SANDIA REPORT
SAND2020-6298
Printed June 2020

Sandia National Laboratories

MELCOR 2.2 Benchmarks of Peach Bottom NUREG/CR-7155 Uncertainty Analysis

Kenneth C. Wagner
Chris Faucett
Kyle Ross
Brad Beeny
Dusty Brooks

Prepared by
Sandia National Laboratories
Albuquerque, New Mexico
87185 and Livermore,
California 94550

Issued by Sandia National Laboratories, operated for the United States Department of Energy by National Technology & Engineering Solutions of Sandia, LLC.

Available to DOE and DOE contractors from
U.S. Department of Energy
Office of Scientific and Technical Information
P.O. Box 62
Oak Ridge, TN 37831

Telephone: (865) 576-8401
Facsimile: (865) 576-5728
E-Mail: reports@osti.gov
Online ordering: http://www.osti.gov/scitech

Available to the public from
U.S. Department of Commerce
National Technical Information Service
5301 Shawnee Rd
Alexandria, VA 22312

Telephone: (800) 553-6847
Facsimile: (703) 605-6900
E-Mail: orders@ntis.gov
Online order: https://classic.ntis.gov/help/order-methods/

ABSTRACT

The U.S. Nuclear Regulatory Commission (NRC) performed a first-of-a-kind uncertainty analysis (UA) of the accident progression, radiological releases, and offsite consequences for the State-of-the-Art Reactor Consequence Analyses (SOARCA) of an unmitigated long-term station blackout (LTSBO) severe accident scenario at the Peach Bottom Atomic Power Station. The objective of the UA was to evaluate the robustness of the SOARCA deterministic "best estimate" results and conclusions documented in NUREG-1935, and to develop insight into the overall sensitivity of the SOARCA results to uncertainty in key modeling inputs. The study was completed in 2015 and documented in NUREG/CR-7155. Since 2015, two other SOARCA UAs were completed for two pressurized water reactor (PWR) plants. The PWR UAs incrementally updated the approach and methodology, including using the latest release of the MELCOR 2.2 computer code. There were also advances made in the state-of-the-art modeling related to NRC efforts using the Peach Bottom model in NUREG-2206, which provided the technical basis for the containment protection and release reduction rulemaking for boiling water reactors with Mark I and Mark II containments. This report documents the input model changes from the NUREG/CR-7155 study and performs a small number of reference calculations to assess the changes of the new computer code and the model input updates. The objective of the work is to verify whether the updated Peach Bottom MELCOR model and updated version of MELCOR support the conclusions formed in the Peach Bottom SOARCA UA by performing these representative calculations.

This page left blank

CONTENTS

LIST OF FIGURES

LIST OF TABLES

ACRONYMS AND DEFINITIONS

Abbreviation	Definition
AC	alternating current
BWR	boiling water reactor
CEA	Atomic Energy and Alternative Energies Commission
CDF	core damage frequency
DC	direct current
FPT	fission product test
FSAR	final safety analysis report
FTC	fail to close
LER	Licensee Event Reports
LHF	lower head failure
LTSBO	long-term station blackout
MSIV	main steam isolation valve
MSL	main steam line
NPP	nuclear power plant
NRC	U.S. Nuclear Regulatory Commission
ORNL	Oak Ridge National Laboratory
PDF	probability distribution function
PWR	pressurized water reactor
RCIC	reactor core isolation cooling
RCP	reactor coolant pumps
RCS	reactor coolant system
RMI	reflective metallic insulation
RP	recirculation pump
RPV	reactor pressure vessel
Sandia	Sandia National Laboratories
SOARCA	State-of-the-Art Reactor Consequence Analyses
SRV	safety relief valve
SV	safety valve
SVRLAM	SRV stochastic failure cycle
TAF	top of active fuel
UA	uncertainty analysis

This page left blank

1. INTRODUCTION

This document describes updates to the Peach Bottom nuclear power plant models supporting the U.S. Nuclear Regulatory Commission's (NRC's) uncertainty analysis (UA) of the accident progression, radiological releases, and offsite consequences for the State-of-the-Art Reactor Consequence Analyses (SOARCA). The SOARCA project [1] is a program that estimates the outcomes of postulated severe accident scenarios which could result in release of radioactive material from a nuclear power plant (NPP) into the environment.

The NRC performed a first-of-a-kind SOARCA UA of the accident progression, radiological releases, and offsite consequences of an unmitigated long-term station blackout (LTSBO) severe accident scenario at the Peach Bottom Atomic Power Station. The objective of the SOARCA UA was to evaluate the robustness of the SOARCA deterministic "best estimate" results and conclusions documented in NUREG-1935 [1], and to develop insight into the overall sensitivity of the SOARCA results to uncertainty in key modeling inputs. The study was completed in 2015 and documented in NUREG/CR-7155 [2]. Since 2015, two other SOARCA UAs were completed for two pressurized water reactor (PWR) plants [3][4]. The PWR UAs incrementally updated the approach and methodology, including using the MELCOR 2.2 computer code. There were also advances made in the state-of-the-art modeling related to NRC efforts using the Peach Bottom model in NUREG-2206 [5], which provided the technical basis for the containment protection and release reduction rulemaking for boiling water reactors (BWRs) with Mark I and Mark II containments. This report documents the model changes from the NUREG/CR-7155 study and performs a select number of reference calculations to assess the changes with the new computer code and the model input updates. The objective of the work is to verify whether the updated Peach Bottom MELCOR model and updated version of MELCOR support the conclusions formed in the Peach Bottom SOARCA UA by performing representative calculations.

Section 2 discusses the key input model updates to the Peach Bottom model made since the NUREG/CR-7155 study as well as uncertainty parameter updates that increase the scope of the uncertainty investigations and update the uncertainty parameter selection and formulation based on insights from the two PWR UAs. Section 3 presents the selection of reference cases for comparison with the NUREG/CR-7155 study. The comparisons of the historical NUREG/CR-7155 results with new MELCOR 2.2 results is presented in Section 4. A summary of the results is provided in Section 5.

This page left blank

2. SUMMARY OF PEACH BOTTOM MODEL UPDATES

The NUREG/CR-7155 study was completed in 2015 using MELCOR 1.8.6. The subsequent PWR UAs incrementally updated the approach and methodology, including using the latest release of the MELCOR 2.2 computer code. This section documents the key model changes made since the NUREG/CR-7155 study. Section 2.1 summarizes the changes from the NUREG/CR-7155 study to a major post-Fukushima venting study that was documented in NUREG-2206 [5]. Section 2.2 summarizes recent changes to improve the Peach Bottom model. Finally, Section 2.3 summarizes uncertainty parameter updates to increase the scope of the uncertainty investigations and update the uncertainty parameter selection and formulation based on insights from the two PWR UAs.

2.1. Peach Bottom Model Updates from NUREG/CR-7155 to NUREG-2206

Since the Peach Bottom model was used in NUREG/CR-7155, the model has been advanced to support other non-SOARCA activities. The model was converted to Version 2.1 and used in the NUREG-2206 study [5]. A limited set of model corrections and model enhancements were implemented to improve areas of the model known to be incorrect, weak, or under-represented. The key changes are listed below:

1. The junction elevation on a flow path connected to the separator was changed to prevent pool formation at reduced reactor pressure vessel (RPV) water levels.
2. The RPV lower head failure (LHF) that opens to fluid flow is limited to 0.01 m^2 (4.4" diameter), or the size of lower head penetration.
3. The minimum unoxidized clad thickness used in the rod collapse model was updated.
4. The control function logic that operates the vacuum breakers between the wetwell and the drywell previously assumed that only atmosphere exists in the downcomer vents. The logic was updated to also include liquid water.
5. The junction opening of the vertical flow path representing the wetwell hard-pipe vent was updated from 8" below the bottom of the pipe to 2" to prevent non-physical entrainment of water.
6. The thickness of the insulation layers on the RPV cylindrical wall and upper head were corrected using plant information (i.e., the final safety analysis report [FSAR]). The insulation was not added to the RPV lower head due to a MELCOR 2.1 code limitation to accept reflective metallic insulation (RMI).
7. The user-defined convective heat transfer coefficient for heat transfer from the RPV to the drywell was updated from ~1 W/m^2-K to 10 W/m^2-K. The previous small value was taken directly from the FSAR apparently without realizing that the design value is small because it incorporates the insulation benefits of the RMI on the RPV.
8. A heat structure representing the containment downcomer vents was added.
9. The control function logic that manages core debris spreading toward the drywell liner was changed to require molten steel as opposed to liquid concrete.
10. As suggested by the MELCOR code development group, Sensitivity Coefficient 4408 (SC-4408)[1] was used to disable the revised treatment of non-equilibrium model, which prevented bubble collapse in swollen pools.

[1] At the time of NUREG-2206 study, the MELCOR code development group recommended using SC-4408 to address occasionally challenging numerical conditions with superheated gas bubbles flowing through saturated pools. The revised method did not address the convergence issues and was assessed to be less effective than the default bubble treatment.

The most significant update, Item 9, was changed with consideration of the debris spreading research performed at Oak Ridge National Laboratory (ORNL) [6]. The spreading of the ex-vessel debris is most influenced by the viscosity of the debris rather than the solidus or liquidus temperature of the concrete substrate. The spreading control logic was modified to start debris movement above the melting temperature of steel (1700 K) and have maximum fluidity at the sampled effective melting temperature of the zircaloy and fuel eutectic mixture (i.e., sampled between 2240 K and 2800 K). Previously, the logic linearly extrapolated from the solidus temperature of the cavity concrete (1420 K) to the liquidus temperature (1670 K).

The MELCOR Peach Bottom model uses three regions or cavities to represent the pedestal region under the reactor and the drywell. When debris leaves the pedestal region, it flows into the drywell. The spreading rate in the drywell cavities is also updated to use the new temperature criteria. The spreading logic from the pedestal cavity to the drywell cavity uses the debris height and temperature-based criteria for flow into the drywell. The height-based criteria is sampled as an uncertain variable. Consequently, this update requires hotter debris to flow from the pedestal and expand into the drywell.

2.2. Recent changes to the Peach Bottom Model

The Peach Bottom model was also updated as part of the current work documented in this report. Several new updates are added to improve the realism of the modeling and associated accident progression. The updates include the addition of recirculation pump (RP) seal leakage, main steam isolation valve (MSIV) leakage, individual safety relief valve (SRV) fail to close (FTC) models, a torus water mixing model, and a new setting for the falling debris heat transfer coefficient. A description of the updates is provided in Sections 2.2.1 through 2.2.5.

2.2.1. Recirculation Pump Seal Leakage

Similar to the PWR reactor coolant pumps (RCPs), the BWR RPs have a coolant flow that provides cooling around the pump shaft. When the AC-powered seal cooling system is available, water flows around the pump shaft into the reactor. On the loss-of-power, the seal cooling pump stops. Without the high-pressure seal flow, the flow around the pump shaft reverses and spills onto the drywell floor. The water leakage on the drywell floor is important for cooling ex-vessel debris after the RPV LHF and initially retarding the movement to the drywell shell.

Exelon assumed an 18 gpm/pump leakage rate in their MAAP analyses for implementing post-Fukushima Orders EA-12-049 and EA-12-051 at the Peach Bottom plant [7]. This value appears conservative if there are no seal failures. The 18 gpm/pump was maintained for the present analyses but could be considered as an uncertain parameter. Based on historical events, the nominal leakage is approximately 5 gpm without seal failures but 45 gpm and 63 gpm in two events with seal failures [8].

2.2.2. Main Steam Isolation Valve Leakage

The BWR MSIVs have some leakage. The maximum BWR MSIV leakage is controlled by technical specifications and regularly monitored. It is conservatively assumed that any leakage past the MSIVs reaches the environment. Consequently, the MSIV leakage can be an early radioactive release, albeit very small. The nominal leakage was assumed to fall within the technical limits for a BWR (<11.5 scfh) [9].

2.2.3. Individual SRV FTC Modeling

In the NUREG/CR-7155 Peach Bottom model, only the lowest opening pressure SRV had logic for stochastic or thermal failure. This was adequate because the stochastic failure was assumed to leave the SRV fully open, which immediately depressurized the RPV without any other SRV cycling. Similarly, the thermal failure stuck-open area distribution used a minimum value that also depressurized the RPV and prevented any other SRV cycling. Since a new stochastic FTC valve area was implemented for the updated model (i.e., see Section 2.3.1), there were concerns that multiple valves could fail open. Consequently, the input model was updated to include stochastic and thermal FTC logic for the five lowest-pressure opening SRVs. The updated logic reads uncertainty parameters for FTC cycle and the FTC area for stochastic failures, and for thermal valve failures on five SRVs. In test calculations with 1200 samples, there was only one or two occurrences of three failed valves and no realizations where there were four or five SRVs. Therefore, the expanded failure modeling for five of the eleven SRVs at the Peach Bottom plant is adequate.

2.2.4. Torus Mixing Model

In the NUREG/CR-7155 Peach Bottom model, the containment torus or wetwell was modeled with a single control volume. One of the insights from the Fukushima accident is that persistent SRV or reactor core isolation cooling (RCIC) operation can lead to localized heating of the torus fluid and an accelerated containment pressurization. Consequently, the torus was subdivided into two control volumes. The $1/16^{th}$ sector represented the location of the first stuck-open SRV and the RCIC steam exhaust discharge.[2] The $15/16^{th}$ sector corresponds to the remainder of the torus. The smaller torus control volume was divided in the $1/16^{th}$ region based on the segmented weld lines on the torus and associated spacing between adjacent spargers. The connecting flow path configuration follows the MELCOR torus modeling recommendations documented in Reference [10] that was benchmarked to the plant data [11]. The model shows preferential heating of the $1/16^{th}$ sector during SRV operation and mixing back to the bulk temperature thereafter.

2.2.5. Falling Debris Heat Transfer Coefficient

The specification of the falling debris heat transfer coefficient was also reviewed. The MELCOR 2.2 default value is 100 W/m^2-K, which is reflective of a film boiling heat transfer coefficient. The value used in the SOARCA and NUREG/CR-7155 studies was 2000 W/m^2-K, which was used with a very small particle diameter to maximize debris quenching in lieu of better multi-dimensional heat transfer models [12]. Historical work by V. K. Dhir showed a dependency of the heat transfer coefficient on the falling velocity and the water subcooling [13]. The heat transfer coefficients ranged from 242 W/m^2-K to 1090 W/m^2-K as the fall velocity and pool subcooling varied of 0.02 m/s and T_{sat} to 0.45 m/s and 50 K subcooling. The median sampled debris size and corresponding velocity is 0.032 m and 0.94 m/s. Dhir's data stopped at 0.45 m/s, whereas the range is expected to span 0.52 m/s to 1.58 m/s. The extrapolated, median heat transfer coefficient at 0.94 m/s is estimated to be 1320 W/m^2-K (see Figure 2-1). The scoping calculations with variable falling debris heat transfer behavior (i.e., particle size, fall rate, and heat transfer coefficient) suggested that the heat transfer coefficient is significantly less important relative to the debris size.

---

[2] A single SRV operation is essentially the only configuration required for decay heat removal in a station blackout. Similarly, a single stuck-open SRV is the most likely configuration. Reference [10] suggested that the complications of more control volumes had limited benefit. Furthermore, if multiple SRVs are open, then there is more vigorous mixing. Consequently, a simplified two-control volume representation is used in the present approach to address the localized heat loading from one stuck-open SRV.

Consequently, an extrapolated rate of 1320 W/m^2-K is judged adequate when the uncertainty of the debris size is considered.

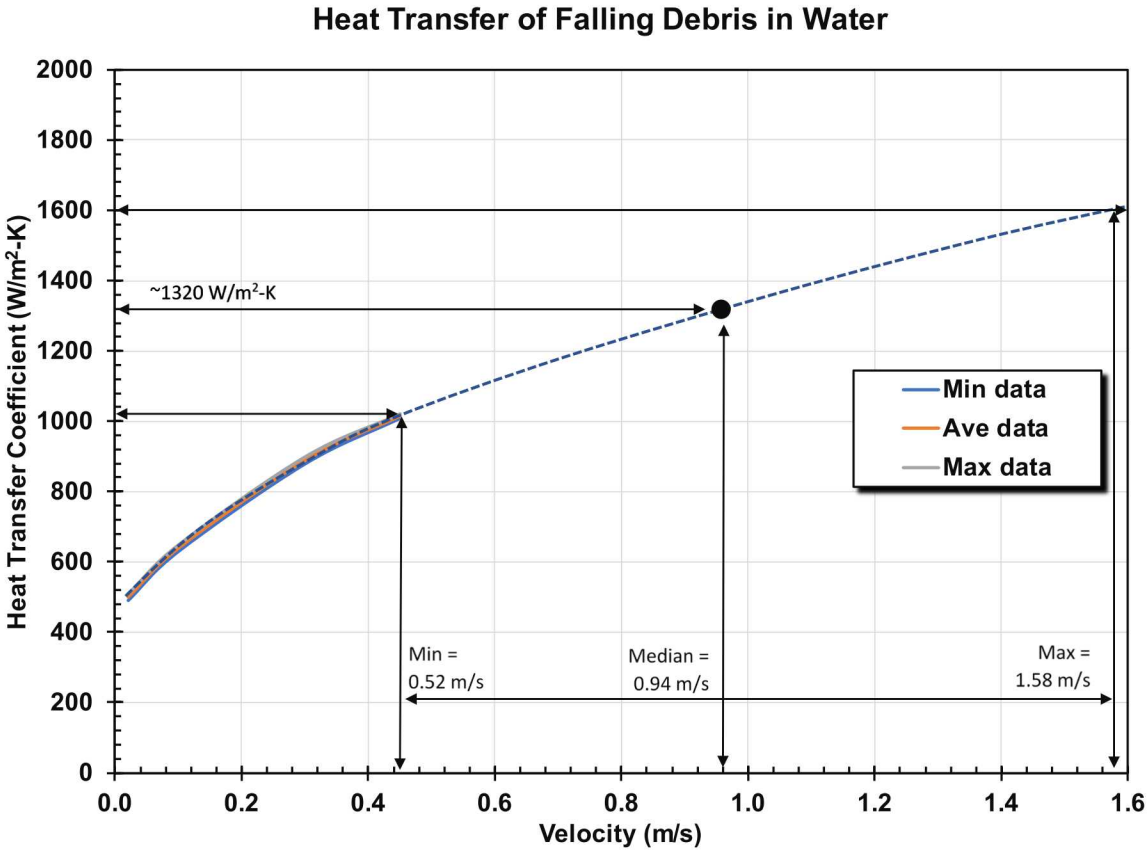

Figure 2-1. Estimation of the film boiling heat transfer coefficient versus falling debris velocity[3]

2.2.6. Ex-vessel Debris Melt Spreading

An important containment failure mechanism in BWR Mark I accident sequences is thermal failure (melting) of the drywell liner following contact with hot ex-vessel core debris (i.e., drywell liner melt-through). Following the RPV LHF, the hot core debris is expected to flow out of the reactor pedestal onto the main drywell floor. If the debris temperatures remain sufficiently high as it spreads across the drywell floor and contacts the drywell liner, the liner would melt and fail. The precise conditions under which core debris would flow out of the pedestal and across the drywell floor are uncertain. NUREG/CR-7155 addressed these uncertainties [2] by assuming debris mobility and the potential for liner failure are represented by two key parameters: debris mass (i.e., static head) necessary for lateral flow and debris temperature (which characterizes debris rheological properties and internal energy available to challenge the liner).

The Peach Bottom containment drywell floor is subdivided into three regions for the purposes of modeling molten core/concrete interactions in the MELCOR model. The first region, which receives core debris exiting the RPV lower head, corresponds to the reactor pedestal floor and sump

[3] Data is from Reference [13]. Expected range of velocities is 0.52 m/s to 1.58 m/s. Median heat transfer coefficient is ~1320 W/m^2-K.

areas (CAV 0). Debris that accumulates in CAV 0 can flow out through a doorway in the pedestal wall to a second region representing a 90-degree sector of the drywell floor (CAV 1). If debris accumulates in this region to a sufficient depth, it can spread further around the annular drywell floor into the third region (CAV2). This discrete representation of debris spreading is illustrated in Figure 2-2.

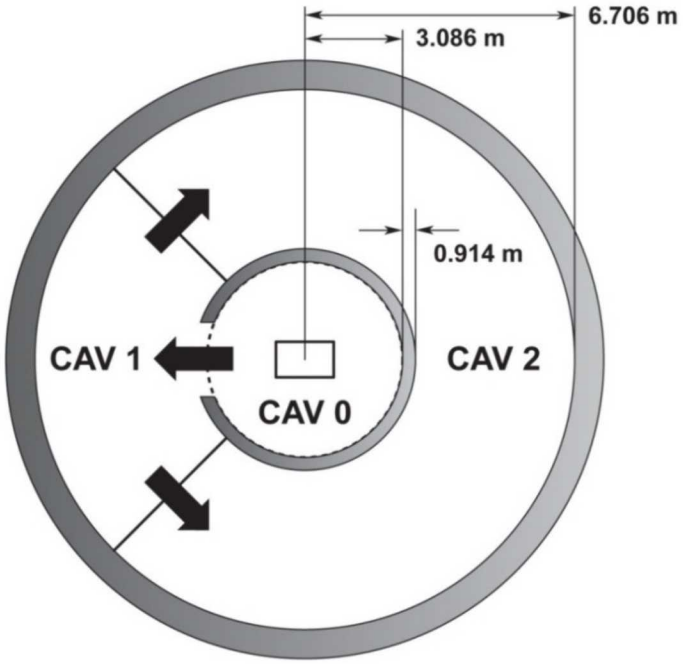

CAV	FLOOR AREA	EQUIV RADIUS	PERIMETER RATIO
0	29.92	3.086	0.95

1	22.75	2.691	0.94
			0.62
2	68.25	4.661	1.72
			1.08

Figure 2-2. Pedestal and drywell floor regions

The NUREG/CR-7155 parametric model that monitors the debris elevation and temperature within each drywell floor region has been retained until better modeling can be developed (i.e., but including the changes noted in Footnote 4). The NUREG/CR-7155 uses uncertain modeling parameters that define threshold values for debris to move from one region to its neighbor. More specifically, when debris in a cavity is at or above the molten fuel (i.e., as specified by the effective eutectic melting temperature[4]) and exceeds uncertain parameter specification for movement, the debris can flow from CAV 0 to CAV 1 and CAV 1 to CAV 2. When the debris in a cavity is at or below the melting temperature of the steel (i.e., unoxidized steel has the lowest metallic constituent

[4] Also see the discussion in Section 2.1, Item 9 for changes in the modeling for the mobility of the ex-vessel debris after the NUREG/CR-7155 study. NUREG/CR-7155 used the solidus and liquidus temperature of the concrete (i.e., the debris substrate) for an estimation of the mobility of the ex-vessel debris versus the debris temperature in subsequent studies.

melting temperature of the significant metals in the ex-vessel debris), no flow is permitted. Between these two debris temperatures, restricted debris flow is permitted by increasing the required elevation difference in debris between the two cavities (i.e., more debris head required to flow).

In NUREG/CR-7155, other parametric models managed the debris spreading radius across the drywell floor within the cavities. The parametric spreading model specified the velocity of the debris spreading using the same temperature logic as above. The debris is assumed immobile below the melting temperature of steel. At or above the effective eutectic melting temperature of the fuel, the ex-vessel debris will traverse CAV 1 in 10 minutes and transverse across CAV 2 in 30 minutes. A linear interpolation is performed to determine the debris front velocity at temperatures between these two values.

In sensitivity calculations presented in Section 4, the new MELCOR meltspreading model is used to control the transport of the debris. When the meltspreading model is activated, the movement of the ex-vessel debris within the three cavities is controlled by the meltspreading model. The meltspreading model was reformulated for this study using the Stokes flow radial momentum equation (axisymmetric):

$$g\frac{\partial H}{\partial r} = \left(\frac{\mu}{\rho}\right)\frac{\partial^2 u_r}{\partial z^2}, \qquad for\ u_r = \frac{dr}{dt}, the\ spreading\ velocity$$

Dimensionally,

$$g\frac{H}{R} \sim \left(\frac{\mu}{\rho}\right)\frac{{}^{dR}/_{dt}}{H^2}$$

Or,

$${}^{dR}/_{dt} \sim \left(\frac{\rho g H^3}{\mu R}\right)$$

Treating debris volume as approximately constant and as a circular cylinder,

$$V = \pi R^2 H \rightarrow H^3 \sim {}^{V^3}/_{\pi^3 R^6}$$

The momentum equation is, dimensionally,

$${}^{dR}/_{dt} \sim \left(\frac{\rho g}{\mu}\right)\left({}^{V^3}/_{\pi^3 R^7}\right) = {}^{K}/_{R^7}, \qquad K = \frac{\rho g V^3}{\mu \pi^3}$$

To solve $R(t)$ with dimensional analysis, define a non-dimensional quantity ε:

$$\varepsilon = \frac{Kt}{R^8}$$

Then:

$$R = \left(\frac{Kt}{\varepsilon}\right)^{1/8}$$

With equations $R(\varepsilon)$ and $^{dR}/_{dt}\,(K,R)$, the dimensionless parameter ε can be shown to equal 1/8 (by taking the derivative of $R(\varepsilon)$ with respect to t, equating to $^{dR}/_{dt}\,(K,R)$, and solving for ε). Using this result, an $R(t-t_0)$ expression can be obtained as a general solution:

$$R(t) = \left(2^{3}/_{8}\right)\left(K^{1}/_{8}\right)(t-t_0)^{1}/_{8}$$

Substituting for K:

$$R(t) = \left(\frac{2}{\pi}\right)^{3}/_{8}\left(\frac{\rho g V^3}{\mu}\right)^{1}/_{8}(t-t_0)^{1}/_{8}$$

Computing a time derivative with this general solution:

$$\frac{dR}{dt} = \left(\frac{2}{\pi}\right)^{3}/_{8}\left(\frac{\rho g V^3}{\mu}\right)^{1}/_{8}\left(\frac{1}{8}\right)(t-t_0)^{-7}/_{8}$$

This time derivative expression can be used to solve for debris radius:

$$R(t) = R(t_0) + \left(\frac{dR}{dt}\right)(t-t_0)$$

$$R(t) = R(t_0) + \left(\left(\frac{2}{\pi}\right)^{3}/_{8}\left(\frac{\rho g V^3}{\mu}\right)^{1}/_{8}\left(\frac{1}{8}\right)(t-t_0)^{-7}/_{8}\right)(t-t_0)$$

Noting that:

$$\frac{1}{8} = \left(\frac{1}{8}\right)^{7}/_{8}\left(\frac{1}{8}\right)^{1}/_{8}$$

Leads to a modified expression for the debris radius:

$$R(t) = R(t_0) + \left[\left(\frac{2}{\pi}\right)^{3}/_{8}\left(\frac{1}{8}\right)^{7}/_{8}\right]\left(\left(\frac{1}{8}\right)\left(\frac{\rho g V^3}{\mu}\right)(t-t_0)\right)^{1}/_{8}$$

The term in square brackets equals 0.136, which is Huppert's "suggested constant" $C1$ as mentioned in the current CAV debris spreading model reference manual entry.

An important input into the melt spreading model is the Ramacciotti viscosity model constant. The value of the Ramacciotti viscosity was specified using guidance from Argonne National Laboratory research on melt spreading [14]. Reference [14] recommends a value of 7.26 for Ramacciotti viscosity model constant based on curve fits from the experimental reactor material melt spreading database. This is an important uncertainty parameter that was not varied in this study.

2.2.7. Ex-vessel Debris Water Ingression

When water is present above the ex-vessel debris, there is important heat transfer from the ex-vessel debris to the water. This is particularly important with the consideration of RP leakage (see Section 2.2.1), which can generate a relatively deep pool of water in the drywell. Previously, the

surface heat transfer was specified using multipliers to the heat transfer coefficient to approximate experiment finding that suggested enhanced heat transfer rates (e.g., see References [18] and [12]). However, a new water ingression model was recently added to MELCOR [15]. The updated model calculates the permeability of the top surface crust layer. The new modeling adds an improved calculation of the surface heat transfer based on the debris crust temperature, depth, and composition. Similar to the new melt spreading model described in Section 2.2.6, the water ingression model is used in sensitivity calculations presented in Section 4 to illustrate the impact of the updated surface heat transfer modeling.

2.3. Summary of New Peach Bottom Uncertainty Distributions

The Peach Bottom uncertain parameters used in NUREG/CR-7155 covered the following phenomenological areas:

- sequence uncertainty,
- in-vessel accident progression uncertainty,
- ex-vessel accident progression issues,
- containment severe accident behavior uncertainty, and
- fission product release, transport, and deposition uncertainty.

The accident progression phenomenological uncertainties span the temporal domain of the severe accident progression and span sequence variations as affected by SRV behavior to uncertainties in the core damage and melt progressions, especially those affecting the rate of core degradation and amount of hydrogen generation. Consequently, the parameters selected in the NUREG/CR-7155 study included parameters that impacted both melt progression and fission product release and transport. The scope of the parameters also addressed key accident progression phenomena taking place following vessel lower head melt-through, such as melt attack of the drywell liner; containment response uncertainty, such as uncertainty in onset of drywell head flange leakage; and uncertainties in radioactive aerosol transport mechanics. The selection of uncertain parameters ensures a commensurate representation of uncertainties in the major phases of the accident evolution.

Table 2-1 summarizes the updated list of uncertainty parameters and an indication whether it was updated for this study. The non-changed parameters are fully discussed in NUREG/CR-7155 and not repeated here. However, based on insights from the Surry and Sequoyah UAs, some changes were made to update the modeling approach for Peach Bottom. The updated uncertain parameters are summarized in following sub-sections. The updated list also includes discussion of two new uncertain parameters; one for the stochastic SRV FTC area and one for debris quenching behavior in the vessel lower head.

Table 2-1. MELCOR uncertain parameter groups

Uncertain Parameter	Revision
Sequence Issues	
SRV stochastic failure to reclose (SRVLAM)	Same as NUREG/CR-7155 but sampled for 5 SRVs
SRV stochastic failure area (SRV_AREA)	New, separate samples for 5 SRVs
Battery Duration (BATTDUR)	Same as NUREG/CR-7155
In-Vessel Accident Progression Parameters	
Zircaloy melt breakout temperature (SC1131(2))	Same as NUREG/CR-7155
Molten clad drainage rate (SC141(2))	Same as NUREG/CR-7155
SRV thermal seizure criterion (SRVFAILT)	Same as NUREG/CR-7155
SRV open area fraction (SRVOAFRAC)	Same as NUREG/CR-7155
Main steam line creep rupture area fraction (SLCRFRAC)	Same as NUREG/CR-7155
Effective eutectic melting temperature	Updated from time-at-temperature approach
Radial debris relocation time constants (RDMTC, RDSTC)	Same as NUREG/CR-7155
Lower plenum particulate debris hydraulic diameter (DYHPD) and correlated settling velocity (VFALL)	New
Ex-Vessel Accident Progression Parameters	
Debris lateral relocation – cavity spillover and spreading rate (DHEADSOL, DHEADLIQ)	Same as NUREG/CR-7155
Containment Behavior Parameters	
Drywell liner failure flow area (FL904A)	Same as NUREG/CR-7155
Hydrogen ignition criteria (H2IGNC)	Same as NUREG/CR-7155
Railroad door open fraction (RRIDRFAC, RRODRFAC)	Same as NUREG/CR-7155
Drywell head flange leakage (K, E, δ)	Same as NUREG/CR-7155
Chemical Forms of Iodine and Cesium	
Cesium chemical forms (CHEMFORM)[5]	Updated to sample 5 continuous variations of cesium allocated to cesium hydroxide versus cesium molybdate
Aerosol Deposition	
Aerosol aerodynamic shape multiplier (CHI)	Updated from aerosol density approach

[5] At this time, the complications of uncertain iodine sampling were not addressed. A constant fraction of iodine gas was used in all the distributions. A model-specific Python script was developed for the Surry UA to support coupled uncertain iodine and cesium speciation sampling that was not implemented for the Peach Bottom model at this time (see Appendix D in Reference [4]).

2.3.1. SRV Stochastic FTC Area Distribution

Following the draft Surry UA, the safety valve (SV) failure attributes were changed based on discussions with nuclear valve testing personnel and closer examination of Licensee Event Reports (LERs). The discussions and LER examinations indicated a higher likelihood of either a mostly closed (slowly leaking) or a mostly open failure position. The new Peach Bottom model stochastic failure distributions were updated to follow the approach in the Sequoyah UA [3] and the final Surry UA [4]. The following discussion was adapted from the approach used for the PWR SV approach [3], which may have some relevance for BWR SRVs.[6]

Small open area fractions that do not lead to depressurization and large open area fractions that cause rapid depressurization are judged the most likely events for PWR SVs. This suggests that the distribution on open area fractions should result in more sampling at the extremes of the interval than in the middle of the distribution. The lower end of the distribution with small open areas represents a leaking or weeping valve, which is something observed in valve failure events during operations [16]. The higher end with a large open area represents a valve that energetically opens but suffers a mechanical deformation of internal parts that prevents re-closure. There are no substantiated failure mechanisms observed to result in the middle part of the distribution for open areas, and hence these open areas are judged less likely to fail. However, given the sparse data on valve failures during actual operating events, the intermediate areas are assigned a non-zero probability (i.e., also not possible to conclude this was impossible). The lower end was truncated at 0.01. Although a small open area fraction is possible, a valve cannot fail to close and also have an open area fraction of 0.0. The value of 0.01 was chosen so if multiple SRVs fail to close and all valves have small open area fractions, the combined open area fraction of the valves will still fall within a realistic range for an FTC mode.

The SRV_AREA uncertainty uses a piecewise distribution between 0.01 and 1.0 with four sub-regions. The sub-regions are the intervals of open area fraction from 0.1% to 10%, from 10% to 30%, from 30% to 90%, and from 90% to 100%. All of the open area fractions within a sub region have the same probability. However, the first and last sub regions are more likely to be sampled than the middle sub-regions reflecting expert opinion that valves are likely to either weep/leak or fail to fully open. The region 10% to 30% was assigned a slightly higher probability than the region 30% to 90% because for one of the 16 failure to close events on which the SV failure probability is based, the event description indicated a ~20% flow area. The density function that illustrates the sub intervals is plotted in Figure 2-4. The cumulative distribution is shown in Figure 2-3.

In addition to an updated FTC area distribution, the final Surry and Sequoyah UAs also updated the SRV stochastic FTC probability distributions. The PWR SV behavior was updated to reflect the expert judgment that the probability of the FTC on the first challenge is weighted differently and higher than subsequent challenges. However, the Peach Bottom SRVs use BWR-specific data for the FTC distributions. Consequently, it was not possible to directly adopt the PWR valve failure distributions used in the Sequoyah and Surry UAs. The BWR SRVs are also expected to have a higher failure probability on the first challenge versus successive openings but this complication was not implemented. The only update is for the stochastic FTC is the SRV failure.

---

[6] The following PWR SV failure area distribution was added as an option for the Peach Bottom SRV sampling. Due to the limited investigation of only three refence cases in this report, it has not been fully adopted and applied in an SRV uncertainty study. It is recommended that applicable BWR LERs with SRV FTC be reviewed to confirm the appropriateness for BWR SRV applications.

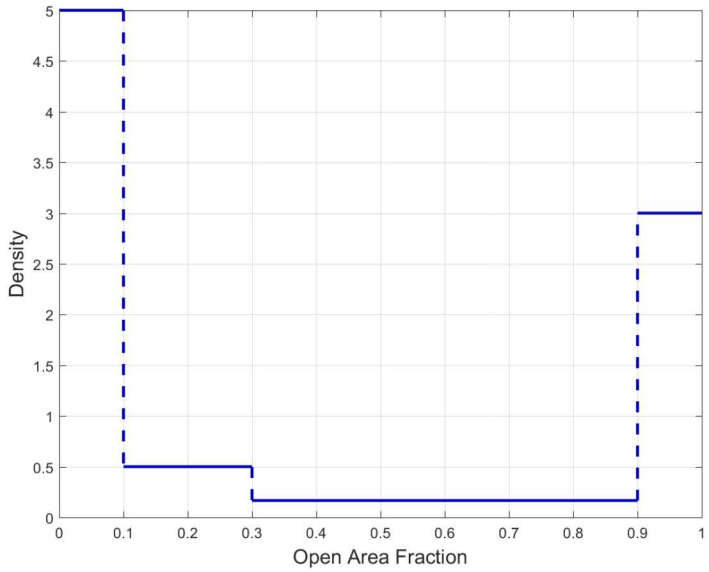

Figure 2-3. The density function for SV open area fraction (SRV_AREA) for each SRV[7]

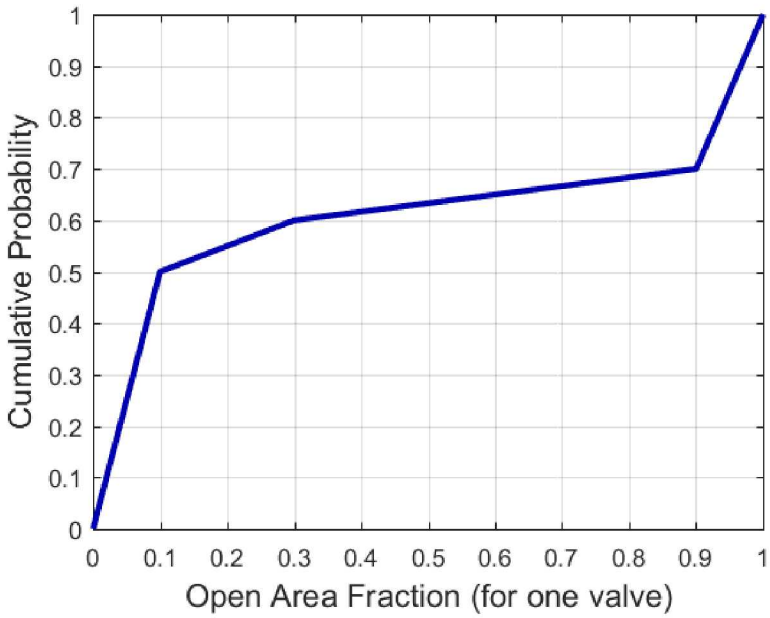

Figure 2-4. The density function for SRV open area fraction (SRV_AREA) for each SRV

2.3.2. Effective Temperature at which the Eutectic Formed from Zircaloy Oxide and Uranium Oxide Melts

MELCOR lacks a deterministic model for evaluating the fuel mechanical response to the effects of material interactions (i.e., eutectic formation) and other processes that occur at very high

[7] Separate uncertainty samples were made for each of the five lowest opening pressure SRVs.

temperatures. NUREG/CR-7155 modeled the uncertainty in the material degradation processes using a time-at-temperature criteria. The time-at-temperature based criterion is consistent with other severe accident codes (e.g., MAAP) and only one of several mechanisms that could lead to the fuel rod collapse.[8] In the subsequent Surry and Sequoyah UAs, an alternate approach was used based on a review of material phase diagrams and experimental observations for fuel collapse. The new method has additional ramifications of not only impacting the collapse of the fuel rod but also the subsequent debris behavior and formation of molten pools. The following discussion was adapted from the PWR approach [3] but judged to be equally applicable for the BWR fuel degradation and response.

The binary phase diagram for ZrO_2/UO_2 suggests the melting point for equilibrium conditions is approximately 2800 K for a 50/50 molar mixture; hence, this was the historical MELCOR default value [2][18][19]. Any liquefaction below this temperature accounts for the effect of molten Zircaloy metal or alpha-Zr(O) 'wetting' the oxide surfaces. Observations of the Phebus and VERCORS experiments suggest that irradiated fuel and oxidized cladding exhibit eutectic liquefaction at significantly lower temperatures; thus, the MELCOR default was subsequently modified to 2500 K. Following significant local cladding oxidation, the effective liquefaction of ZrO_2 and UO_2 mixtures results in local rod collapse as molten material, rather than as rubble or debris. The parameter treatment for this work attempts to approximate the combined uncertainties associated with burnup, eutectic composition, material properties, and non-equilibrium effects in the ZrO_2/UO_2 eutectic reactions.

The fuel melt associated with this parameter is a localized effect. This means that MELCOR evaluates the temperature for each core cell independently and allows the fuel in that specific cell to melt when it reaches a failure temperature, such as the temperature at which the eutectic formed from UO_2 and ZrO_2 melts. Thus, the entire core will not collapse when the hottest location reaches the sampled temperature. However, the melting of a core cell can cause the subsequent failure of fuel above and in the same radial ring that was previously supported by the failed cell. This is a physical effect and still only affects a section of a single ring, thus keeping it a localized effect.

The eutectic reactions are approximated by a user-modification of melting and failure temperatures in model input. Thus, to effectively represent the temperature at which the eutectic formed from UO_2 and ZrO_2 melts, the user must modify:

- The sensitivity coefficient SC1132(1), which defines the cladding temperature resulting in rod collapse without Zr-metal cladding remaining, and
- The melting temperatures of both UO_2 and ZrO_2 in the input deck (MP_PRC records).

Six experimental data points for eutectic induced core collapse are readily available from the VERCORS experiments to help inform the uncertainty distribution [17]. Table 2-2 shows the VERCORS test results along with the mean and standard deviation.

[8] The fuel rod collapse is complicated with the interaction of the molten zircaloy breakout (i.e., see SC1131(2) parameter in Table 2-1). Once the molten zircaloy is released, the additional heating from the cladding oxidation significantly decreases and the remaining oxide structural fragility increases. The time-at-temperature model is an alternate collapse criterion that addressed uncertainties in the rod structural integrity. The structural integrity is simplified to predict an increasing likelihood to collapse as a function of increasing temperature and time.

Table 2-2. VERCORS test results for collapse temperature

Test	Collapse Temperature (K)
T1	2525
HT1	2550
HT2	2400
HT3	2525
V_6	2525
RT6	2350
Mean	2479
Standard Deviation	83

In selecting this experimental data, the observed core slump is projected to a eutectic reaction. This was strongly indicated by the test results but cannot be definitively confirmed due to a lack of instrumentation.

The selection of a specific distribution is complicated by the lack of detailed experimental data over the ranges of severe accident conditions and reactor operation (e.g., high burnup). While the VERCORS testing matrix does not provide randomly distributed evidence of eutectic formation temperatures, these tests do provide a range of temperatures over which eutectics were significant enough to cause core collapse. A normal distribution was fitted to the data and used to assess the uncertainty in the average core collapse temperature for higher burnup fuel. The simple parameter treatment is not intended to rigorously quantify eutectic effects on severe accidents and core degradation. Rather, the proposed treatment roughly evaluates the influences that the physical state of the core debris has on core degradation kinetics and the subsequent severe accident progression. A lower temperature for this parameter results in an increased generation of molten pools in the RPV during the core disassembly. Alternatively, a higher temperature for this parameter results in a decreased generation of molten pool formation for the ZrO_2 and UO_2 debris.

The VERCORS testing data was derived from independent tests with varying environmental conditions. A normal distribution was fitted to the VERCORS data in order to describe the general range of potential collapse temperatures (see Figure 2-5). The normal distribution has a mean of 2479 K and a standard deviation of 83 K. The red star identifies the value used in the original SOARCA [18] and NUREG/CR-7155 [2] studies. Consequently, the new distribution will always result in lower oxide debris melting temperatures in an uncertainty assessment. However, the new uncertainty parameter addresses the fuel collapse in a different manner than the time-at-temperature uncertainty parameter. Therefore, its impact on the fuel collapse timing is not necessarily at the extreme maximum.

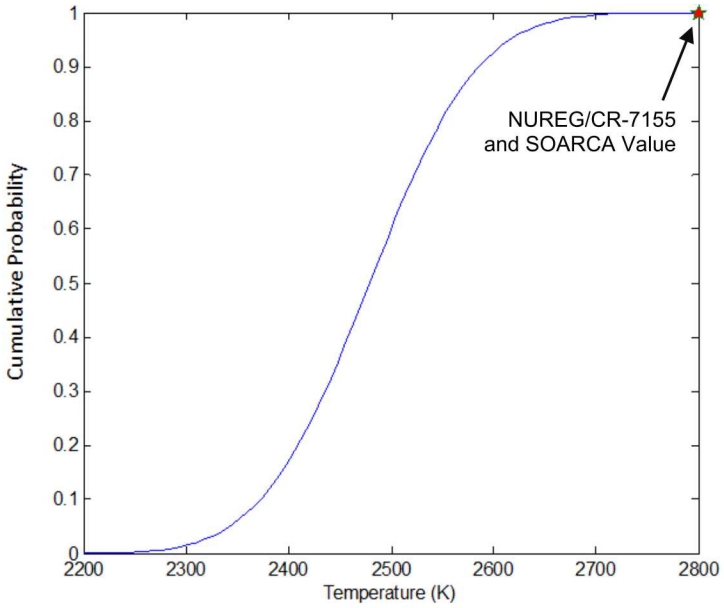

Figure 2-5. CDF of eutectic melting temperature

2.3.3. Lower Plenum Falling Debris Size

The BWR RPV has a large lower plenum under the core to hold the control blades (i.e., the PWR control rod insert from above the core). When the core plate fails in a severe accident, the debris will fall through the deep water pool to the vessel lower head. A new uncertainty parameter was added to vary the average size of the falling debris particulates and the corresponding settling velocity. The amount of heat transfer between the falling particles and the water changes the magnitude of the associated vessel pressurization. The previous SOARCA and NUREG/CR-7155 treatment of these variables exaggerated heat transfer to match experimental debris quenching data and account for multi-dimensional effects not treated in the MELCOR model [12]. NUREG/CR-7155 showed a sensitivity to the likelihood of the MSL failure due to the vessel pressurization following the relocation of hot debris into the lower plenum. Consequently, new uncertainty parameters are introduced to address debris-water heat transfer uncertainties using the characteristic debris size and its corresponding settling velocity in water.

The sampled average particle size is exactly correlated to the size-dependent settling velocity of uranium dioxide debris falling through the water between the core plate to the lower head (i.e., confirmed be to approximately equal to the terminal particle velocity using a Stokes' Law formulation, see Figure 2-6). The sampled particle size is bounded by the diameter of a UO_2 fuel pellet size (~1 cm) and 1 mm. The minimum value was selected to bound the previous SOARCA value (0.2 cm) and reflect observed molten particle breakup in debris quenching experiments. A uniform log distribution is used between these bounds (see Figure 2-7).

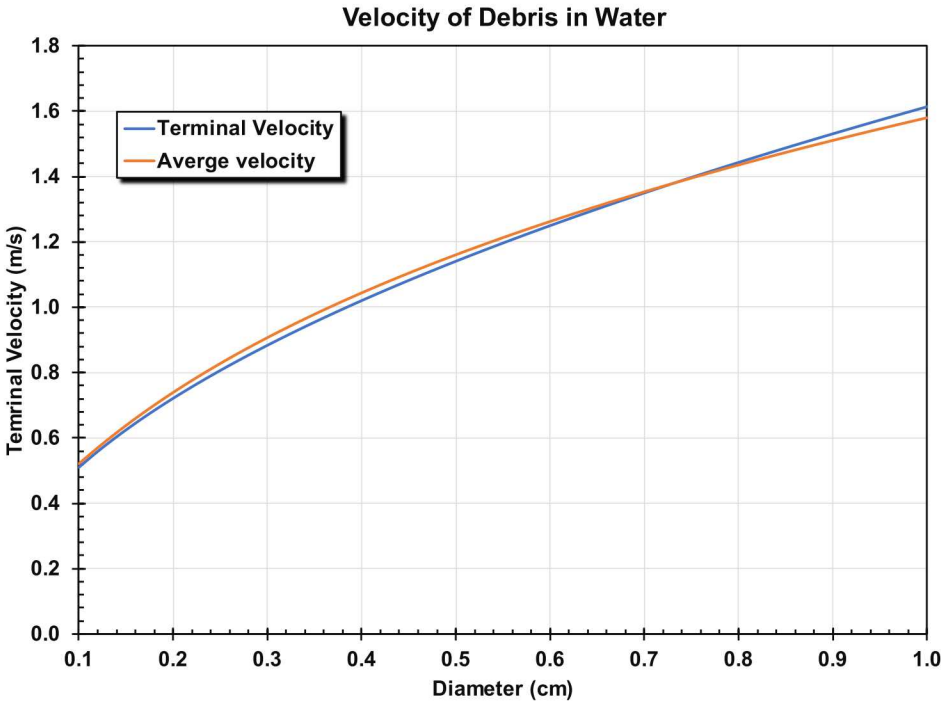

Figure 2-6. Particle terminal velocity of UO_2 debris in water

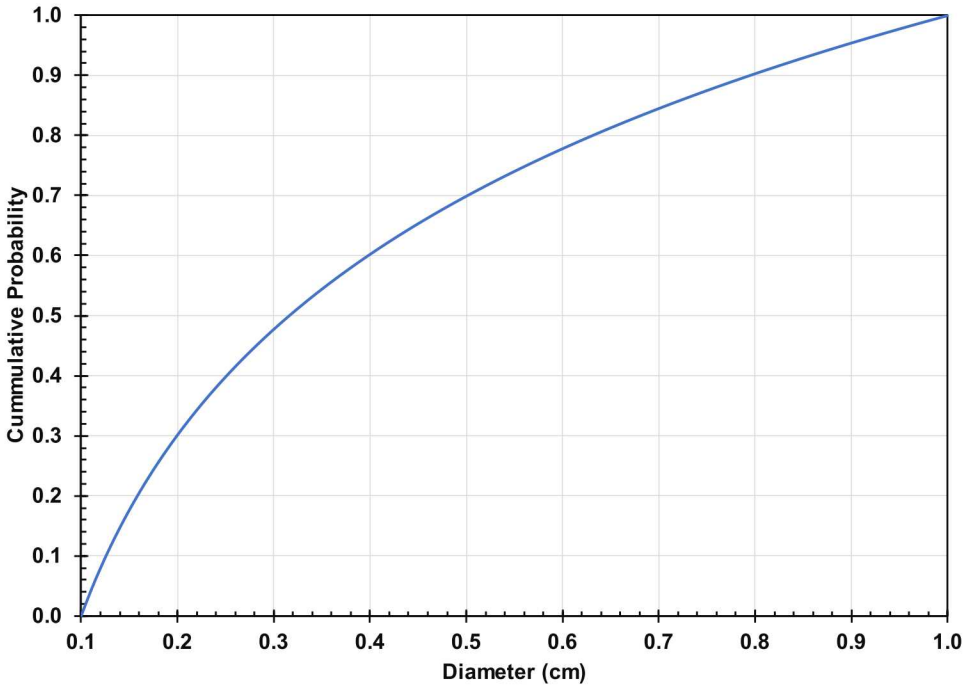

Figure 2-7. CDF of debris particle size in the lower plenum

2.3.4. Cesium Speciation

The uncertainty parameter for the cesium speciation was updated from the NUREG/CR-7155 approach. The NUREG/CR-7155 speciation had five variations of cesium and iodine speciation that did not vary in a continuous manner (see Table 2-3). The interpretation of the corresponding regression analysis was less informative because any trends from Distribution 1 to Distribution 5 did not linearly indicate the influence of the various compounds. Consequently, the cesium speciation was updated to continuously vary from low to high fractions of cesium molybdate using the continuous distribution developed in the Surry UA [4]. The following discussion was adapted from the PWR approach [4] but judged to be equally applicable for the BWR radionuclide behavior.

The speciation of cesium described in the original Peach Bottom SOARCA analysis [18] was based on a detailed chemical analysis of the deposition and transport of the volatile fission products in the Phebus facility tests [20]. The chemical analysis revealed molybdenum combined with cesium and formed cesium molybdate (Cs_2MoO_4). This is based on cesium and molybdenum having been found deposited in the same locations that were at temperatures too high for cesium hydroxide to remain deposited. However, there was also evidence from the Phebus tests that cesium is revaporized at temperatures consistent with the cesium hydroxide chemical form. It is presumed that reactions between cesium molybdate and steam cause cesium hydroxide to form during the release from the fuel. Prior to the SOARCA analysis, the MELCOR default chemical form of remaining cesium (beyond the creation of CsI) was 100% cesium hydroxide. Understanding the uncertainty regarding chemical form of cesium is important because cesium chemical behavior affects the amount and timing of the cesium release from containment into the environment (e.g., late phase revalorization of cesium).

Table 2-3. NUREG/CR-7155 uncertain parameters for chemical forms of iodine and cesium

Parameter			Distribution		
CHEMFORM: Five alternative combinations of RN classes 2, 4, 16, and 17 (CsOH, I2, CsI, and Cs2MoO4)			Discrete distribution Combination #1 = 0.125 Combination #2 = 0.125 Combination #3 = 0.125 Combination #4 = 0.125 Combination #5 = 0.500		
Five Alternatives			**Species (MELCOR RN Class)**		
		CsOH (2)	I_2 (4)	CsI (16)	Cs_2MO_4 (17)
Combination #1	fraction iodine	--	0.03	0.97	--
	fraction cesium[a]	1	--	--	0
Combination #2	fraction iodine	--	0.002	0.998	
	fraction cesium	0.5	--	--	0.5
Combination #3	fraction iodine	--	0.00298	0.99702	--
	fraction cesium	0	--	--	1
Combination #4	fraction iodine	--	0.0757	0.9243	--
	fraction cesium	0.5	--	--	0.5
Combination #5	fraction iodine	--	0.0277	0.9723	--
	fraction cesium	0	--	--	1
SOARCA estimate	Fraction iodine	--	0.0	1.0	--
	Fraction cesium	0.0	--	--	1.0

[a] This represents the distribution of 'residual' cesium which is the mass of cesium remaining after first reacting with the amount of iodine assumed to form CsI.

The updated cesium uncertainty parameter (i.e., CHEMFORM) determines the fraction of total cesium, which is not bound to iodine and becomes Cs_2MoO_4. There are clear limits at 0.0 and 1.0. The limits also represent the spread in what was considered 'best practice' for cesium in past work, where in SOARCA it was considered 100% cesium molybdate and prior to SOARCA, the best practice had been 100% cesium hydroxide. So, for this parameter, 0.0 and 1.0 will be used as the lower and upper limits, respectively. The best-estimate for cesium partitioning based on examination of Phebus results indicates that outside of the primary system (and in containment) cesium will have a speciation of 80% Cs_2MoO_4 and 20% CsOH. This may not represent the cesium distribution at the time of release from fuel, but within MELCOR there is no model for the cesium molybdate and steam reaction to form cesium hydroxide, so the environmental release forms need to be initialized within the fuel [21].

The fractional distribution of elemental Cs as Cs_2MoO_4 is a beta distribution with shape parameters α equal to 9 and β equal to 3 (see Figure 2-8). The beta distribution is naturally bounded between zero and one, which makes it well-suited for a fractional sampling. The shape parameters were selected to give a mode of 80% Cs_2MoO_4, which agrees with Phebus data while also possessing a noticeable amount of negative skewness to explore the effects of higher CsOH concentrations.

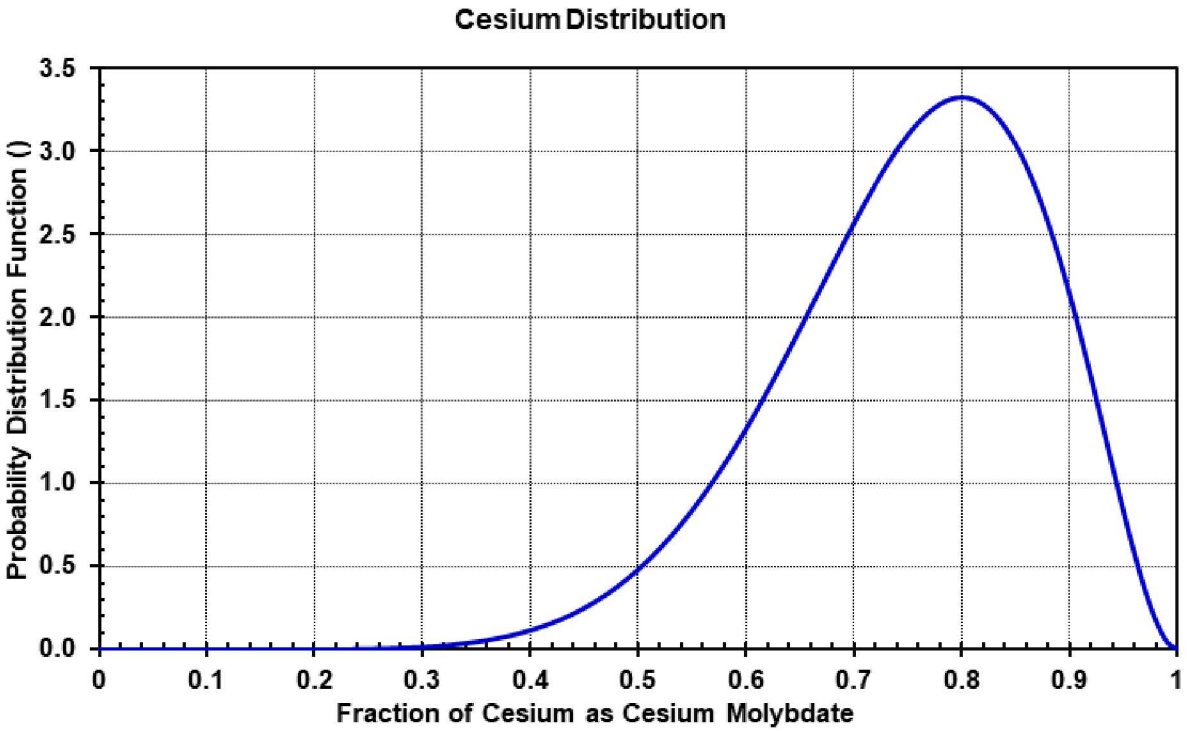

Figure 2-8. The Beta distribution used to sample the fraction of cesium as cesium molybdate [6]

Partitioning the initial core inventory of cesium among its defined chemical forms for release and transport is managed within MELCOR input files that define the initial spatial mass distribution of the various chemical species and their associated decay heat. The sampled changes to the mass fractions directly affect the mass fractions of other chemical groups, and hundreds of individual input records within the MELCOR model for Peach Bottom. Similar to NUREG/CR-7155, five distributions were developed to span the range of cesium speciation represented by Figure 2-8. The beta distribution in Figure 2-8 was divided into seven uniform intervals. The conditional probability

of each distribution (i.e., C.Prob. in Figure 2-9) is evaluated by the integral probability of the Beta distribution within each of the sampled intervals. However, only five radionuclide input data sets were developed due to the low conditional probabilities of the first two intervals. Unlike the non-continuous distributions used in NUREG/CR-7155 (see Table 2-3), the new cesium speciation uncertainty parameter has a continuous distribution across uniformly sized intervals.

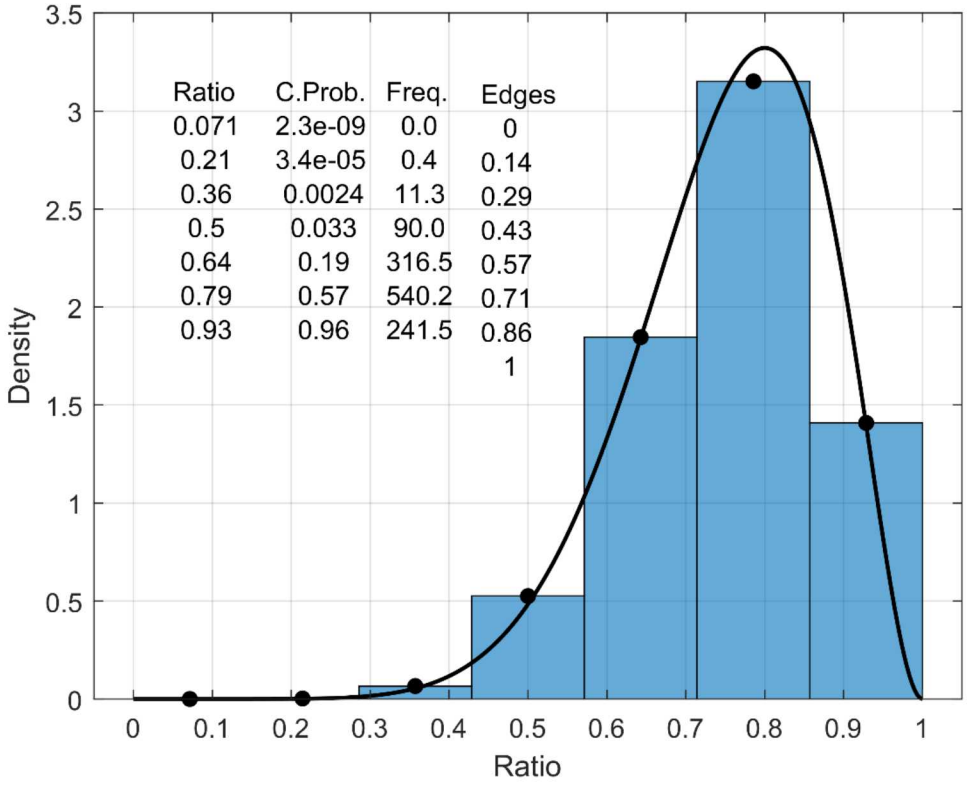

Figure 2-9. The discrete sampling of the Beta distribution used to represent the fraction of cesium as cesium molybdate

Iodine speciation

It is complicated to simultaneously sample the uncertainty in the iodine and cesium speciation. The complications of uncertain iodine sampling were not addressed, and a constant fraction of iodine gas and cesium iodide was used in all the distributions. A model-specific Python script was developed for the Surry UA to support coupled uncertain iodine and cesium speciation sampling that was not implemented for the Peach Bottom model at this time (see Appendix D in Reference [4]). The Surry UA also simultaneously incorporated the radionuclide inventory variations as a function of the time in the cycle. The combined cesium and iodine speciation approach used in the Surry SOARCA UA would be applicable to Peach Bottom. However, it would require additional Peach Bottom-specific results from ORIGEN radionuclide inventory calculation, which were not available.

The amount of gaseous iodine is uncertain and complicated. A constant iodine gaseous fraction of 0.25% was selected for the Peach Bottom model, which is the midpoint of Distribution 2 and 3 in the Peach Bottom UA [2] (see Table 2-3). NUREG/CR-7155 based the iodine uncertainty sampling on the Phebus FPT experiment with the FPT3 experiment having significantly higher release of

gaseous iodine. Only the FPT3 accident showed a high initial concentration of iodine. Analysis of the iodine behavior in the Phebus FPT3 test concluded,

> "Despite the high concentrations of gaseous iodine arriving in the containment, the overall behavior of this gaseous form did not significantly depart from that in previous Phebus FP tests and is characterized by a fast depletion due to adsorption on containment surfaces at short term and constant low residual concentrations in the long term." [22]

Consequently, the high gaseous iodine release is not representative of the airborne concentration at containment failure due to the short-term absorption on containment surfaces, which is not modeled in the Peach Bottom MELCOR model. The Surry UA sampling used Atomic Energy and Alternative Energies Commission (CEA) measurements from irradiated fuel rods, which had median gaseous iodine concentrations between 0.2% to 0.5% across the fuel cycle. Since the speciation of iodine remains uncertain, future updates to the Peach Bottom model should consider the simultaneous uncertainty sampling of iodine and cesium.

2.3.5. Aerosol Aerodynamic Multiplier

After the NUREG/CR-7155 study, the aerosol settling rate uncertainty was changed from varying the aerosol density to changing the aerodynamic shape factor. Sandia's aerosol subject matter expert indicated that water condensation on aerosols and fog droplets skew the overall aerosol density towards the default value of water. Instead of varying the density, it was recommended to use the aerodynamic shape factor to characterize the uncertainty in the aerosol settling, which was also done in the Surry and Sequoyah UAs [3][4]. The following discussion was adapted from the PWR approach [3] but judged to be equally applicable for the BWR aerosol behavior.

The dynamic shape factor is defined as "the ratio of the actual resistance force of the non-spherical particle to the resistance force of a sphere having the same volume and velocity" [26]. This unitless dynamic shape factor is used to account for the stringing out of aerosol agglomerates in a linear or complex manner as opposed to growing as a perfect sphere.

A value of 1 is a perfect sphere and it is the lower limit for the dynamic shape factor. This value is also the default value in MELCOR and was used in NUREG/CR-7155. The upper limit requires more consideration. The aerosol model in MELCOR is used to determine the mass concentration evolution of aerosols in a spatially homogenous volume, as well as deposition on surfaces and injection/removal from volumes. One of the critical assumptions of this model is that non-spherical particle effects are adequately parameterized with the dynamic shape factor, the collision shape factor, and the effective material density. The importance of these parameters is demonstrated in several uncertainty analyses of the MAEROS aerosol model performed in support of the development of the MELCOR program [23][24]. To determine the uncertainty of this model, the uncertainty of the dynamic shape factor is addressed.

As shown in Figure 2-10, Kasper et al. (Tables 9 and 10 [25]) experimentally measured values for the dynamic shape factor for linear chains with their long axis either parallel or perpendicular to the settling direction. As seen in Figure 2-10, the shape factor is reasonably linear with respect to the number of spheres. This data supports an upper bound of 2.8, with a weighting toward values less than 2.0. Compiled data from Hinds (pg. 48 [26]) also supports a range of 1.0 to 2.04. However, Brockmann, et al. [27] compiled data and models that yield a range of 1 to 10 for the dynamic shape factor. The same report includes a correlation for loosely-packed spheres which calculates dynamic shape factors will be in the range of 1 to 5 for void volumes ranging from 26 to 99%. Based on

these sources, a range of 1 to 5 is judged reasonable. The dynamic shape factor is sampled directly, and the uncertainty of it is represented with a scaled beta distribution with the parameters of $\alpha=1$ and $\beta=5$ and bounds of 1 and 5.

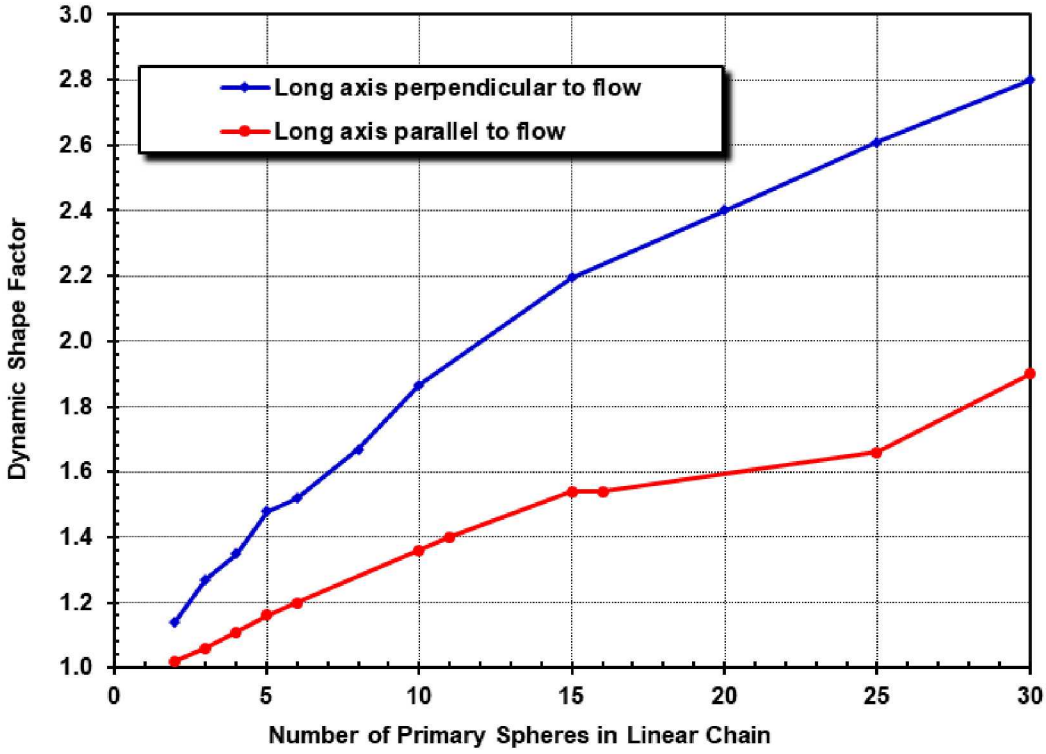

Figure 2-10. Dynamic shape factor compared to number of spheres within a chain

Although the bounds of the distribution were informed by the experiments described, these works cannot inform the shape of the distribution since they do not contain information on the normal shape of aerosols during a severe accident. Kissane compiled information on aerosols from a number of nuclear accident experiments, including the Phebus fission product tests (FPT) [28]. The report concluded, "Concerning particle shape, relatively compact particles without branching chain-like structures appear to be typical in the RCS;" (reactor coolant system) although a visual inspection of post-test deposition images did show slight evidence of aerosol chains. Since a compact, spherical particle has a shape factor of 1, the distribution is weighted more heavily toward the lower end of the range (i.e., 1.0). Additionally, most references support weighting more heavily in the 1 to 2 range. Because of this weighting, a beta distribution is used, with the parameters of $\alpha=1$ and $\beta=5$, and the core damage frequency (CDF) of the distribution is shown in Figure 2-10. The α parameter yields a function that has a peak as close as possible to the lower bound of 1, while the β parameter gives the desired shape to the probability distribution function (PDF) and yields about 75% of samples between 1 and 2 while still allowing some samples at physically possible values up to 5.

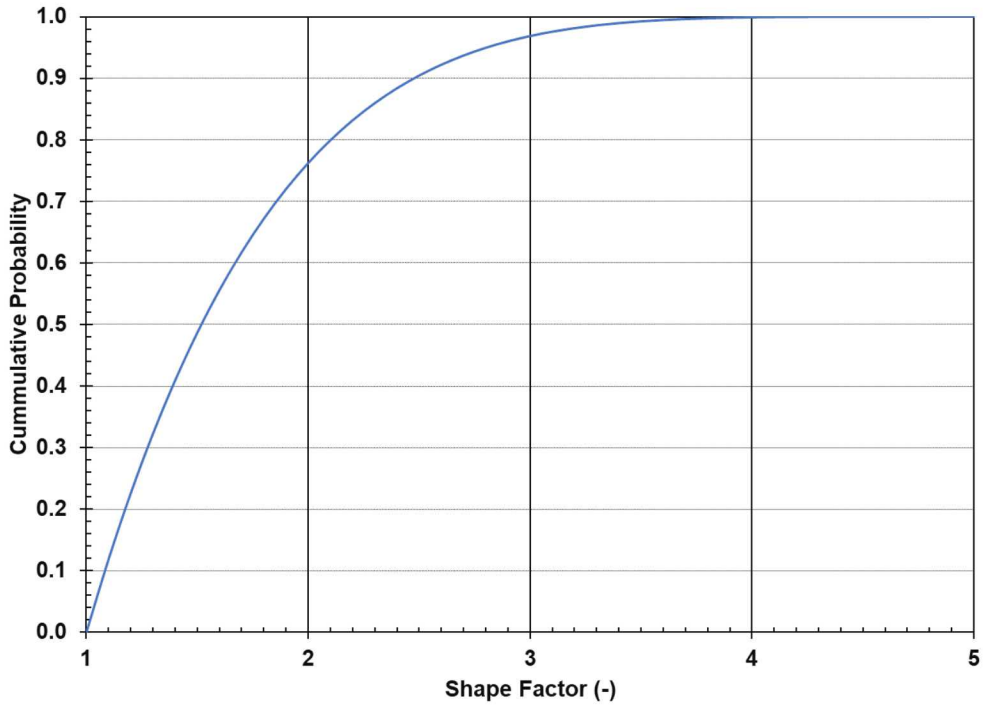

Figure 2-11. CDF of the dynamic shape factor

This page left blank

3. SELECTION OF THE REFERENCE CASES

Three reference calculations from the NUREG/CR-7155 study were selected for comparison with the updated Peach Bottom model. Section 3.1 identifies the three reference realizations from NUREG/CR-7155. Section 3.2 describes the updated uncertainty settings used in the updated model for parameters not used in the NUREG/CR-7155 study.

3.1. Identification of Reference Cases from NUREG/CR-7155

As a first step in qualifying the new MELCOR 2.2 Peach Bottom model for future applications, a small number of reference calculations from the historical NUREG/CR-7155 are compared to new calculations with MELCOR 2.2 and the updated Peach Bottom model. Some differences are expected between the two code versions for the following reasons:

- The MELCOR 2.2 code includes substantial updates since the application of MELCOR 1.8.6 in NUREG/CR-7155. To give some perspective, the NUREG/CR-7155 calculations were performed using MELCOR 1.8.6, Revision 3704, which was built in 2011. The current calculations use MELCOR 2.2, Revision 15596 using a code built in January 2020. The MELCOR code developers use subversion code maintenance software that tracks each change or revision to code. Consequently, there were many code revisions (and changes) since the MELCOR 1.8.6 code version used in NUREG/CR-7155.[9] The MELCOR code development group provides the code updates, model corrections, and new models in quick look reports and status update presentations for international code releases (e.g., [29][30][31][32]).[10]
- The Peach Bottom input includes model updates and corrections as identified in Sections 2.1 and 2.2.
- Some of the formulations of the parameter uncertainty parameters and their impact on the accident progression have changed as identified in Section 2.3. This is a continuous process as understanding of severe accident modeling and phenomena changes and improves with time.
- Finally, the severe accident models have inherent variabilities due to complex numerical and physical interactions. Consequently, some variations are expected as subtle interactions accumulate and change model responses (e.g., generating just enough debris to fail a core plate structure and the associated fuel assemblies prior to a sampled SRV thermal failure or not).[11]

The results and corresponding uncertainty analysis and regressions revealed three important outcomes of the Peach Bottom calculations, (1) a stochastic failure of an SRV prior to significant core degradation (~1/2 of the realizations), (2) a thermal failure of an SRV after the start of core degradation without a failure of the main steam line (MSL) (~1/3 of the realizations), and (3) a thermal failure of an SRV and a thermal failure of the MSL after the significant core degradation (~1/6 of the realizations). Consequently, NUREG/CR-7155 includes a significant number of

---

[9] The Sandia MELCOR subversion system also includes the large plant input models, which are part of the same numbering system as the code revisions. Approximately five years ago, thousands of uncertainty sampling files and outputs were inadvertently added to the system. The Peach Bottom SOARCA UA calculations were performed in 2012 using MELCOR 1.8.6 Revision 3704, which was built in 2011 before the large jump in revision numbers.

[10] Appendix C of NUREG/CR-7155 includes a comparison of SOARCA calculations [18] using MELCOR 1.8.6 Version 540 and MELCOR 1.8.6 Version 3704 used in NUREG/CR-7155 before any model changes. These two provide an example of variabilities of responses using identical input.

[11] A strong motivation for a SOARCA uncertainty analysis is to perform a significant number of calculations to explore the range of possible outcomes through variation of model inputs of uncertain phenomena.

individual realization analysis results from each of these three accident categories. All realizations fell into one of these three categories (e.g., no realizations without an SRV failure).

Figure 3-1 illustrates the overall impact of the three accident categories on the total cesium release to the environment. If an SRV fails stochastically early prior to significant core damage, a significant portion of the volatile radionuclide releases are vented into the torus and captured in the water. The blowdown of the SRV leads to an accelerated core uncovery but a slower, low-pressure core damage progression. The vented, low-pressure vessel condition retained a smaller quantity of radionuclides in the vessel. The important impact of the low-pressure vented state prior to core damage was less volatile radionuclide material for revaporization after the containment failure. The lower fraction of vulnerable radionuclides retained in the vessel had the combined benefits of less radioactive heating in the vessel, a slower heatup of the vessel internals, and a smaller mass of available radionuclides during the revaporization release. The blue lines of the stochastic SRV failure generally had the lowest cesium releases of the three accident progression (see Figure 3-1).

The realizations with a thermally failed SRV and no MSL failure are shown with the black lines in Figure 3-1. In contrast to the realizations with an earlier stochastic SRV failure, the volatile radionuclide release started at high pressure prior to the SRV failure. As the hot gases vented through the cycling SRV, it was predicted to heat and fail in a partially open position (i.e., the failure open area was an uncertain parameter). A much higher quantity of released radionuclides condensed and deposited on the internal structures. The high-pressure conditions resulted in more in-vessel hydrogen production (i.e., high steam density for oxidation at high pressure) and rapid in-vessel radionuclide releases. The important impacts from the high-pressure core damage phase were more volatile radionuclide material circulating and retained in-vessel that were available for a subsequent revaporization after the containment failure. The higher initial in-vessel retention of radionuclides had the combined effects of more radioactive heating in the vessel, a faster heatup of the vessel internals, and a larger amount of volatile material released during the revaporization phase. The black lines of the thermal SRV failure generally had the second highest cesium releases of the three accident progressions (see Figure 3-1).

Finally, approximately $1/6^{th}$ of the realization had a thermally-failed SRV and a subsequent MSL creep rupture failure. The realizations with a smaller sampled leakage area from the thermally-failed SRV maintained a higher vessel pressure, which had the similar adverse consequences cited for a thermally-failed SRV without an MSL failure. The smaller SRV leakage area promoted high thermal and mechanical stresses on the MSL, which resulted in its failure. The failure of the MSL had two adverse impacts, (1) an immediate release of airborne volatile radionuclides to the drywell and (2) an efficient natural circulation pathway for radionuclides after vessel failure (i.e., up the vessel failure location, through the vessel, and out the failed MSL). The realizations with an MSL failure generally had the highest cesium releases as shown in the green lines on Figure 3-1.

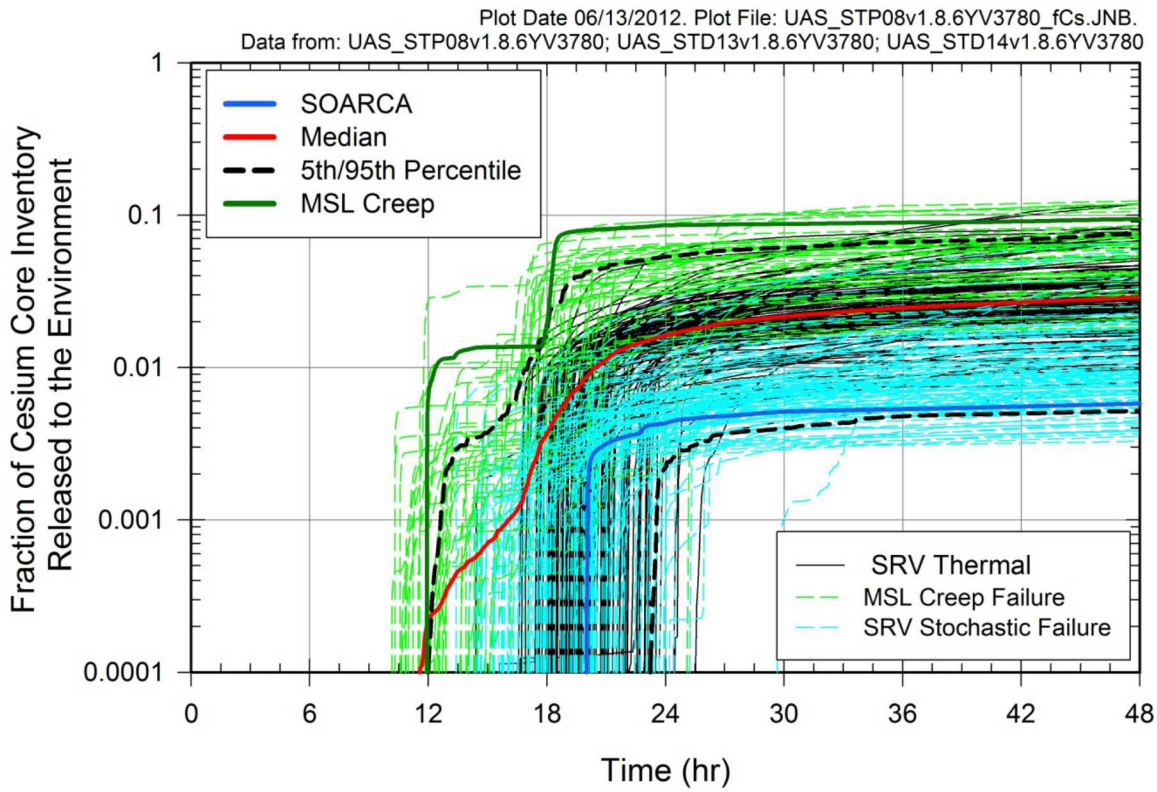

Figure 3-1. Distribution for the fraction of cesium core inventory released to the environment for Replicate 1 of the source term uncertainty analysis of the SOARCA Peach Bottom unmitigated LTSBO scenario

As part of the analysis and identification of the important phenomena in NUREG/CR-7155, individual realizations from each accident progression category identified in Figure 3-1 were selected from the three categories of calculations. Figure 3-2 separates the cesium environmental releases results into the three accident progression categories and identifies the individual realizations analyzed in NUREG/CR-7155. A typical realization from each grouping was identified for comparison with the new MELCOR 2.2 model (i.e., a realization with median tendencies and not an extreme response). Of the 865 successful realizations, the individual realizations presented in Figure 3-1 and analyzed in NUREG/CR-7155, these were the most logical candidates for reference cases (i.e., their availability in the NUREG/CR-7155 documentation).

Realization 51 from Figure 3-2 (a) was selected as the reference calculation for an SRV with a stochastic SRV failure prior to significant core damage. Although Realization 51 had the lowest release, the other three realizations were above or close to the 95th percentile for cesium release to the environment and judged not typical of lower median and mean responses.

Realization 18 was selected as the reference realization for an SRV with a thermal failure and no MSL failure. The cesium release to the environment for Realization 18 was near the median response of the realizations from this category.

Finally, Realization 86 was selected as the reference realization for an SRV with a thermal failure and an MSL failure. The cesium release to the environment for Realization 86 was slightly below the median response of the realizations from this category. Realization 62 was also considered but it had

the complication of the one highest iodine releases to the environment and no cesium hydroxide. Consequently, Realization 86 was judged a better choice.

Table 3-1 summarizes the uncertain variables used in the NUREG/CR-7155 study with a comparison to the best-estimate values in the original SOARCA study [18]. As described in NUREG/CR-7155, the uncertain variables were randomly selected using a Monte Carlo approach. As expected, the randomly selected variables in the three reference realizations deviated from the best-estimate values used in the original SOARCA study. Table 3-3 through Table 3-5 ranks the most important uncertain parameters impacting the cesium release to the environment, the iodine release to the environment, and the in-vessel hydrogen generation, respectively.

The key results from the four calculations are summarized in Table 3-2. The timing of events varies due to the impact of the various SRV and MSL failures and the contributing effects from the uncertainty variable settings. However, the cesium releases to the environment show the incremental magnitudes noted in Figure 3-1.

As a consequence of other more complicated factors imbedded in the various uncertain parameters, the in-vessel hydrogen production and iodine release show independent variability from the cesium releases. The complicated interactions are identified in the NUREG/CR-7155 uncertainty regressions as important uncertain parameters that effect cesium release to the environment, iodine release to the environment, and in-vessel hydrogen production. Although the three are somewhat correlated, the uncertainty analysis illustrated how other parameter settings lead to independent variations.

For example, Table 3-3 and Table 3-4 show the NUREG/CR-7155 regression analysis of cesium and iodine releases to the environment at 48 hr. Although both figures of merit show the SRV stochastic failure cycle (SRVLAM) as the most important uncertain parameter, the other identified parameters varied in the two tables. The secondary parameters illustrate their impact the physics of the respective radionuclide release, transport, deposition, and revaporization for cesium and iodine release to the environment, respectively. Similarly, the in-vessel hydrogen production shown in Table 3-5 shows the SRV stochastic failure cycle (SRVLAM). However, the remaining parameters also showed differences from the cesium and iodine results. The uncertainty analyses allowed identification of the important primary and secondary parameters affecting the magnitude of key figures of merit.

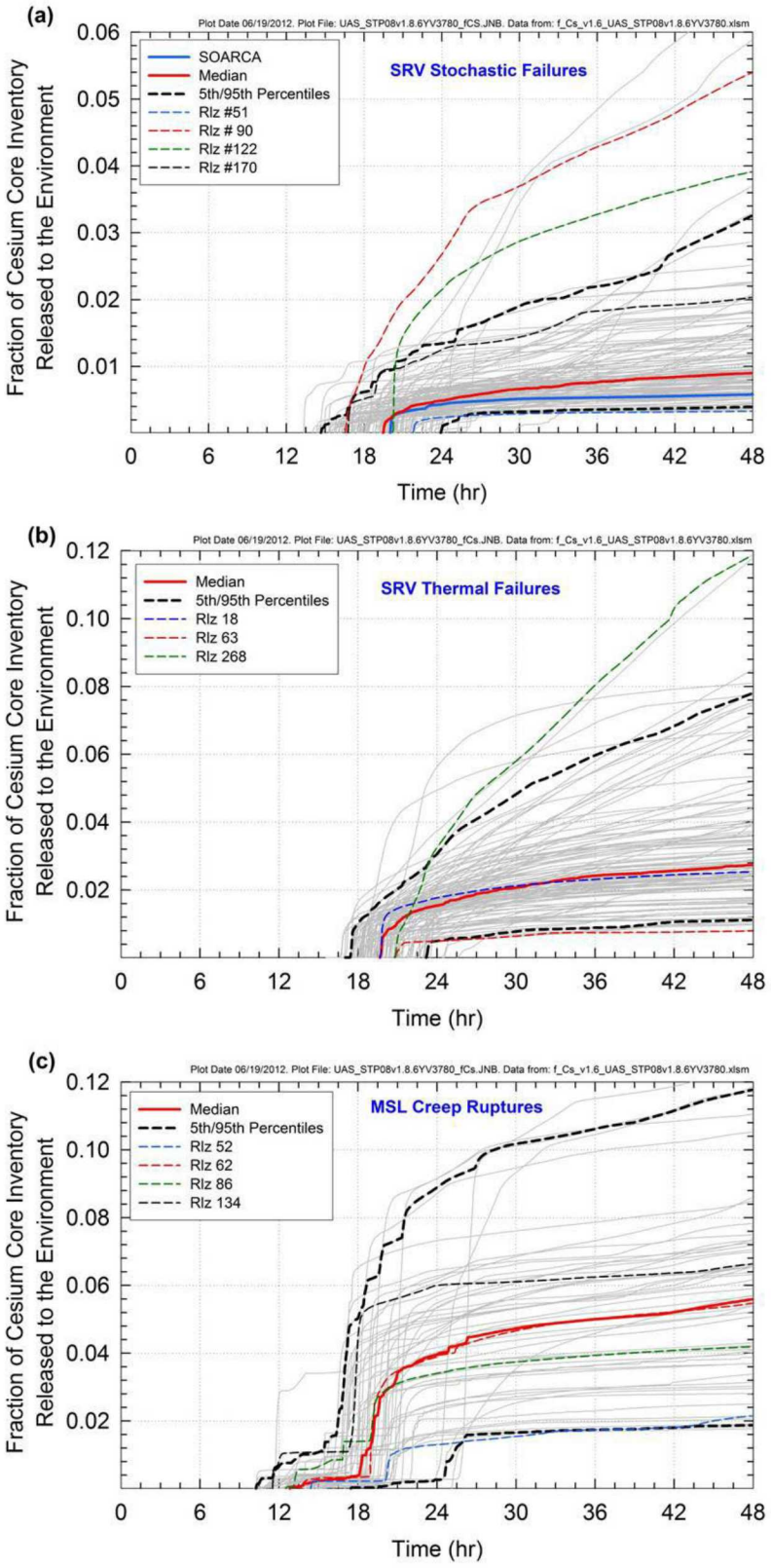

Figure 3-2. Cesium release of individualization realizations from NUREG/CR-7155

Table 3-1. Sampled parameter values for the selected reference realizations

Parameter	SOARCA BE	18 SRV_th	51 SRV_stoc	86 MSL_fail
SRV failure to reclose (SRVLAM), per demand	3.70E-03	7.90E-05	4.45E-03	9.90E-04
Battery duration (BATTDUR), hr	4.00E+00	4.14E+00	5.11E+00	3.72E+00
Zircaloy melt breakout temperature (SC1131(2)), K	2.40E+03	2.26E+03	2.37E+03	2.16E+03
Molten clad drainage rate (SC1141(2)), kg/m-s	2.00E-01	4.56E-01	2.79E-01	3.92E-01
SRV thermal failure criterion (SRVFAILT), K	9.00E+02	8.38E+02	9.50E+02	8.63E+02
SRV open fraction (SRVOAFRAC), unitless	1.00E+00	6.87E-01	5.46E-01	2.46E-01
MSL creep rupture area (SLCRFRAC), unitless	0.00E+00	0.00E+00	0.00E+00	4.00E-01
Fuel failure criterion (FFC), unitless	0.00E+00	1.00E+00	1.00E+00	1.00E+00
Solid debris radial relocation (RDSTC), s	3.60E+02	3.10E+02	4.72E+02	2.83E+02
Molten debris radial relocation (RDMTC), s	6.00E+01	5.31E+01	8.12E+01	4.77E+01
Debris height for solid core-concrete (DHEADSOL), m	5.00E-01	5.56E-01	6.06E-01	6.41E-01
Debris height for molten core-concrete debris (DHEADLIQ), m	1.52E-01	1.47E-01	1.57E-01	1.66E-01
DW liner melt-thru area (FL904A), m2	1.00E-01	1.49E-01	1.38E-01	1.42E-01
H2 ignition criterion (H2IGNC), mole fraction	1.00E-01	1.41E-01	1.08E-01	5.25E-02
Inner RR door open fraction (RRIDFRAC), unitless	5.00E-01	6.90E-01	1.69E-01	2.32E-01
Outer RR door open fraction (RRODFRAC), unitless	5.00E-01	1.28E-01	1.32E-01	6.74E-01
Chemical form of I and Cs (CHEMFORM), unitless	5.00E+00	3.00E+00	3.00E+00	4.00E+00
Aerosol particle density (RHONOM), kg/m3	1.00E+03	4.01E+03	1.20E+03	1.74E+03
DW head bolt torque coeff. (KBOLT), unitless	8.00E-02	2.03E-01	3.52E-01	2.42E-01
DW head bolt modulus of elasticity (EBOLT), psi	1.93E+11	2.01E+11	1.86E+11	1.93E+11
DW head gasket rebound thickness (DGASKET), inch	7.62E-04	6.80E-04	7.02E-04	7.87E-04

Notes:

BE = Best-estimate as determined for the original SOARCA study
SRV_th = Thermal failure of an SRV during core degradation without an MSL failure
SRV_stoc = Stochastic failure of an SRV prior to core degradation
MSL_fail = Thermal failure of an SRV during core degradation with an MSL failure

Table 3-2. Timing of events, key occurrences/attributes, and environmental releases for selected reference realizations

Event Timing (hr)	SOARCA BE	18 SRV_th	51 SRV_stoc	86 MSL_fail
100 °F/hr cooldown initiated (SRV opened, RCIC throttled)	1.00	1.00	1.00	1.00
SRV closes on battery depletion	4.00	4.10	5.10	3.70
RCIC turbine floods failing RCIC	5.19	5.34	6.36	4.91
SRV fails to close due to excessive cycling	8.19	N/A	9.07	N/A
Downcomer level drops to top of active fuel (TAF)	8.40	9.23	9.46	8.68
First fuel-cladding gap release	9.12	10.32	10.35	9.75
SRV fails to close due the excessive temperature	N/A	11.51	N/A	10.95
MSL creep rupture	N/A	N/A	N/A	12.48
First large-scale relocation of core debris to lower plenum	10.69	13.50	11.92	13.01
RPV LHF	19.76	19.49	21.54	18.84
Drywell head flange leakage begins	19.87	14.87	13.61	12.48
Reactor building blowout panels open	19.92	16.20	21.60	12.48
Wetwell rupture (above waterline)	N/A	N/A	N/A	N/A
Drywell liner melt-through	20.00	19.72	21.78	19.07
A large reactor building H_2 burn fails the roof	20.01	19.74	21.68	13.16
Key Occurrences / Events	**SOARCA BE**	**18 SRV_th**	**51 SRV_stoc**	**86 MSL_fail**
Stochastic SRV failure (hr)	8.19	-	9.07	-
Thermal SRV failure (hr)	-	11.51	-	10.95
MSL failure (hr)	-	-	-	12.48
Elapsed time between SRV sticking open and onset of core damage (hr)	0.94	-1.18	1.28	-1.20
Elapsed time between onset of core damage and MSL creep rupture (hr)	N/A	N/A	N/A	2.73
In-vessel H_2 production (kg)	1,083	1,307	1,203	1,257
Surge of water from wetwell up onto drywell floor at liner melt-thru (Yes/No)	N	N	N	N
Railroad Doors blow open (Yes/No)	Y	Y	N	Y
Releases to the Environment	**SOARCA BE**	**18 SRV_th**	**51 SRV_stoc**	**86 MSL_fail**
I release to environment > 0.1% (hr)	20.1	19.8	21.9	15.8
Cs release to environment by 48 hr (fraction)	0.005	0.025	0.003	0.042
I release to environment by 48 hr (fraction)	0.025	0.070	0.015	0.023

Notes:

BE = Best-estimate as determined for the original SOARCA study
SRV_th = Thermal failure of an SRV during core degradation without an MSL failure
SRV_stoc = Stochastic failure of an SRV prior to core degradation
MSL_fail = Thermal failure of an SRV during core degradation with an MSL failure

Table 3-3. Regression analysis of fraction of cesium released to the environment after 48 Hours

	Rank Regression			Quadratic			Recursive Partitioning			MARS		
Final R^2	**0.61**			**0.64**			**0.90**			**0.66**		
Input name	**R^2 inc.**	**R^2 cont.**	**SRRC**	**S_i**	**T_i**	**p-val**	**S_i**	**T_i**	**p-val**	**S_i**	**T_i**	**p-val**
SRVLAM	0.50	0.50	-0.72	0.39	0.64	0.00	0.43	0.70	0.00	0.57	0.68	0.00
FL904A	0.53	0.03	0.19	0.01	0.04	0.12	0.06	0.02	0.44	0.00	0.03	0.10
FFC	0.55	0.02	0.19	0.04	0.05	0.31	0.02	0.10	0.00	0.01	0.08	0.00
RRDOOR	0.58	0.03	0.33	0.02	0.10	0.00	0.02	0.03	0.19	---	---	---
SRVOAFRAC	0.59	0.02	-0.13	0.07	0.19	0.00	0.11	0.33	0.00	0.12	0.27	0.00
CHEMFORM	0.60	0.01	0.09	0.00	0.08	0.38	0.01	0.18	0.00	0.02	0.00	0.87
SC1131_2	0.60	0.01	-0.07	0.02	0.01	0.63	0.00	0.07	0.00	0.00	0.04	0.01
RRIDFRAC	0.61	0.00	0.06	0.05	0.00	1.00	0.00	0.01	0.57	0.01	0.03	0.07
BATTDUR	0.61	0.00	0.04	0.03	0.02	0.49	0.00	0.02	0.47	0.00	0.01	0.53

Table 3-4. Regression analysis of fraction of iodine to the environment released after 48 Hours

	Rank Regression			Quadratic			Recursive Partitioning			MARS		
Final R^2	0.69			0.76			0.93			0.80		
Input name	**R^2 inc.**	**R^2 cont.**	**SRRC**	**S_i**	**T_i**	**p-val**	**S_i**	**T_i**	**p-val**	**S_i**	**T_i**	**p-val**
SRVLAM	0.49	0.49	-0.72	0.46	0.68	0.00	0.55	0.78	0.00	0.64	0.70	0.00
CHEMFORM	0.58	0.09	0.30	0.10	0.16	0.00	0.07	0.22	0.00	0.09	0.12	0.00
FL904A	0.64	0.06	0.26	0.05	0.06	0.22	0.02	0.12	0.00	0.05	0.08	0.00
RRDOOR	0.67	0.03	0.28	0.01	0.06	0.03	0.04	0.07	0.00	---	---	---
SRVOAFRAC	0.69	0.02	-0.12	0.06	0.13	0.00	0.05	0.20	0.00	0.06	0.16	0.00
FFC	0.69	0.00	0.06	0.03	0.03	0.17	---	---	---	0.02	0.00	1.00
RRIDFRAC	0.69	0.00	0.03	---	---	---	---	---	---	0.00	0.02	0.09
KBOLT	0.69	0.00	-0.04	0.04	0.00	1.00	0.00	0.00	1.00	---	---	---

Table 3-5. Regression analysis of in-vessel hydrogen production after 48 Hours

	Rank Regression			Quadratic			Recursive Partitioning			MARS		
Final R^2	0.55			0.63			0.88			0.65		
Input name	**R^2 inc.**	**R^2 cont.**	**SRRC**	**S_i**	**T_i**	**p-val**	**S_i**	**T_i**	**p-val**	**S_i**	**T_i**	**p-val**
SRVLAM	0.39	0.39	-0.64	0.48	0.65	0.00	0.50	0.70	0.00	0.66	0.75	0.00
SC1131_2	0.53	0.14	0.37	0.19	0.29	0.00	0.17	0.33	0.00	0.25	0.26	0.00
SC1141_2	0.54	0.01	-0.11	0.03	0.08	0.01	0.03	0.14	0.00	0.05	0.05	0.03
RDSTC	0.54	0.01	0.07	0.02	0.00	0.73	0.02	0.04	0.10	0.00	0.02	0.18
CHEMFORM	0.55	0.00	0.04	0.01	0.09	0.00	---	---	---	0.03	0.01	0.19
BATTDUR	0.55	0.00	0.06	0.00	0.00	1.00	---	---	---	0.00	0.02	0.04
SRVFAILT	0.55	0.00	0.05	0.03	0.07	0.01	0.02	0.00	1.00	0.00	0.00	1.00
DGASKET	0.55	0.00	0.04	---	---	---	0.04	0.00	1.00	---	---	---
EBOLT	0.55	0.00	0.03	0.01	0.00	1.00	0.01	0.00	1.00	---	---	---
RRIDFRAC	0.55	0.00	0.03	---	---	---	0.00	0.04	0.04	0.01	0.00	1.00

3.2. Model Setting for Updated Uncertainty Parameters

As described in Section 2.3, several of the uncertainty parameters were updated for the MELCOR 2.2 model. Consequently, the new MELCOR 2.2 reference calculations require specifications for these new and updated uncertainty parameters. Table 3-6 summarizes the updated setting used in the reference calculations. If not explicitly cited in Table 3-6, then the same parameter setting shown in Table 3-1 was used. The rationale for each setting is provided in the following sub-sections.

Table 3-6. Uncertainty settings for the updated MELCOR 2.2 Peach Bottom uncertainty parameters

Parameter	18 SRV_th	51 SRV_stoc	86 MSL_fail
SRV failure to reclose (SRVLAM), per demand	7.90E-05	4.45E-03	9.90E-04
SRV failure to reclose cycle number [Note A]	12,658	224	1,010
SRV stochastic failure area, unitless	1.0	1.0	1.0
Fuel failure criterion (FFC), unitless	-	-	-
Effective eutectic melting temperature, K	2479	2479	2479
SC-1132(1) – fuel collapse temperature, K	2479	2479	2479
Lower plenum falling debris size, (m)	0.0032	0.0032	0.0032
Lower plenum falling debris velocity, (m/s)	1.215	1.215	1.215
Chemical form of Cs, unitless [Note B]	New Dist. 5	New Dist. 5	New Dist. 3
Aerosol aerodynamic shape factor, unitless	1.5	1.5	1.5

Note:

A. SOARCA and NUREG/CR-7155 used a per demand failure probability, λ_{SRV} (i.e., SRVLAM). The median failure cycle is calculated as $1/\lambda$, which was used in the subsequent PWR UA work. Although the Peach Bottom model was updated to simulate five SRVs individually, only the lowest opening pressure SRV cycled in these realizations. In Realizations 18 and 86, the SRV cycled until thermal failure. In Realization 51, the SRV stuck fully-open on the 224th cycle, which immediately depressurized the vessel (i.e., no cycles on the next lowest pressure SRV).

B. New Distribution 5 had 93% of the available cesium after the formation of cesium iodide as cesium molybdate versus cesium hydroxide (see Section 2.3.4).

3.2.1. SRV Stochastic FTC Area and Per Demand Failure Probability

Previously, the SRV stochastic FTC area was set to fully open and not sampled as an uncertain parameter. NUREG/CR-7155 specified the SRV would remain fully open upon failing. Using the updated MELCOR 2.2 model flexibility with five SRVs and the new insights on likely valve failure positions, multiple valves could fail in multiple positions. However, the reference calculations will use the same assumptions (i.e., fail fully open) to ensure a similar response when there is a stochastic valve failure (see SRV stochastic failure pressure response in Section 4.1).

The Peach Bottom MELCOR model for the SOARCA study and NUREG/CR-7155 used a per demand failure probability, λ_{SRV} (i.e., SRVLAM) in the SRV control logic. The median failure cycle is calculated as $1/\lambda_{SRV}$, which was used in the subsequent PWR UA work. The MELCOR 2.2 reference calculations use the failure cycle ($1/\lambda_{SRV}$) rather than the per demand failure rate, λ_{SRV} (see Table 3-6). The failure cycle number for the MELCOR 2.2 model gives the same cycle count to an FTC as the per demand failure rate in the NUREG/CR-7155 MELCOR 1.8.6 model. The SRVLAM distribution and corresponding FTC cycle is shown in Figure 3-3.

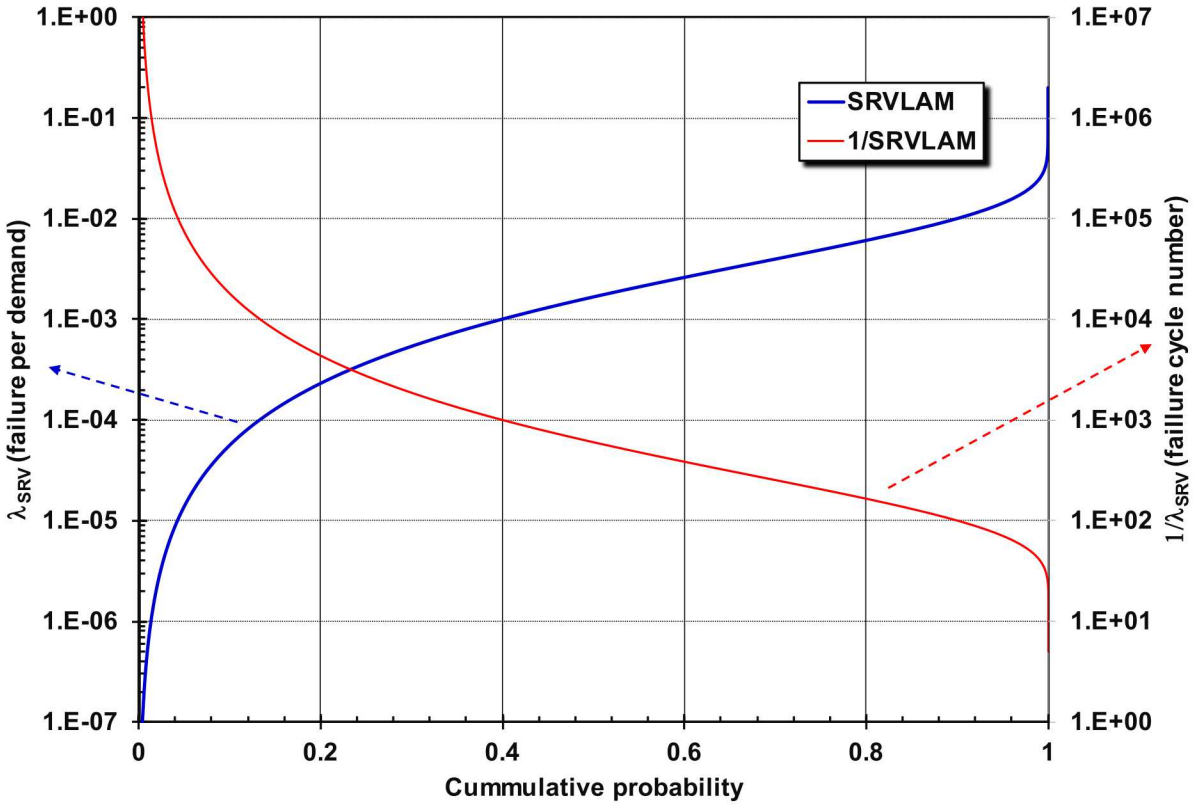

Figure 3-3. SRVLAM and FTC cycle distribution for the SRVs

3.2.2. Effective Eutectic Melting Temperature

NUREG/CR-7155 varied the time-to-temperature criteria to vary uncertainty in the fuel collapse. The MELCOR 2.2 reference cases will use the median value (2479 K) from the uncertainty distribution (see Section 2.3.2). The fuel collapse temperature criterion is set to the same

temperature using SC-1132(1) = 2479 K (i.e., exactly correlated). The fuel in each core cell collapses when the local temperature reaches the effective melting temperature, which is the same approach as the PWR UAs [3][4].[12]

3.2.3. Falling Particulate Debris Size and Velocity

The falling debris particulate hydraulic diameter is set to the median value of (i.e., 0.0055 m) the falling debris size uncertainty distribution (see Section 2.2.5). The corresponding falling velocity is 0.94 m/s as described in Section 3.2.3. The particulate velocity is correlated to the particulate diameter and not an independent uncertain parameter. It is prescribed as a second input based on the sampled value of the falling debris hydraulic diameter (see Figure 2-6).

3.2.4. Cesium Chemical Form

NUREG/CR-7155 defined five independent distributions of cesium and iodine. Realizations 18 and 51 selected Distribution 3, which had 100% cesium molybdate and 0% cesium hydroxide. New Distribution 5 with 93% cesium molybdate was selected as the closest distribution to the 100% NUREG/CR-7155 cesium molybdate specification (see Section 2.3.4).

Realization 86 in NUREG/CR-7155 used Distribution 4 with 50% distribution of cesium molybdate. New Distribution 3 with 50% cesium molybdate was selected as the closest distribution to the NUREG/CR-7155 50% cesium molybdate specification (see Section 2.3.4).

3.2.5. Aerosol Aerodynamic Shape Factor

NUREG/CR-7155 sampled the aerosol density whereas the new Peach Bottom model and the subsequent Surry and Sequoyah uncertainty analyses sampled the aerosol aerodynamic shape factor. The median of the uncertainty distribution (i.e., 1.5) is used for all realizations.

[12] Each core intact fuel cell monitors various collapse criteria including SC-1132(1). The fuel in the core cell collapses from its intact geometry when temperature reaches the temperature specified in SC-1132(1). If a middle section of a fuel rod fails first, then the portion of the fuel rods above the failure location also fails (i.e., supported from below as a column).

This page left blank

4. REFERENCE CASES

This section describes the comparisons of the new MELCOR 2.2 results with the NUREG/CR-7155 MELCOR 1.8.6 results. As described in Section 3, NUREG/CR-7155 had three basic outcomes that had first-order impacts on the key figures of merit for environmental radionuclide releases. Sections 4.1 through 4.3 describe the comparisons of the reference calculations with a stochastically-failed SRV, a thermally-failed SRV, and a thermally-failed SRV with a thermally-failed MSL, respectively.

Each section presents four calculations:

1. the original MELCOR 1.8.6 result from NUREG/CR-7155 (i.e., labeled Version 1.8.6),
2. MELCOR 2.2 with recirculation pump (RP) seal leakage and all the modifications noted in Section 2 except the new ex-vessel debris melt spreading and water ingression models (i.e., labeled Version 2.2),
3. MELCOR 2.2 without RP seal leakage and all the modifications noted in Section 2 except the new ex-vessel debris melt spreading and water ingression (i.e., labeled Version 2.2 No RP leak), and
4. MELCOR 2.2 with RP seal leakage and all modifications noted in Section 2 including the new ex-vessel debris melt spreading and water ingression models (i.e., labeled Version 2.2 Meltspread + Ingress)

Table 4-1 summarizes some of the important modeling differences between the four calculations that contributed to the variations noted in Sections 4.1 through 4.3. These modeling attributes were the most significant parameters explaining the differences in the four calculations.

Table 4-1. Comparison of results modeling differences highlighted in calculation differences

Modeling Attribute	NUREG/CR-7155	MELCOR 2.2 No RP leak	MELCOR 2.2 w/RP leak	MELCOR 2.2 w/Meltspread
Code version	MELCOR 1.8.6	MELCOR 2.2		
SRV operator action	Open 1 SRV at 1 hr	Open 1 SRV at 1 hr but close control between 200 to 400 psia		
Lower plenum debris modeling	Small debris size and slow falling rate.	Correlated debris size, falling rate, and heat transfer rate.		
Wetwell-drywell vacuum breakers	ΔP_{open} based on gas only	ΔP_{open} based on gas and liquid forces on the vent.		
Temperature criteria for debris spill to adjacent cavity	Between concrete solidus to liquidus temperature	Variable rate based on steel solidus to the effective fuel eutectic melting temperature (see Section 2.1)		
RP seal leakage	No		18/gpm-RP	
Ex-vessel debris spreading model	Variable rate based on concrete solidus to liquidus temperature range (see NUREG/CR-7155)	Variable rate based on steel solidus to the effective fuel eutectic melting temperature (see Section 2.1)		MELCOR 2.2 melt spread model

Modeling Attribute	NUREG/CR-7155	MELCOR 2.2 No RP leak	MELCOR 2.2 w/RP leak	MELCOR 2.2 w/Meltspread
Ex-vessel debris water-interaction model	Specified heat transfer multipliers			MELCOR 2.2 water ingression model

4.1. Reference Realization 51 with a Stochastically-failed SRV

This section documents the comparison of the updated MELCOR 2.2 model with Realization 51 from NUREG/CR-7155 with a stochastically failed SRV on the 224th valve cycle, which defined the accident progression (see Section 3.1). All calculations predicted a stochastically-failed SRV using the uncertain parameters in Table 3-1 with the MELCOR 2.2 updates noted in Table 3-6. A comparison of the key timings, calculated quantities, and events between the NUREG/CR-7155 result and the updated MELCOR 2.2 calculations are presented in Table 4-2.

Figure 4-1 through Figure 4-9 show comparisons of key accident progression and source term quantities for the NUREG/CR-7155 result (labeled Version 1.8.6), the updated base case using MELCOR 2.2 (labeled Version 2.2), the updated base case without RP seal leakage (labeled Version 2.2 No seal leak), and a MELCOR 2.2 sensitivity calculation using the new melt spreading (see Section 2.2.6) and water ingression models (see Section 2.2.7), which is labeled "Version 2.2 Meltspread + Ingress". Some of the key differences contributing to differences in the results are summarized in Table 4-1. The specific findings are summarized below.

Key observations –

- An operator action was included at 1 hr that opened an SRV to depressurize the RPV. All of the new MELCOR 2.2 calculations included operator actions to control the RPV pressure above 200 psia. Without these simulated actions, the RPV pressure dropped below the RCIC shutoff head, which terminated RCIC injection prematurely. The inclusion of the RP seal and the MSIV leakage in the new MELCOR 2.2 caused the higher RPV depressurization versus the original calculations without these leakages (see Table 4-1).
- The SRV closed at 5.1 hr following the loss of DC power control (see Figure 4-1). The subsequent RPV pressurization in the MELCOR 2.2 calculations started at a higher pressure than the original calculation because the drywell pressure was maintained between 200 psi to 400 psi. Consequently, the timing to the start of the SRV cycling was earlier than in the original calculation.
- The SRV cycled after the RPV pressurized until the hot gases exiting the core caused its failure between ~8.3 to 9.1 hr. The two calculations with RP seal leakage reached this condition approximately 0.8 hr before the original case (see Figure 4-1 and Table 4-2). The MELCOR 2.2 calculation without RP seal leakage had the earliest SRV failure, which was a function of the higher starting RPV pressure when the SRV closed at 5.1 hr (i.e., dictated by the operator actions to maintain the RPV pressure above 200 psia).
- The RPV and drywell pressure response is the same for the "Version 2.2" and "Version 2.2 with melt spreading and water ingression" until the RPV LHF (see Figure 4-1 and Figure 4-2). Both calculations include RP seal leakage (i.e., see buildup of the drywell water level in Figure 4-6).
- The accelerated timings in the new MELCOR 2.2 calculations persisted through LHF, which occurred 1.3 to 1.5 hr earlier (see Table 4-2).
- The calculation labeled MELCOR 2.2 without RP seal leakage and the original MELCOR 1.8.6 calculation did not include RP seal leakage. Consequently, there is significantly less water in the

drywell than in the calculations with RP seal leakage (see Figure 4-6), which impacts the ex-vessel debris behavior.

- The two MELCOR 2.2 calculations with RP seal leakage had lower in-vessel hydrogen production (i.e., ~1010 kg) than the original calculation (i.e., 1203 kg) and the MELCOR 2.2 calculation without RP seal leakage (i.e., 1213 kg). The RP seal leakage cases progressed to core damage more quickly, which led to a faster fuel collapse and a corresponding lower in-vessel hydrogen generation (i.e., oxidation slows significantly after the collapse of the fuel into a debris bed).
- The drywell pressure increased early in the MELCOR 2.2 calculations with RP seal leakage, which led to earlier and more sustained leakage drywell leakage prior to the RPV failure (see Figure 4-3).
- All the new MELCOR 2.2 calculations show a surge of water from the wetwell onto the drywell floor at drywell liner failure (see Figure 4-6). The water surge also carried some radionuclides previously captured in the wetwell. The consistent surge of water in the new calculations is attributed to the changes in the vacuum breaker modeling noted in Section 2.1. The vacuum breakers are less likely to open to relieve the pressure difference in the new calculations, which promotes backflow through the downcomer pipes.
- Following the RPV LHF and the debris ejection to the containment, the drywell responses varied in the four calculations. The drywell liner failed at 0.22 hr after RPV failure in the original calculation. The MELCOR 2.2 calculation without RP leakage failed next fastest after RPV LHF (i.e., 2.14 hr), due to limited water to slow the debris movement to the drywell liner.[13]
- The Version 2.2 calculation and the Version 2.2 calculation with the new melt spreading and water ingress models included RP seal leakage, which delayed the failure of the drywell liner melt-through after the RPV LHF (i.e., 6.69 hr and 5.02 hr, respectively).
- The drywell head leakage (see Figure 4-3) continued until the drywell liner failure (see Figure 4-4), which depressurized the containment (see Figure 4-2) and resealed the drywell head (see Figure 4-3).
- In the two cases with RP seal leakage, the base MELCOR 2.2 calculation used the ex-vessel debris heat transfer multiplier approach whereas the other calculation used the new melt spreading and water ingression models.[13,14] The base MELCOR 2.2 calculation predicted a higher heat transfer rate between the water and debris than the new MELCOR 2.2 model with water ingression heat transfer,[15] which caused the following:

---

[13] The new MELCOR 2.2 calculations also included the new changes noted in Section 2.1 that required molten debris versus molten concrete for movement between the cavities.

[14] The default heat transfer rate from the debris surface to the water was increased using a multiplier to match observed maximum heat transfer rates in CCI experiments [2]. The debris spreading rate was linearly varied from 0 m/s to a maximum rate of 0.37 m/min as the temperature varied from 1700 K to the eutectic melting temperature of the fuel (i.e., assumed to be 2479 K in these calculations). In the original model, the spreading rate was varied between the solidus (1420 K) and the liquidus (1670 K) temperature of the concrete (see Section 2.1). The new melt spreading and water ingression models replaced these models.

[15] This calculation does not characterize the uncertainty in the new melt spreading model. The ex-vessel debris movement has uncertainties that are better examined within the scope of many calculations in a UA. The MELCOR 2.2 calculation paused twice in the debris spreading before reaching and failing the liner. The "MELCOR 2.2 Meltspread + Ingress" calculation also paused but was impacted by successive flows of hot debris from the pedestal region that caused incremental movements to the wall. The debris flow rates, surface heat transfer, and debris spreading responses are highly coupled. While the new MELCOR 2.2 melt spreading and water ingression models are believed to be an improvement over the NUREG/CR-7155 approach, the new models have uncertainties

- The base MELCOR calculation using the debris heat transfer multipliers had a faster and higher pressurization of the drywell (see Figure 4-2), which immediately resulted in more drywell head leakage (see Figure 4-3). The drywell leakage can be considered a surrogate for ex-vessel debris heat transfer rate to the water (i.e., the magnitude of the steam production and resultant drywell pressurization is directly related to the debris to water heat transfer during this phase of the accident).
- A greater delay in the debris transport to the drywell liner (see Figure 4-5).

- The timing on the drywell liner failure shows new behavior in the MELCOR 2.2 calculations. In the original calculation and the MELCOR 2.2 case without RP seal leakage, the debris spread quickly after the RPV LHF and failed the drywell liner. The two cases with RP seal leakage showed 6.31 and 5.02 hr delays between the RPV LHF and the drywell liner failure. The calculation with the new melt spreading and water ingression models showed less vigorous heat transfer versus the previous approach. The older ex-vessel debris heat transfer approach[14] predicted more debris cooling and a greater delay until the drywell liner failure.[15]
- The xenon gas release to the environment is almost identical between all four cases (see Figure 4-7). The xenon gas did not deposit and therefore somewhat reflected the leakage rate of the containment.
  - The RP seal leakage cases with a delayed drywell liner failure slowed the release of the xenon, which occurred through the drywell head leakage. However, once the drywell liner failed, the remaining xenon was rapidly released when the vacuum breakers opened during the sharp containment depressurization.
  - About half of the xenon (~240 kg) was held up in the wetwell airspace until the sharp containment depressurization that opens the vacuum breakers and discharges the captured gases.

- The cesium release to the environment is similar in all four cases (see Figure 4-8). The original result was lower than the new MELCOR 2.2 results but not significantly considering the variations noted in NUREG/CR-7155 for results with a stochastically-failed valve. The following factors contributed to the differences:
  - The MELCOR 2.2 cases included a surge of water from the wetwell that was not calculated in the original calculation. The higher release in the Version 2.2 calculations is partially attributed to the surge of radionuclides from the wetwell water that boiled away on the drywell debris. However, the amount that reaches the environment is impacted by hydrogen burns in the reactor building, which has variable behavior based on the local conditions at the ignition site (i.e., ignition sources are assumed throughout the reactor building).
  - The pump seal leakage pathway also contributed to direct cesium leakage into the drywell rather than exclusively to the wetwell prior to the RPV LHF. For example, there was ~30 kg of cesium and iodine leaked to the drywell via the RP seal leakage in the Version 2.2 calculation versus essentially none in the Version 2.2 calculation with no RP leakage. The cesium and iodine released to the drywell contributed to an increase in the source term when the drywell water evaporated and lofted the radionuclides.

---

and are still coupled to NUREG/CR-7155 uncertainty parameter logic that determines when the debris flows from the pedestal to the drywell floor (see Figure 2-2).

- The differences in the magnitude of the cesium releases were not affected by the delayed drywell liner failure during the drywell head leakage phase. The leakage through the drywell head was also effective at releasing cesium aerosols prior the liner failure.

- The new MELCOR 2.2 iodine releases to the environment showed some differences as compared to the original calculation. Two of the cases had a similar total release, albeit trending higher at 48 hr. The difference in the base case with RP leakage is attributed to the pump seal leakage and the water surge from the wetwell.
  - The pump seal leakage pathway contributed to higher cesium iodide leakage into the drywell rather than exclusively to the wetwell. For example, ~8% iodine inventory (~1.7 kg) leaked to the drywell in the Version 2.2 calculation versus essentially none in the Version 2.2 calculation with no RP leakage. The iodine released to the drywell contributed to an increase in the source term as the drywell water evaporated and lofted and/or revaporized the radionuclides.
  - As discussed in NUREG/CR-7155, a surge of water into the drywell increases the magnitude of the source term. The surge of water carries radionuclides from the wetwell to the drywell floor. The boiling water also helps push airborne radionuclides from the drywell into the reactor building. A surge of water up the wetwell downcomers was more likely with the new vacuum breaker modeling (see Section 2.1 and Table 4-1), which happened in all the new MELCOR 2.2 calculations.
  - The differences in the magnitude of the iodine releases were not affected by the delayed drywell liner failure during the drywell leakage phase. The leakage through the drywell head was also effective at releasing cesium aerosols prior to the liner failure.

This page left blank

Table 4-2. Comparison of Realization 51 key events and timing between NUREG/CR-7155 and MELCOR 2.2

Event Timing (hr)	NUREG/CR-7155	MELCOR 2.2 No RP leak	MELCOR 2.2 w/RP leak	MELCOR 2.2 w/Meltspread
Loss-of-offsite power, Reactor SCRAM, MSIV closes, FW stops, RPs stop	~0	~0	~0	~0
Start of RP seal leakage	N/M	N/M	0.00	0.00
100 °F/hr cooldown initiated (SRV opened, RCIC throttled)	1.00	1.00	1.00	1.00
SRV closes on battery depletion	5.10	5.10	5.10	5.10
RPV overfills failing RCIC turbine	6.36	6.08	6.19	6.19
SRV fails to close due to excessive cycling	9.08	8.28	8.42	8.42
Downcomer level drops to TAF	9.47	8.58	8.64	8.64
First fuel-cladding gap release	10.36	9.47	9.44	9.44
SRV fails to close due the excessive temperature	N/A	N/A	N/A	N/A
MSL creep rupture	N/A	N/A	N/A	N/A
First large-scale relocation of core debris to lower plenum	11.92	12.03	11.84	11.84
RPV LHF	21.56	20.25	20.03	20.03
Drywell head flange leakage begins	13.61	16.17	15.50	15.50
Reactor building blowout panels open	21.61	20.28	20.19	20.69
Wetwell rupture (above waterline)	N/A	N/A	N/A	N/A
Drywell liner melt-through	21.78	22.39	26.33	25.06
A large reactor building H_2 burn fails the roof	21.67	20.33	20.35	20.69
Key Occurrences / Events	**NUREG/CR-7155**	**MELCOR 2.2 No RP leak**	**MELCOR 2.2 w/RP leak**	**MELCOR 2.2 w/Meltspread**
Elapsed time between SRV sticking open and onset of core damage (hr)	1.28	1.19	1.03	1.03
Elapsed time between LHF and drywell liner melt-through (hr)	0.22	2.14	6.31	5.02
Elapsed time between onset of core damage and MSL creep rupture (hr)	N/A	N/A	N/A	N/A
In-vessel H_2 production (kg)	1,203	1,213	1,011	1,014
Surge of water from wetwell up onto drywell floor at liner melt-thru (Yes/No)	N	Y	Y	Y
Railroad Doors blow open (Yes/No)	N	Y	Y	N

Releases to the Environment	NUREG/CR-7155	MELCOR 2.2 No RP leak	MELCOR 2.2 w/RP leak	MELCOR 2.2 w/Meltspread
I release to environment > 0.1% (hr)	21.9	20.4	20.4	20.7
Cs release to environment by 48 hr (fraction)	0.003	0.008	0.012	0.006
I release to environment by 48 hr (fraction)	0.015	0.052	0.067	0.020

Notes:

N/A – Not applicable.
N/M – Not modeled.

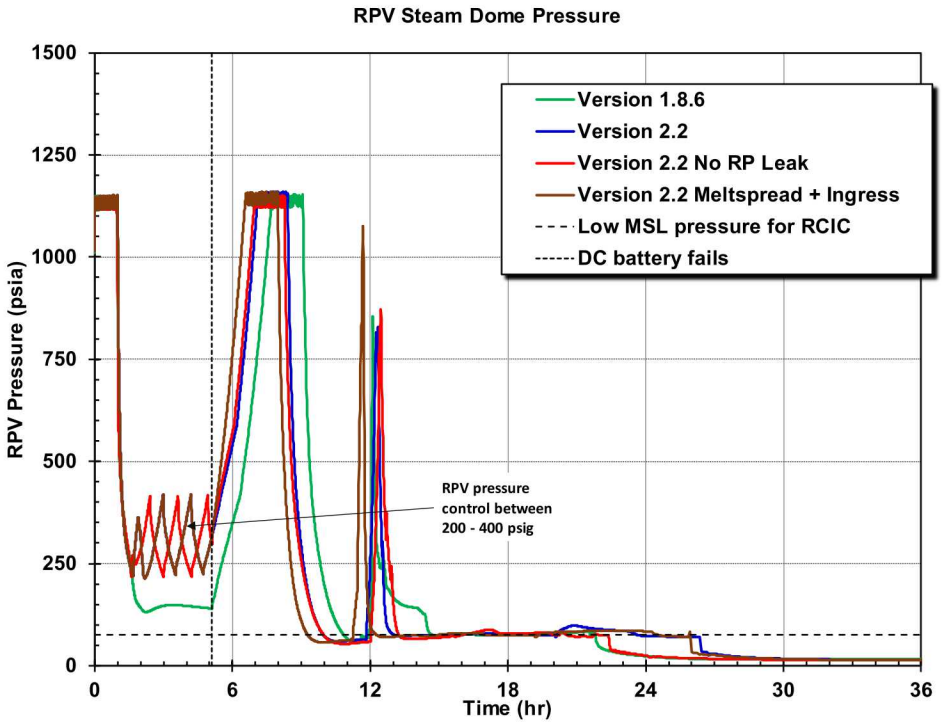

Figure 4-1. Comparison of the RPV pressure with NUREG/CR-7155 and MELCOR 2.2 for Realization 51 with a stochastically-failed SRV

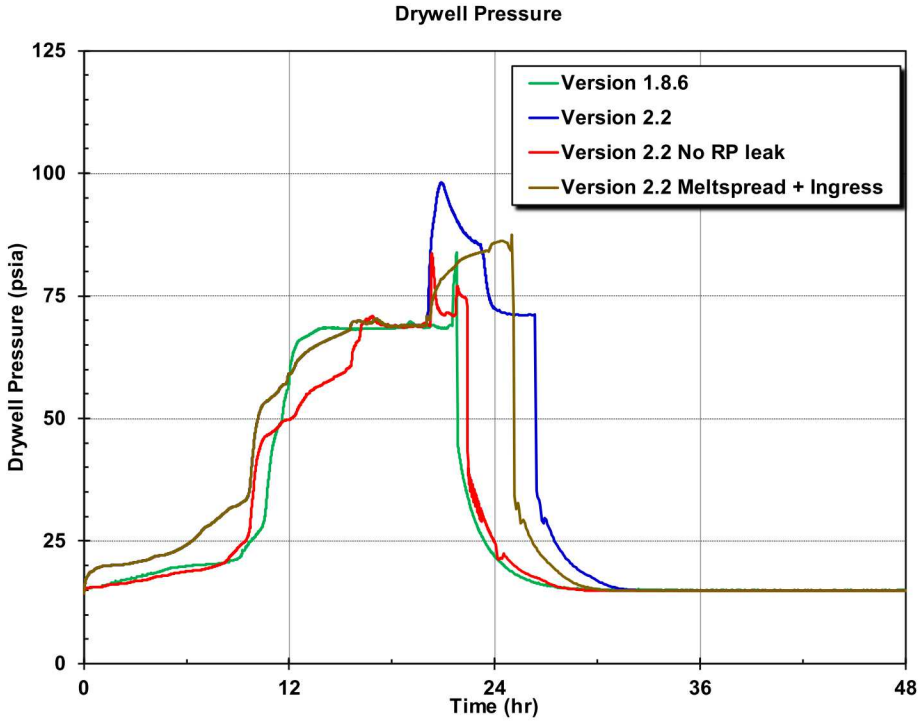

Figure 4-2. Comparison of the drywell pressure with NUREG/CR-7155 and MELCOR 2.2 for Realization 51 with a stochastically-failed SRV

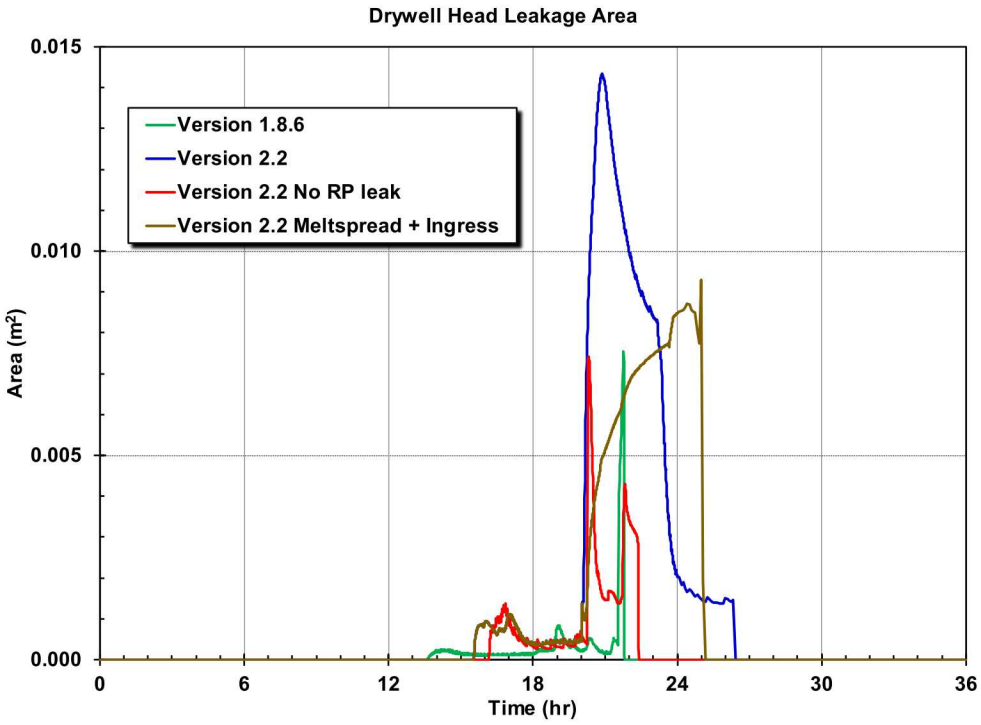

Figure 4-3. Comparison of the drywell head leakage area with NUREG/CR-7155 and MELCOR 2.2 for Realization 51 with a stochastically-failed SRV

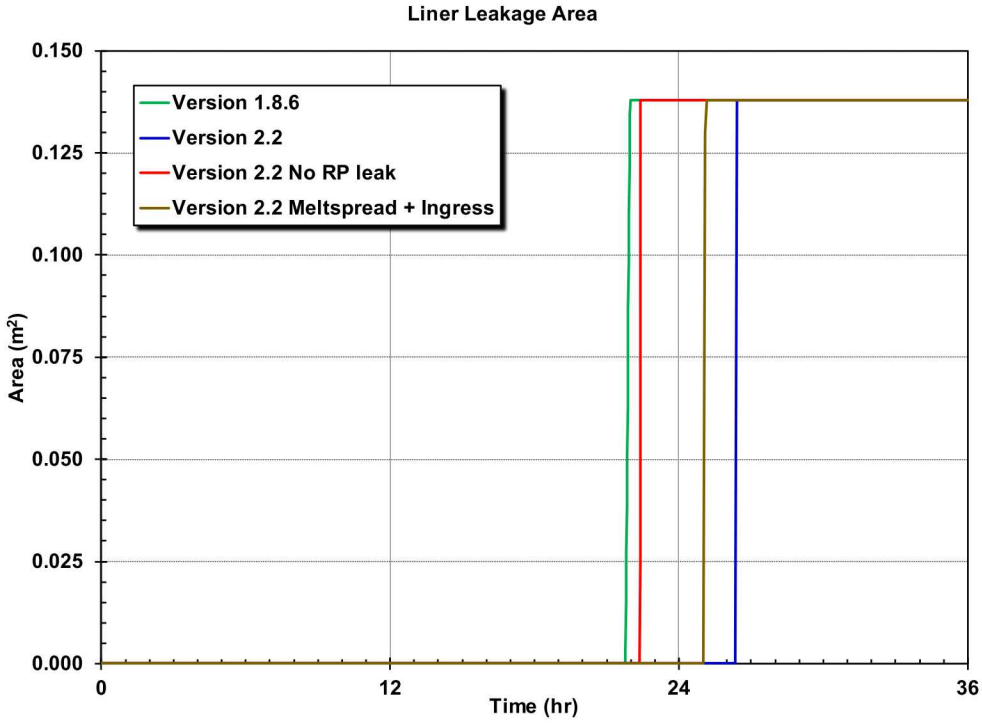

Figure 4-4. Comparison of the drywell liner failure area with NUREG/CR-7155 and MELCOR 2.2 for Realization 51 with a stochastically-failed SRV

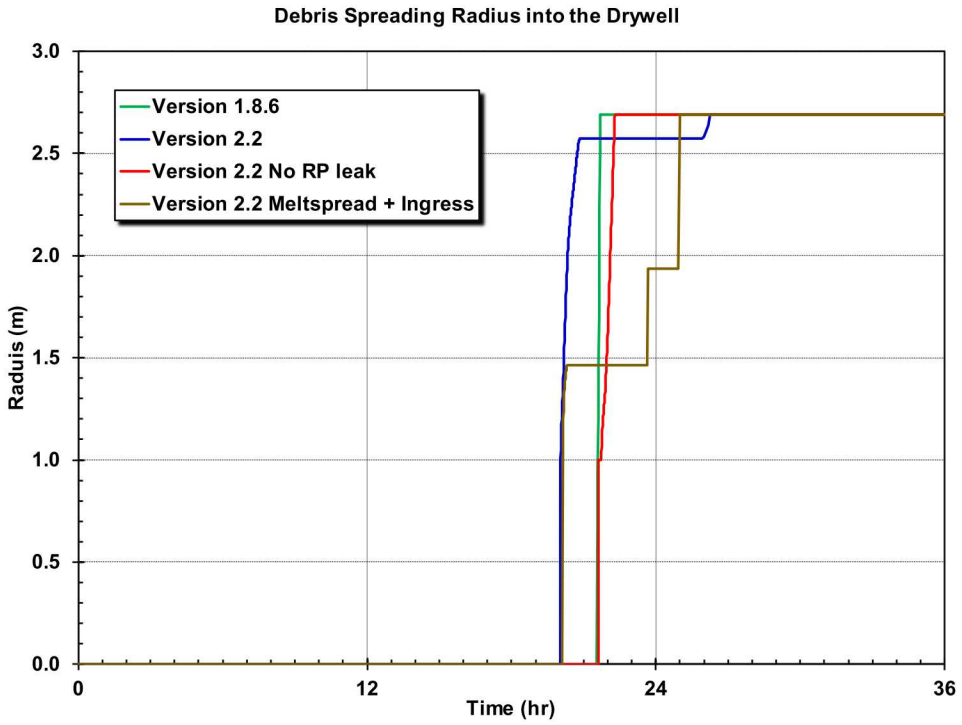

Figure 4-5. Comparison of the debris spreading radius into the drywell with NUREG/CR-7155 and MELCOR 2.2 for Realization 51 with a stochastically-failed SRV

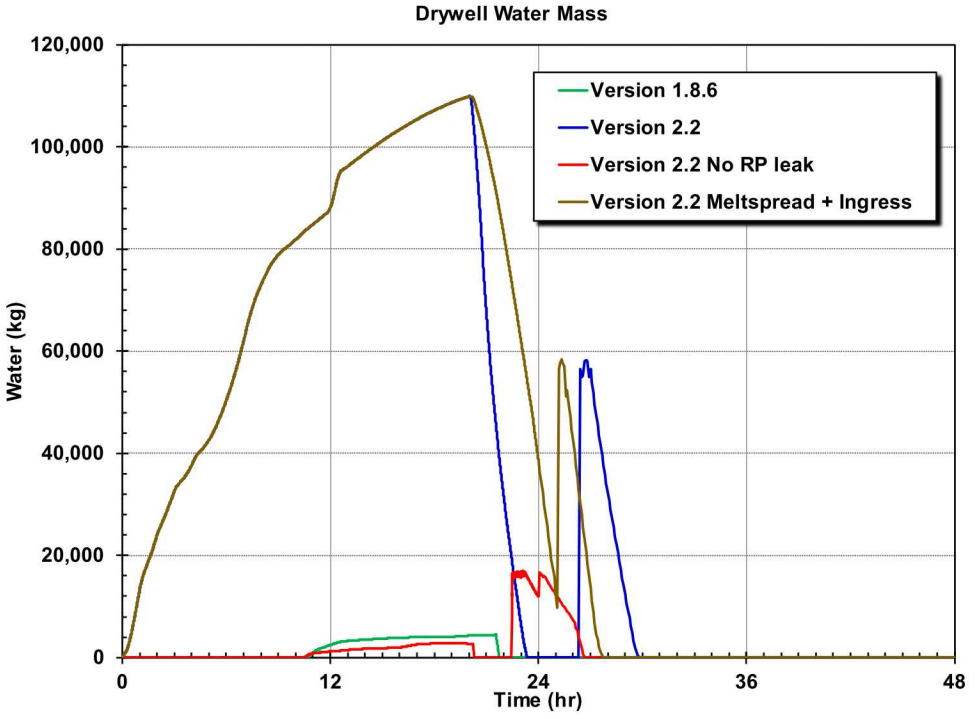

Figure 4-6. Comparison of the water mass in the drywell with NUREG/CR-7155 and MELCOR 2.2 for Realization 51 with a stochastically-failed SRV

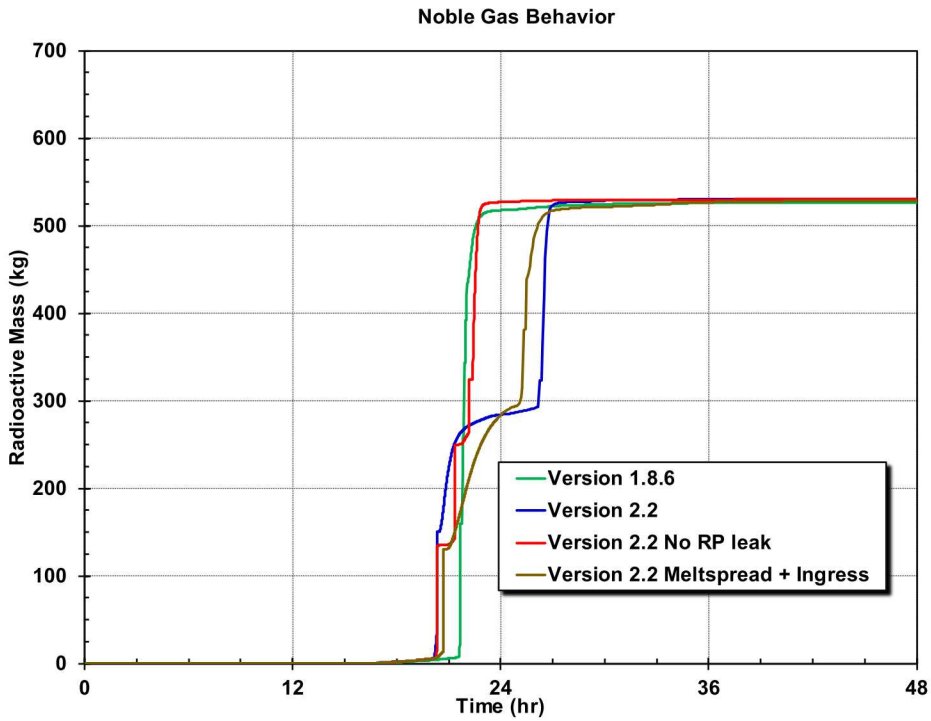

Figure 4-7. Comparison of the xenon release to the environment with NUREG/CR-7155 and MELCOR 2.2 for Realization 51 with a stochastically-failed SRV

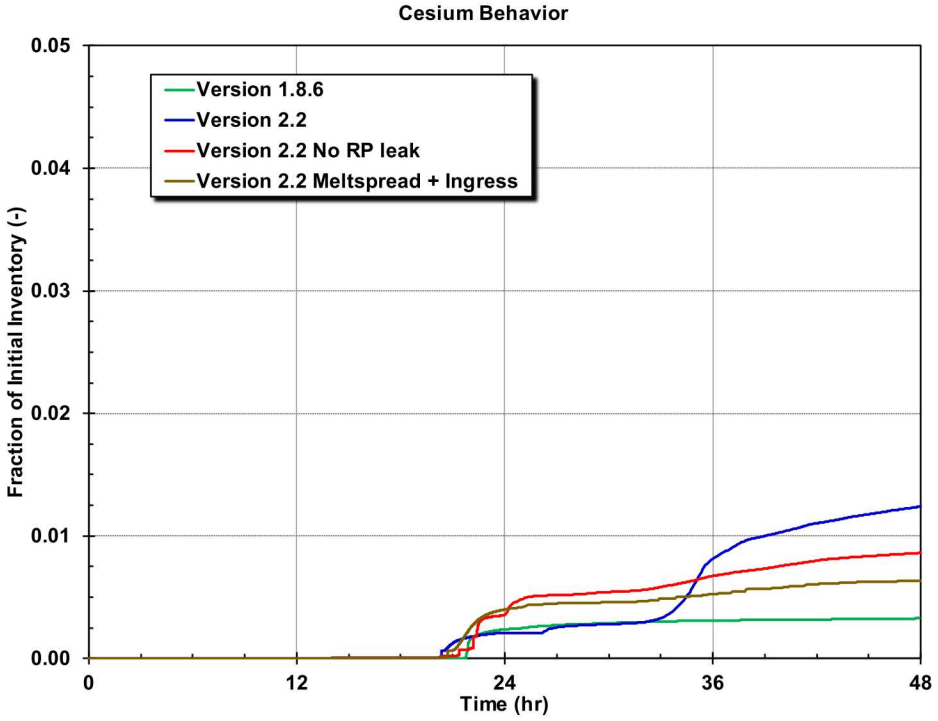

Figure 4-8. Comparison of the cesium release to the environment with NUREG/CR-7155 and MELCOR 2.2 for Realization 51 with a stochastically-failed SRV

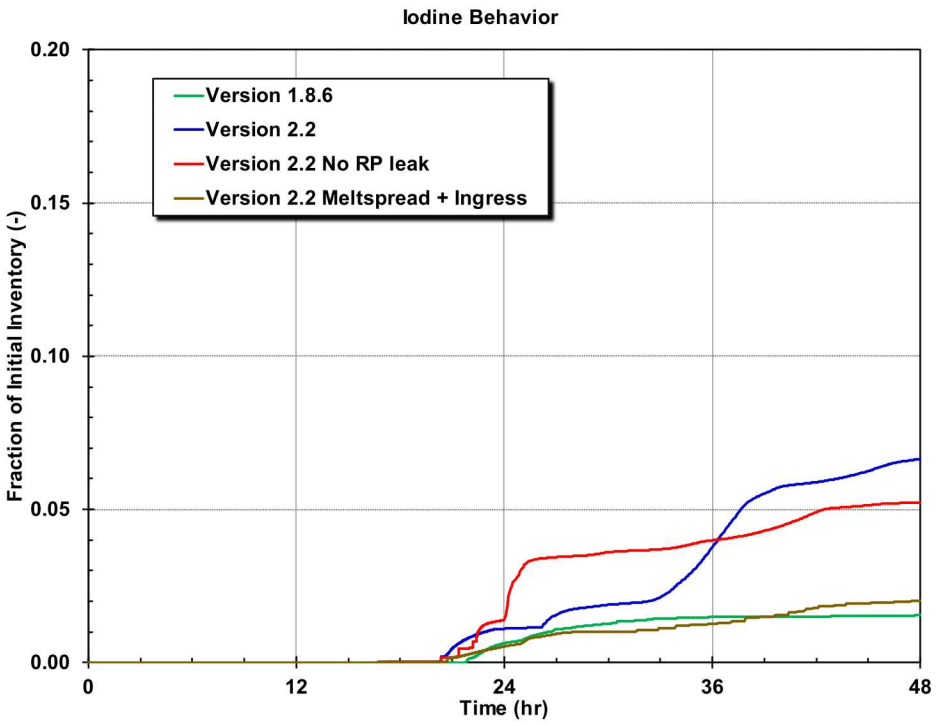

Figure 4-9. Comparison of the iodine release to the environment with NUREG/CR-7155 and MELCOR 2.2 for Realization 51 with a stochastically-failed SRV

4.2. Reference Realization 18 with a Thermally-failed SRV

This section documents the comparison of the updated MELCOR 2.2 model with Realization 18 from NUREG/CR-7155 with a thermally-failed SRV, which defined the accident progression (see Section 3.1). All 4 calculations predicted a thermally-failed SRV using the uncertain parameters in Table 3-1 with the MELCOR 2.2 updates noted in Table 3-6. A comparison of the key timings, calculated quantities, and events between the NUREG/CR-7155 result and the updated MELCOR 2.2 calculations are presented in Table 4-3.

Figure 4-10 through Figure 4-18 show comparisons of key accident progression and source term quantities for the NUREG/CR-7155 result (labeled Version 1.8.6), the updated base case using MELCOR 2.2 (labeled Version 2.2), the updated base case without RP seal leakage (labeled Version 2.2 No seal leak), and a MELCOR 2.2 sensitivity calculation using the new melt spreading (see Section 2.2.6) and water ingression models (see Section 2.2.7), which is labeled "Version 2.2 Meltspread + Ingress". Some of the key differences contributing to differences in the results are summarized in Table 4-1. The specific findings are summarized below.

Key observations –

- An operator action was included at 1 hr that opened an SRV to depressurize the RPV. All of the new MELCOR 2.2 calculations included operator actions to control the RPV pressure above 200 psia (see Figure 4-10). Without these simulated actions, the RPV pressure dropped below the RCIC shutoff head, which terminated RCIC injection prematurely. The inclusion of the RP seal and the MSIV leakage in the new MELCOR 2.2 caused the higher RPV depressurization versus the original calculations without these leakages (see Table 4-1).

- The SRV closed at 4.14 hr following the loss of DC power control. The subsequent RPV pressurization in the MELCOR 2.2 calculations started at a higher pressure than the original calculation because the drywell pressure was maintained between 200 psi to 400 psi. Consequently, the timing to the start of the SRV cycling was earlier than in the original calculation (see Figure 4-10).
- The SRV cycled after the RPV pressurized until the hot gases exiting the core caused its failure between 10.25 to 11.50 hr. The two calculations with RP seal leakage reached this condition approximately 1 hr before the two cases without RP seal leakage (see Table 4-3 and Figure 4-10).
- The RPV and drywell pressure response is the same for the "Version 2.2" and "Version 2.2 with melt spreading and water ingression" until the RPV LHF (see Figure 4-11). Both calculations include RP seal leakage (i.e., see buildup of the drywell water level in Figure 4-15).
- The accelerated timings in the new MELCOR 2.2 calculations persisted through LHF, which occurred 2 hr earlier in the MELCOR 2.2 calculation without RP seal leakage and 3.2 hr earlier with RP seal leakage (i.e., see Table 4-3, depending on the calculation).
- The calculation labeled MELCOR 2.2 without RP seal leakage and the original NUREG/CR-7155 MELCOR 1.8.6 calculation did not include RP seal leakage. Consequently, there is significantly less water in the drywell than in the calculations with RP seal leakage (see Figure 4-15), which impacts the ex-vessel debris behavior.
- The two MELCOR 2.2 calculations with RP seal leakage had significantly lower in-vessel hydrogen production (i.e., ~1015 kg) than the original calculation (i.e., 1307 kg) and the MELCOR 2.2 calculation without RP seal leakage (i.e., 1170 kg). These two cases with RP seal leakage progressed to core damage more quickly, which led to a faster core collapse and a corresponding lower in-vessel hydrogen generation (i.e., oxidation slows significantly after the collapse of the fuel into a debris bed). The differences in the original calculation and the MELCOR 2.2 calculation without RP seal leakage are attributed to variations in the accident specifications (i.e., see Table 2-1 and Table 4-1) and code version changes (see discussion in Section 3.1), which includes important changes to the oxidation routines.
- The drywell pressure increased earlier in the MELCOR 2.2 calculations with RP seal leakage, which led to an earlier and more sustained leakage drywell leakage prior to the RPV failure (see Figure 4-11).
- All the new MELCOR 2.2 calculations show a surge of water from the wetwell onto the drywell floor at drywell liner failure (see Figure 4-15). The water surge also carried some radionuclides previously captured in the wetwell. The consistent surge of water in the new calculations is attributed to the changes in the vacuum breaker modeling noted in Section 2.1. The vacuum breakers are less likely to open to relieve the pressure difference in the new calculations, which promotes backflow through the downcomer pipes.
- Following the RPV LHF and the debris ejection to the containment, the drywell responses varied in the four calculations. The drywell liner failed at 0.22 hr after RPV failure in the original calculation. The MELCOR 2.2 calculation without RP leakage failed next fastest after RPV LHF (i.e., 1.22 hr), due to limited water to slow the debris movement to the drywell liner.[13]
- The base MELCOR 2.2 calculation and the MELCOR 2.2 calculation with the new melt spreading and water ingress models included RP seal leakage, which delayed the failure of the drywell liner melt-through after the RPV LHF (i.e., 6.21 hr and 4.31 hr, respectively).
- The drywell head leakage (see Figure 4-12) continued until the drywell liner failure (see Figure 4-13), which depressurized the containment (see Figure 4-20) and resealed the drywell head.

- In the two cases with RP seal leakage, the base MELCOR 2.2 calculation used the ex-vessel debris heat transfer multiplier approach whereas the other calculation used the new melt spreading and water ingression models.[13,14] The base MELCOR 2.2 calculation predicted a higher heat transfer rate between the water and debris than the new MELCOR 2.2 model with water ingression heat transfer,[15] which caused the following:
    - The base MELCOR calculation using the debris heat transfer multipliers had a faster and higher pressurization of the drywell (see Figure 4-11), which immediately resulted in more drywell head leakage (see Figure 4-12). The drywell leakage can be considered a surrogate for ex-vessel debris heat transfer rate to the water (i.e., the magnitude of the steam production and resultant drywell pressurization is directly related to the debris to water heat transfer during this phase of the accident).
    - A greater delay in the debris transport to the drywell liner (see Figure 4-14).
- The xenon gas release to the environment is almost identical between all four cases (see Figure 4-16). The xenon gas did not deposit and therefore somewhat reflected the leakage rate from the containment.
- The delayed drywell liner failure slowed the release of the xenon, which occurred through the drywell head leakage. However, once the drywell liner failed, the remaining xenon was rapidly released when the vacuum breakers opened during the sharp containment depressurization.
    - The delayed drywell liner failure slowed the release of the xenon, which initially occurred through the drywell head leakage. However, once the drywell liner failed, the remaining xenon was released.
    - Over half of the xenon (~250 kg) was held up in the wetwell airspace until the sharp containment depressurization that opens the vacuum breakers and discharges the captured gases.
- The cesium release to the environment is similar between all four cases (see Figure 4-17). The original result was lower than the new MELCOR 2.2 results but not significantly considering the variations noted in NUREG/CR-7155 for results with a thermally-failed valve. The following factors contributed to the differences:
    - The MELCOR 2.2 cases included a surge of water from the wetwell that was not calculated in the original calculation. The higher release in the Version 2.2 calculations is partially attributed to the surge of radionuclides from the wetwell water that boiled away on the drywell debris and revaporization of cesium iodine in the drywell. However, the amount that reaches the environment is impacted by hydrogen burns in the reactor building, which has variable behavior based on the local conditions at the ignition site (i.e., ignition sources are assumed throughout the reactor building).
    - The pump seal leakage pathway also contributed to cesium leakage into the drywell rather than exclusively to the wetwell prior to the RPV LHF. For example, there was ~15 kg of cesium and iodine leaked to the drywell in the Version 2.2 calculation versus essentially none in the Version 2.2 calculation with no RP leakage. The cesium and iodine released to the drywell contributed to an increase in the source term as the drywell water evaporated and lofted the radionuclides.

- The differences in the magnitude of the cesium releases were not affected by the delayed drywell liner failure during the drywell leakage phase. The leakage through the drywell head was also effective at releasing cesium aerosols prior the liner failure.

- The iodine release to the environment is similar to the original calculation except the base MELCOR 2.2 calculation with RP seal leakage, albeit trending higher at 48 hr (see Figure 4-18). The difference in the base case with RP leakage is attributed to the pump seal leakage and the surge of water from the wetwell.
  - The pump seal leakage pathway also contributed to cesium leakage into the drywell rather than exclusively to the wetwell. For example, ~5% iodine inventory (~1 kg) leaked to the drywell in the Version 2.2 calculation versus essentially none in the Version 2.2 calculation with no RP leakage. The iodine released to the drywell contributed to an increase in the source term as the drywell water evaporated and lofted and/or revaporized the radionuclides.
  - As discussed in NUREG/CR-7155, a surge of water into the drywell increases the magnitude of the source term. The steam source helps push airborne radionuclides from the drywell into the reactor building. A surge of water through the wetwell downcomers was more likely with the new vacuum breaker modeling (see Section 2.1 and Table 4-1), which happened in all the new MELCOR 2.2 calculations.
  - The differences in the magnitude of the iodine releases were not affected by the delayed drywell liner failure during the drywell leakage phase. The leakage through the drywell head was also effective at releasing cesium aerosols prior to the liner failure.

Table 4-3. Comparison of Realization 18 key events and timing between NUREG/CR-7155 and MELCOR 2.2

Event Timing (hr)	NUREG/CR-7155	MELCOR 2.2 No RP leak	MELCOR 2.2 w/RP leak	MELCOR 2.2 w/Meltspread
100 °F/hr cooldown initiated (SRV opened, RCIC throttled)	1.00	1.00	1.00	1.00
SRV closes on battery depletion	4.14	4.14	4.14	4.14
RCIC turbine floods failing RCIC	5.28	5.00	5.28	5.28
SRV fails to close due to excessive cycling	N/A	N/A	N/A	N/A
Downcomer level drops to TAF	9.22	8.96	7.97	7.97
First fuel-cladding gap release	10.33	9.92	8.92	8.92
SRV fails to close due the excessive temperature	11.50	11.14	10.25	10.25
MSL creep rupture	N/A	N/A	N/A	N/A
First large-scale relocation of core debris to lower plenum	13.50	13.52	11.53	11.53
RPV LHF	21.54	19.50	18.19	18.19
Drywell head flange leakage begins	14.86	16.61	12.75	12.75
Reactor building blowout panels open	16.19	19.56	18.31	18.49
Wetwell rupture (above waterline)	N/A	N/A	N/A	N/A
Drywell liner melt-through	19.72	19.86	24.89	22.66
A large reactor building H_2 burn fails the roof	19.75	N/A	24.64	22.96
Key Occurrences / Events	**NUREG/CR-7155**	**MELCOR 2.2 No RP leak**	**MELCOR 2.2 w/RP leak**	**MELCOR 2.2 w/Meltspread**
Elapsed time between SRV sticking open and onset of core damage (hr)	1.17	1.22	1.33	1.33
Elapsed time between LHF and drywell liner melt-through (hr)	0.22	0.36	6.69	4.47
Elapsed time between onset of core damage and MSL creep rupture (hr)	N/A	N/A	N/A	N/A
In-vessel H_2 production (kg)	1,307	1,170	1,015	1,014
Surge of water from wetwell up onto drywell floor at liner melt-thru (Yes/No)	N	Y	Y	Y
Railroad Doors blow open (Yes/No)	Y	Y	Y	Y
Releases to the Environment	**NUREG/CR-7155**	**MELCOR 2.2 No RP leak**	**MELCOR 2.2 w/RP leak**	**MELCOR 2.2 w/Meltspread**
I release to environment > 0.1% (hr)	19.6	19.7	18.4	20.0

Cs release to environment by 48 hr (fraction)	0.021	0.028	0.040	0.050
I release to environment by 48 hr (fraction)	0.070	0.077	0.142	0.155

Notes:

N/A – Not applicable.

N/M – Not modeled.

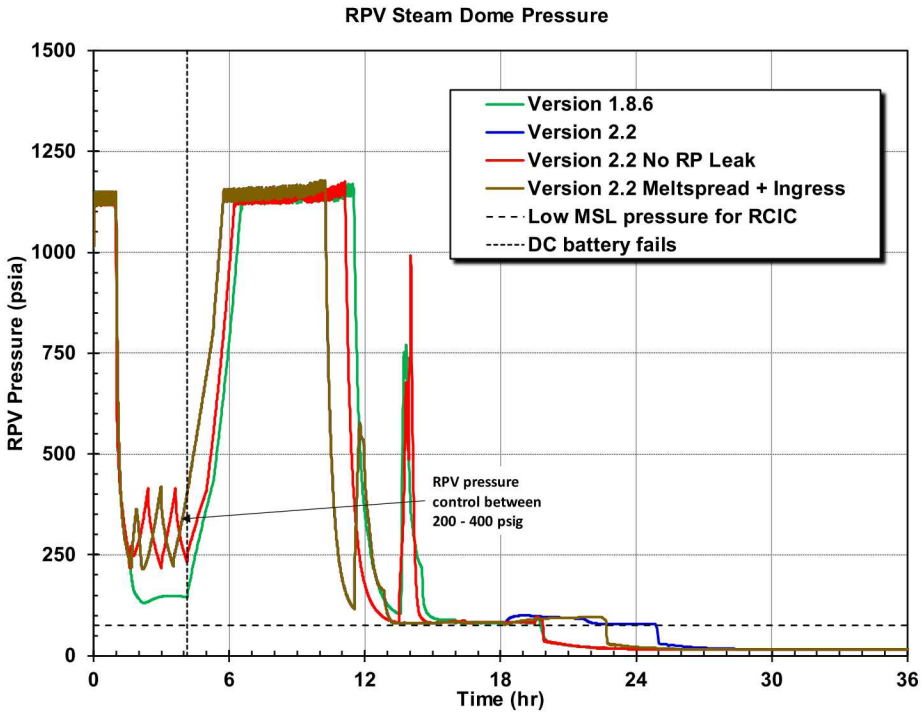

Figure 4-10. Comparison of the RPV pressure with NUREG/CR-7155 and MELCOR 2.2 for Realization 18 with a thermally-failed SRV

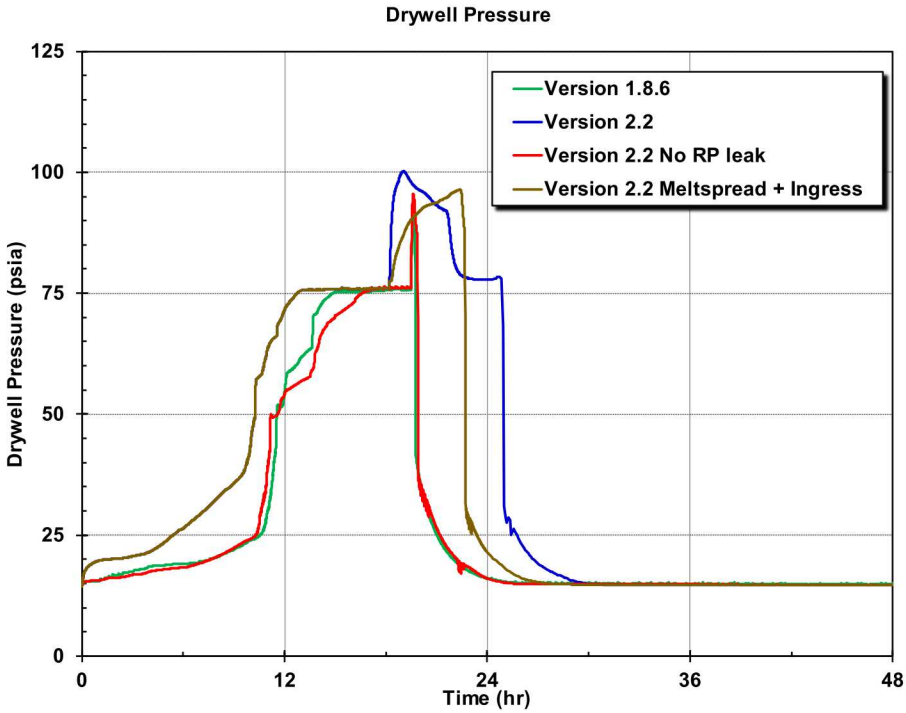

Figure 4-11. Comparison of the drywell pressure with NUREG/CR-7155 and MELCOR 2.2 for Realization 18 with a thermally-failed SRV

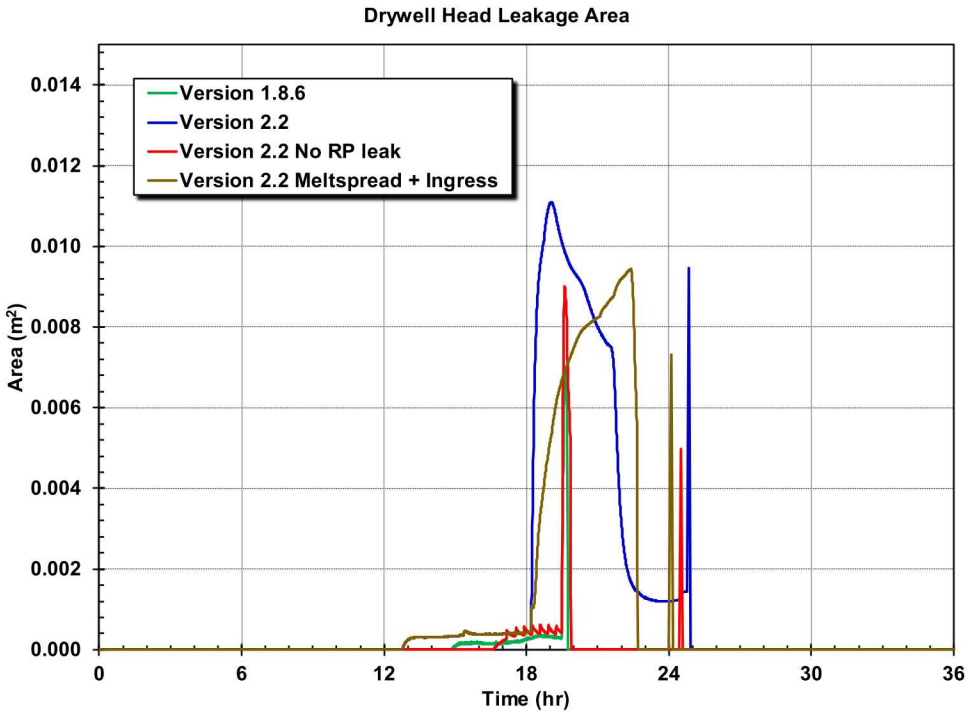

Figure 4-12. Comparison of the drywell head leakage area with NUREG/CR-7155 and MELCOR 2.2 for Realization 18 with a thermally-failed SRV

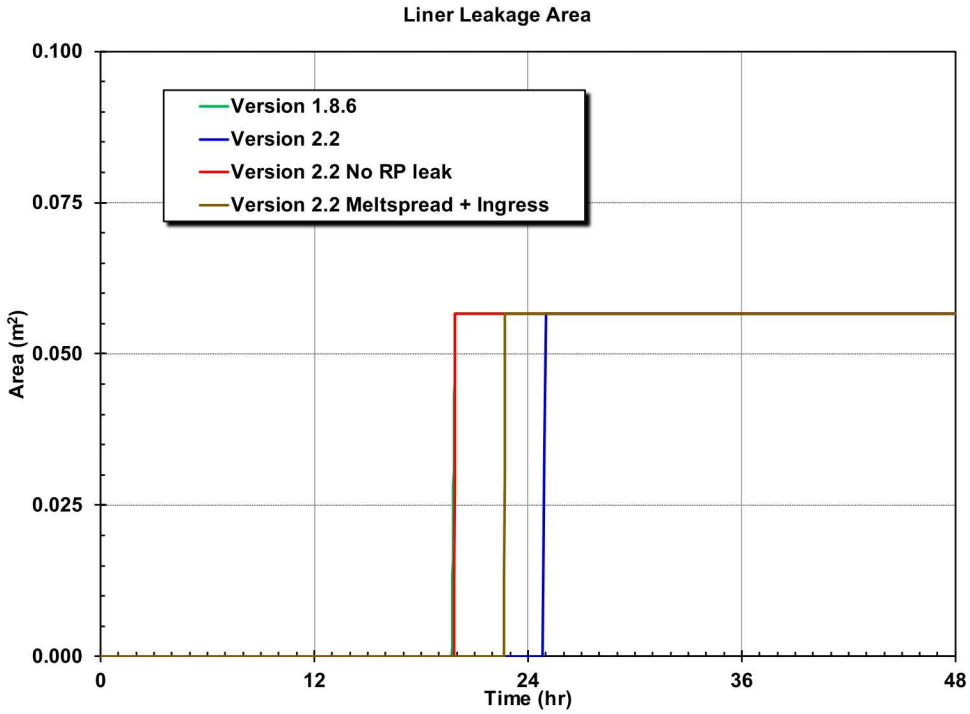

Figure 4-13. Comparison of the drywell liner failure area with NUREG/CR-7155 and MELCOR 2.2 for Realization 18 with a thermally-failed SRV

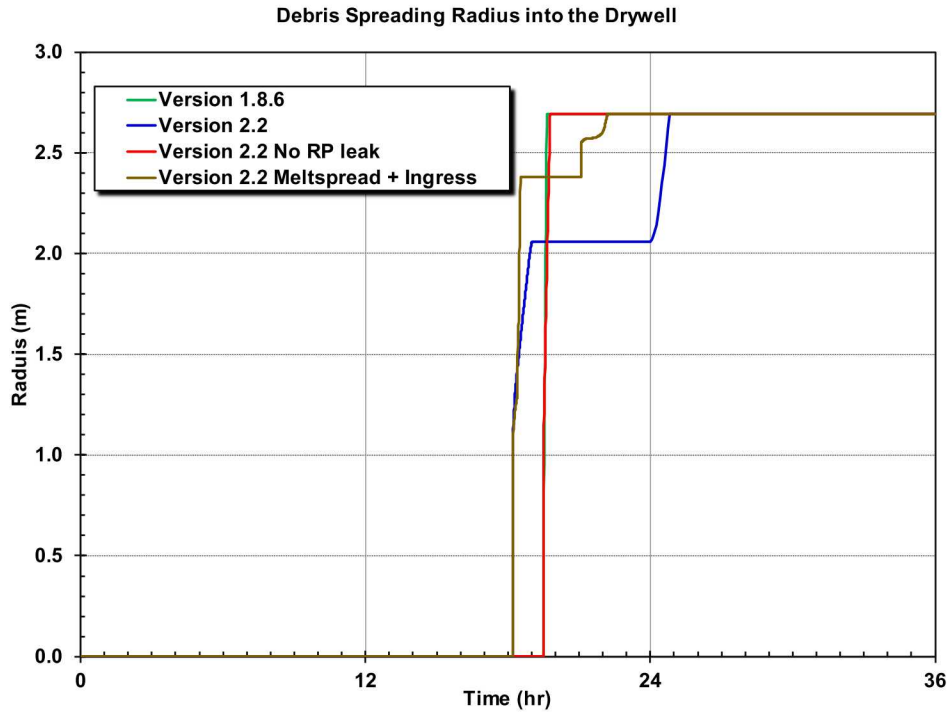

Figure 4-14. Comparison of the debris spreading radius into the drywell with NUREG/CR-7155 and MELCOR 2.2 for Realization 18 with a thermally-failed SRV

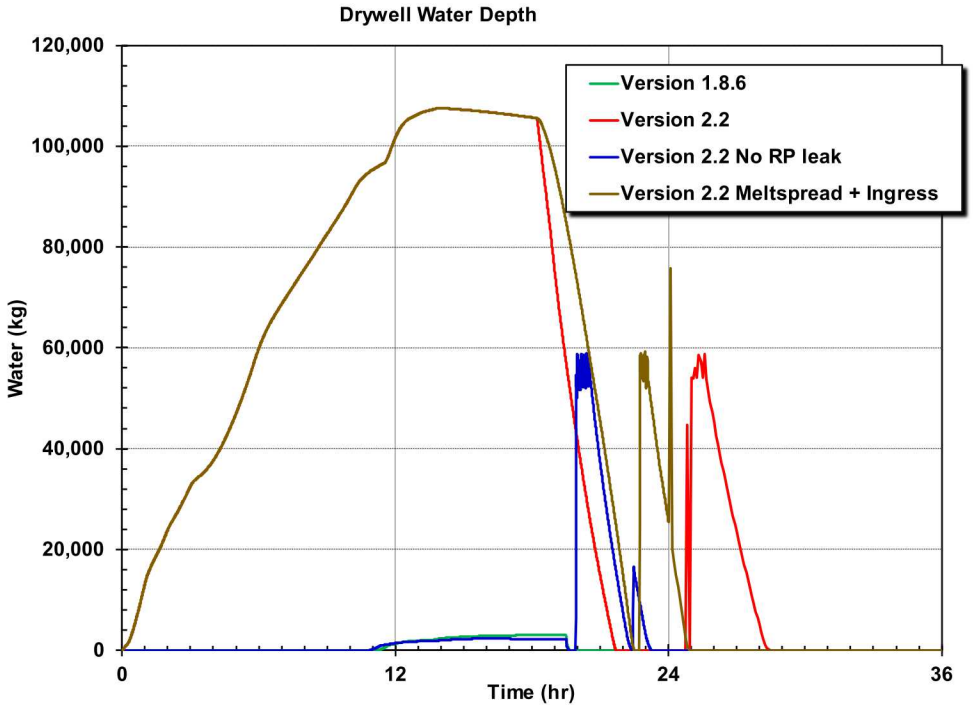

Figure 4-15. Comparison of the water mass in the drywell with NUREG/CR-7155 and MELCOR 2.2 for Realization 18 with a thermally-failed SRV

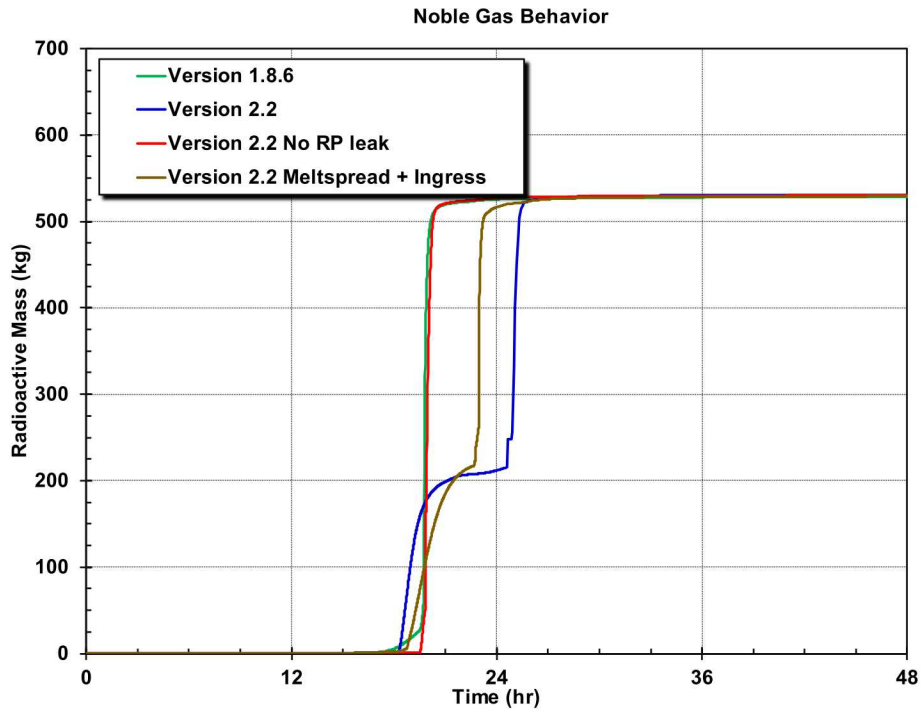

Figure 4-16. Comparison of the xenon release to the environment with NUREG/CR-7155 and MELCOR 2.2 for Realization 18 with a thermally-failed SRV

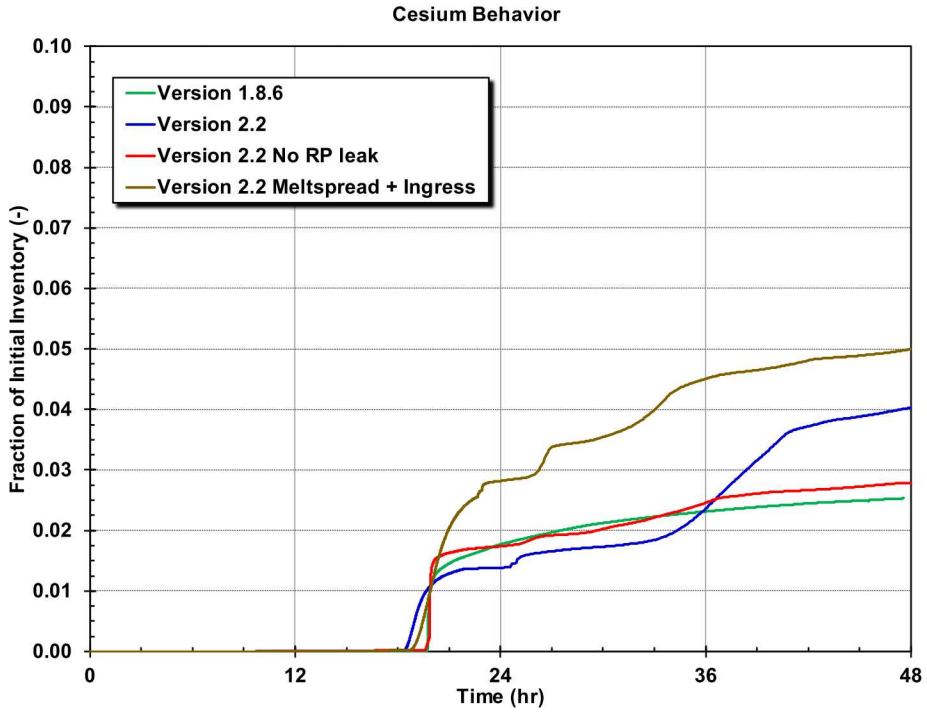

Figure 4-17. Comparison of the cesium release to the environment with NUREG/CR-7155 and MELCOR 2.2 for Realization 18 with a thermally-failed SRV

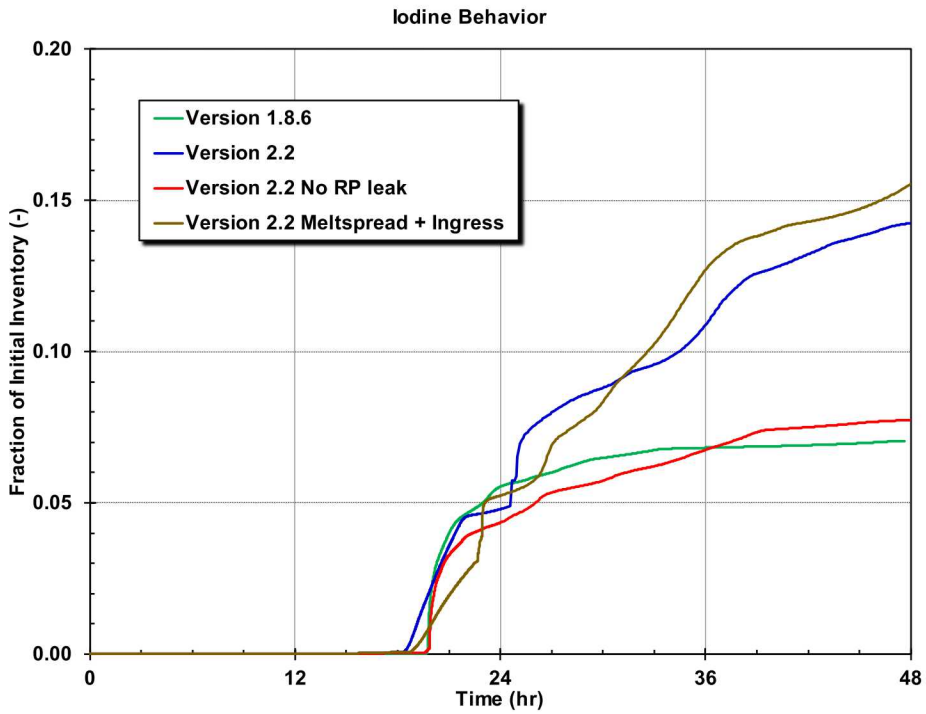

Figure 4-18. Comparison of the iodine release to the environment with NUREG/CR-7155 and MELCOR 2.2 for Realization 18 with a thermally-failed SRV

4.3. Reference Realization 86 with a Thermally-failed SRV and a Failed MSL

This section documents the comparison of the updated MELCOR 2.2 model with Realization 86 from NUREG/CR-7155 with a thermally-failed SRV and a thermally-failed MSL, which defined the accident progression (see Section 3.1). All four calculations predicted a thermally-failed SRV using the uncertain parameters in Table 3-1 with the MELCOR 2.2 updates noted in Table 3-6. The thermally-failed SRV had a small fractional open area (i.e., 0.246), which released hot gases from the core through the steam line while more slowly depressurizing the primary system. The resulting thermal and mechanical strain across the main steam line causes an MSL failure in all 4 calculations. A comparison of the key timings, calculated quantities, and events between the NUREG/CR-7155 result and the updated MELCOR 2.2 calculations are presented in Table 4-4.

Figure 4-19 through Figure 4-27 show comparisons of key accident progressions and source term quantities for the NUREG/CR-7155 result (labeled Version 1.8.6), the updated base case using MELCOR 2.2 (labeled Version 2.2), the updated base case without RP seal leakage (labeled Version 2.2 No seal leak), and a MELCOR 2.2 sensitivity calculation using the new melt spreading (see Section 2.2.6) and water ingression models (see Section 2.2.7), which is labeled "Version 2.2 Meltspread + Ingress". Some of the key differences contributing to differences in the results are summarized in Table 4-1. The specific findings are summarized below.

Key observations –

- An operator action was included at 1 hr that opened an SRV to depressurize the RPV. All of the new MELCOR 2.2 calculations included subsequent operator actions to control the RPV pressure above 200 psia (see Figure 4-19). Without these simulated actions, the RPV pressure dropped below the RCIC shutoff head, which terminated RCIC injection prematurely. The inclusion of RP seal and MSIV leakage in the new MELCOR 2.2 caused the higher RPV depressurization versus the original calculations without these leakages (see Table 4-1).
- The SRV closed at 3.72 hr following the loss of DC power control. The subsequent RPV pressurization in the MELCOR 2.2 calculations started at a higher pressure than the original calculation because the drywell pressure was maintained between 200 psi to 400 psi. Consequently, the timing to the start of the SRV cycling was earlier than in the original calculation (see Figure 4-19).
- The SRV cycled after the RPV pressurized until the hot gases exiting the core caused its failure between 9.94 to 10.95 hr. The two calculations with RP seal leakage reached this condition approximately 15 min after the new MELCOR 2.2 case without RP seal leakage but approximately 58 min after the original calculation (see Table 4-3 and Figure 4-10). The variations in the MELCOR 2.2 results are due to the RPV pressure at the time of the battery failure (i.e., higher in the MELCOR 2.2 calculations with RP seal leakage than the MELCOR 2.2 calculation without seal leakage). The two calculations with seal leakage started SRV cycling earlier. The original calculation lagged the MELCOR 2.2 results due to the later start of SRV cycling after the battery failure and no RP seal leakage (i.e., more RPV water inventory to heat).
- The RPV and drywell pressure response is the same for the "Version 2.2" and "Version 2.2 with melt spreading and water ingression" until the RPV LHF (see Figure 4-20). Both calculations include RP seal leakage (i.e., see buildup of the drywell water level in Figure 4-24).
- The in-vessel accident progressions showed some variations. The three new MELCOR 2.2 calculations had a thermally-induced MSL failure after the first debris relocation to the lower plenum versus before any debris relocations in the original calculation. Since the MSL was failed original calculation prior to the initial core debris relocation into the lower plenum, there was no

containment pressurize spike in the original calculation following the MSL failure. In contrast, the new MELCOR 2.2 calculation had an RPV pressure spike due to the initial debris relocation into the RPV lower plenum that contributed to the MSL failure. The MELCOR 2.2 models also included the updated lower plenum debris modeling (see Table 4-1 with discussions in Sections 2.2.5 and 2.3.3). However, it was the intact MSL at the time of the debris relocation into the lower plenum that allowed a significant RPV pressurization in the MELCOR 2.2 calculations.

- The other in-vessel accident progression timings also showed some differences. The MELCOR 2.2 calculation without RP leakage progressed to LHF more quickly than the other calculations. Although the Ring 2 fuel (i.e., highest power region) was the first to collapse in all the MELCOR 2.2 calculations, the subsequent behavior was different in the MELCOR 2.2 calculation without RP leakage. The differences were traced to an earlier failure of the core plate supporting the Ring 1 fuel (i.e., 112 assemblies), which accelerated the subsequent failures of the remaining fuel and the timing to the LHF.
- The relative timings of the original calculation and the two MELCOR 2.2 calculations with RP leakage remained relatively consistent through the LHF.
- The calculation labeled MELCOR 2.2 without RP seal leakage and the original NUREG/CR-7155 MELCOR 1.8.6 calculation did not include RP seal leakage. Consequently, there is significantly less water in the drywell than in the calculations with RP seal leakage (see Figure 4-24), which impacts the ex-vessel debris behavior.
- The two MELCOR 2.2 calculations with RP seal leakage had significantly lower in-vessel hydrogen production (i.e., ~890 kg) than the original calculation (i.e., 1257 kg) and the MELCOR 2.2 calculation without RP seal leakage (i.e., 1049 kg). The two cases with RP seal leakage progressed to core damage more quickly, which led to a faster core collapse and a corresponding lower in-vessel hydrogen generation (i.e., oxidation slows significantly after the collapse of the fuel into a debris bed). The differences in the original calculation and the MELCOR 2.2 calculation without RP seal leakage are attributed to variations in the accident specifications (i.e., see Table 2-1 and Table 4-1) and code version changes (see discussion in Section 3.1), which includes important changes to the oxidation routines.
- The drywell pressure increased earlier in the MELCOR 2.2 calculations with RP seal leakage, which led to an earlier and more sustained leakage drywell leakage prior to the RPV failure (see Figure 4-21).
- All the new MELCOR 2.2 calculations show a surge of water from the wetwell onto the drywell floor at drywell liner failure (see Figure 4-24). The water surge also carried some radionuclides previously captured in the wetwell. The consistent surge of water in the new calculations is attributed to the changes in the vacuum breaker modeling noted in Section 2.1. The vacuum breakers are less likely to open to relieve the pressure difference in the new calculations, which promotes backflow through the downcomer pipes.
- The time intervals between the LHF and the drywell liner showed different behavior from the two other realization comparisons (see Table 4-2 and Table 4-3).
    - Similar to the other two realizations, the drywell liner failed at 0.22 hr after RPV failure in the original calculation.
    - The MELCOR 2.2 calculation without RP leakage failed next fastest after RPV LHF (i.e., 1.18 hr), due to limited water to slow the debris movement to the drywell liner. This

calculation had a longer delay than observed in the other realizations because the lowest powered fuel in Ring 5 remained in the RPV.[16]
    - The MELCOR 2.2 calculation with the debris heat transfer multipliers had the longest delay (i.e., 6.33 hr), which is consistent with the other two realizations.
    - The MELCOR 2.2 calculation with the new melt spreading and water ingress models only had a 0.9 hr delay, which was faster than in the other two realizations. The spreading to the liner failure also occurred in relatively deep water (i.e., 0.7 m), which also occurred in Realization 51 but not in Realization 18 (see Footnote 15). The result was unexpected but was traced to slightly hotter debris leaving the pedestal region that did not freeze prior to reaching the drywell liner. Nevertheless, the faster drywell liner response provides an alternate outcome to assess any impact on the source term.

- The drywell head leakage (see Figure 4-21) continued until the drywell liner failure (see Figure 4-22), which depressurized the containment (see Figure 4-20) and resealed the drywell head.
- In the two cases with RP seal leakage, the base MELCOR 2.2 calculation used the ex-vessel debris heat transfer multiplier approach whereas the other calculation used the new melt spreading and water ingression models.[13,14] The base MELCOR 2.2 calculation predicted a higher heat transfer rate between the water and debris than the new MELCOR 2.2 model with water ingression heat transfer,[15] which caused the following:
    - The base MELCOR calculation using the debris heat transfer multipliers had a faster and higher pressurization of the drywell (see Figure 4-20), which immediately resulted in more drywell head leakage (see Figure 4-21). The drywell leakage can be considered a surrogate for ex-vessel debris heat transfer rate to the water (i.e., the magnitude of the steam production and resultant drywell pressurization is directly related to the debris to water heat transfer during this phase of the accident).
    - The base calculation evaporated all the water in the drywell before causing the drywell liner failure. The new melt spreading calculation with water ingression failed the drywell liner under 0.7 m of water.
    - Both cases had a greater delay in the debris transport to the drywell liner than the original calculation (see Figure 4-22).

- The xenon gas release to the environment is almost identical between all four cases (see Figure 4-16). The xenon gas did not deposit and therefore somewhat reflected the leakage rate from the containment.
    - The delayed drywell liner failure slowed the release of the xenon in the "Version 2.2" calculation, which occurred through the drywell head leakage. However, once the drywell liner failed, the remaining xenon was rapidly released when the vacuum breakers opened during the sharp drywell depressurization. Over half of the xenon (~250 kg) was held up in

[16] The MELCOR 2.2 calculation without RP seal leakage did not have a complete ejection of all core materials from the RPV. The lowest powered fuel in Ring 5 remained in the RPV. The RPV failed earlier in this calculation before the collapse of the Ring 5 fuel. A natural circulation flow was established through the failed RPV lower head to MSL failure that sufficiently cooled the fuel to prevent its relocation. The fuel was hot but below the melting temperature of the steel core plate. The smaller amount of debris mass in the drywell contributed to the delayed drywell liner failure.

the wetwell airspace until the sharp containment depressurization that opened the vacuum breakers and discharged the captured gases.

- The cesium release to the environment is similar between all four cases (see Figure 4-26). The original result was lower than the new MELCOR 2.2 results but not significantly considering the variations noted in NUREG/CR-7155 for results with a thermally-failed MSL. The MELCOR 2.2 cases included a surge of water from the wetwell that was not calculated in the original calculation. The higher release in the Version 2.2 calculations is attributed to the surge of radionuclides from the wetwell water that boiled away on the drywell debris and the revaporization of cesium iodine in the drywell. However, the amount that reaches the environment is impacted by hydrogen burns in the reactor building, which has variable behavior based on the local conditions at the ignition site (i.e., ignition sources are assumed throughout the reactor building). The differences in the magnitude of the cesium releases were not affected by the delayed drywell liner failure during the drywell leakage phase. The leakage through the drywell head was also effective at releasing cesium aerosols prior the liner failure.
- The iodine release in the MELCOR 2.2 calculation without RP seal leakage to the environment is similar to the original calculation (see Figure 4-27). The two cases with RP seal leakage had higher iodine releases to the environment. The higher environmental release in the MELCOR 2.2 calculation with melt spreading and water ingression was between 23 to 25 hr due to a late release of cesium iodide from the ex-vessel melt after the liner failure. Similarly, the initial sharp rise in the MELCOR 2.2 calculation with the debris heat transfer multipliers ("Version 2.2") also had a significant ex-vessel cesium iodine release from 24 to 25 hr. In contrast, the MELCOR 2.2 calculation without RP seal leakage did not have a significant ex-vessel release, which limited the magnitude of the iodine release to the environment.[17]
    - The higher release in the Version 2.2 calculations is also partially attributed to the surge of radionuclides from the wetwell water that boiled away on the drywell debris and revaporization of cesium iodine in the drywell.
    - The differences in the magnitude of the iodine releases were not affected by the delayed drywell liner failure during the drywell leakage phase. The leakage through the drywell head was also effective at releasing cesium iodide aerosols prior to the liner failure.

[17] The MELCOR calculation without RP seal leakage had a much smaller ex-vessel release of cesium iodide than the other MELCOR 2.2 calculations. The lowest powered fuel in Ring 5 did not collapse and relocate into the drywell. The ex-vessel cesium iodide release primarily originated from the fuel in Ring 5, which had a less complete heatup prior to the collapse of the structures holding the Ring 5 core plate.

This page left blank

Table 4-4. Comparison of Realization 86 key events and timing between NUREG/CR-7155 and MELCOR 2.2

Event Timing (hr)	NUREG/CR-7155	MELCOR 2.2 No RP leak	MELCOR 2.2 w/RP leak	MELCOR 2.2 w/Meltspread
Loss of all AC power, DC power available Reactor trip, feedwater pumps trip, and MSIVs close	0.00	0.00	0.00	0.00
Pump seal leakage increases to 18 gpm/pump	N/A	N/A	>0.0	>0.0
100 °F/hr cooldown initiated (SRV opened, RCIC throttled)	1.00	1.00	1.00	1.00
SRV closes on battery depletion	3.72	3.72	3.72	3.72
RCIC turbine floods failing RCIC	4.92	4.64	4.72	4.72
SRV fails to close due to excessive cycling	N/A	N/A	N/A	N/A
Downcomer level drops to TAF	8.68	7.75	7.89	7.89
First fuel-cladding gap release	9.75	8.75	8.83	8.84
SRV fails to close due the excessive temperature	10.95	9.94	10.16	10.16
MSL creep rupture	12.48	12.89	11.56	11.56
First large-scale relocation of core debris to lower plenum	13.01	12.74	11.33	11.33
RPV LHF	18.84	16.84	18.19	18.19
Drywell head flange leakage begins	12.48	12.89	11.56	11.56
Reactor building blowout panels open	12.48	12.89	11.57	11.57
Wetwell rupture (above waterline)	N/A	N/A	N/A	N/A
Drywell liner melt-through	19.07	18.01	24.51	22.50
A large reactor building H_2 burn fails the roof	13.16	14.88	24.42	N/C
Key Occurrences / Events	**NUREG/CR-7155**	**MELCOR 2.2 No RP leak**	**MELCOR 2.2 w/RP leak**	**MELCOR 2.2 w/Meltspread**
Elapsed time between SRV sticking open and onset of core damage (hr)	-1.19	-1.19	-1.31	-1.31
Elapsed time between LHF and drywell liner melt-through (hr)	0.22	1.18[16]	6.33	0.90
Elapsed time between onset of SRV sticking open and MSL creep rupture (hr)	1.53	2.94	1.41	1.41
In-vessel H_2 production (kg)	1,257	1,049	884	891
Surge of water from wetwell up onto drywell floor at liner melt-thru (Yes/No)	N	Y	Y	Y

Railroad Doors blow open (Yes/No)	Y	Y	Y	Y
Releases to the Environment	**NUREG/CR-7155**	**MELCOR 2.2 No RP leak**	**MELCOR 2.2 w/RP leak**	**MELCOR 2.2 w/Meltspread**
I release to environment > 0.1% (hr)	12.7	12.9	11.9	11.6
Cs release to environment by 48 hr (fraction)	0.042	0.064	0.073	0.078
I release to environment by 48 hr (fraction)	0.085	0.090	0.194	0.230

Notes:

N/A – Not applicable.
N/M – Not modeled.

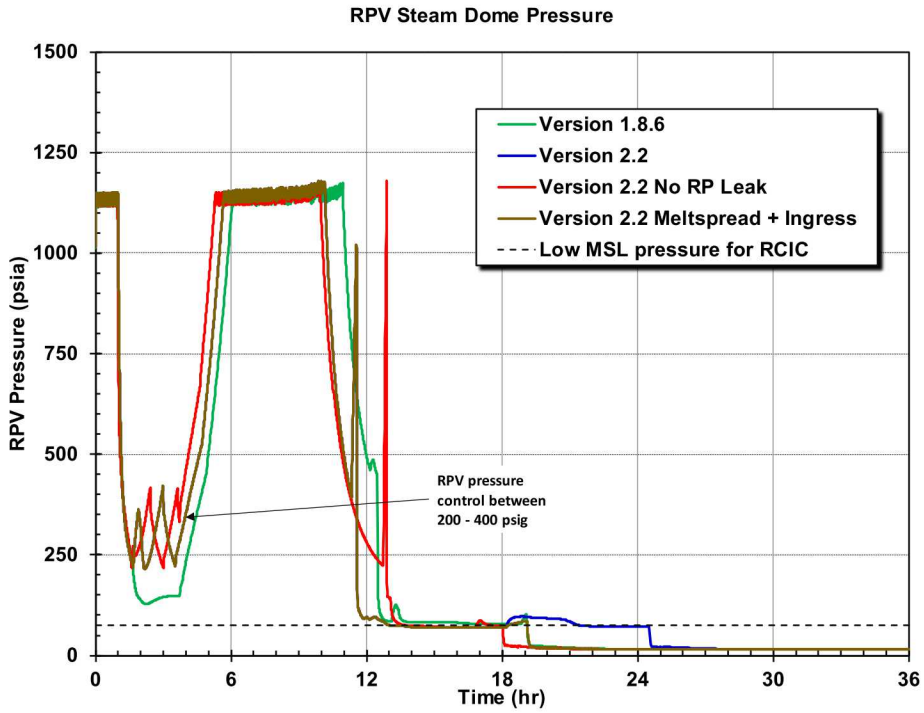

Figure 4-19. Comparison of the RPV pressure with NUREG/CR-7155 and MELCOR 2.2 for Realization 86 with a thermally-failed SRV and thermally-failed MSL

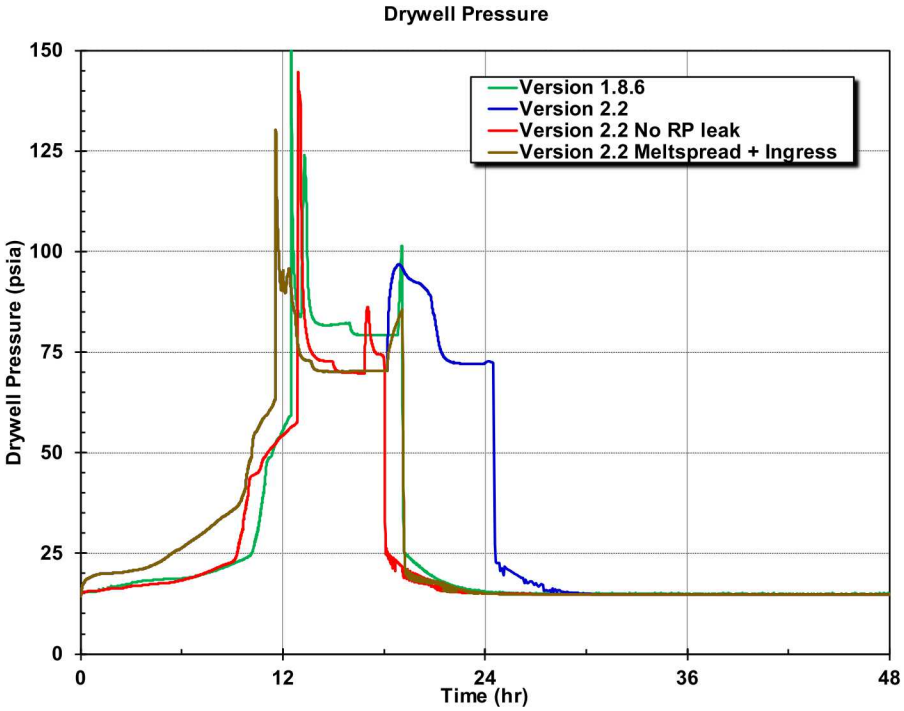

Figure 4-20. Comparison of the drywell pressure with NUREG/CR-7155 and MELCOR 2.2 for Realization 86 with a thermally-failed SRV and thermally-failed MSL

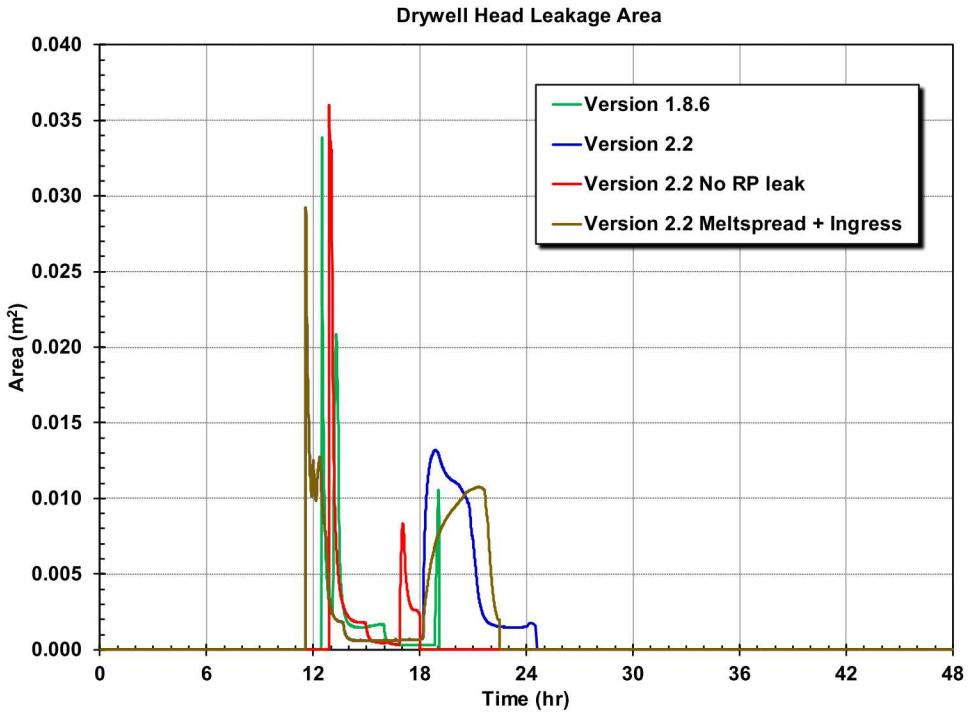

Figure 4-21. Comparison of the drywell head leakage area with NUREG/CR-7155 and MELCOR 2.2 for Realization 86 with a thermally-failed SRV and thermally-failed MSL

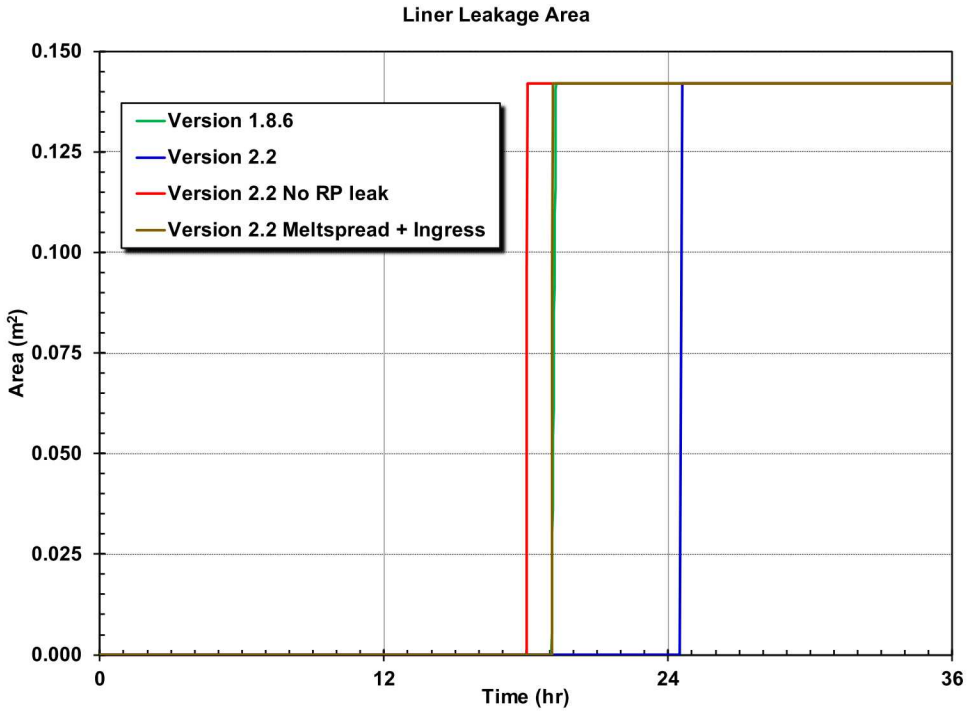

Figure 4-22. Comparison of the drywell liner failure area with NUREG/CR-7155 and MELCOR 2.2 for Realization 86 with a thermally-failed SRV and thermally-failed MSL

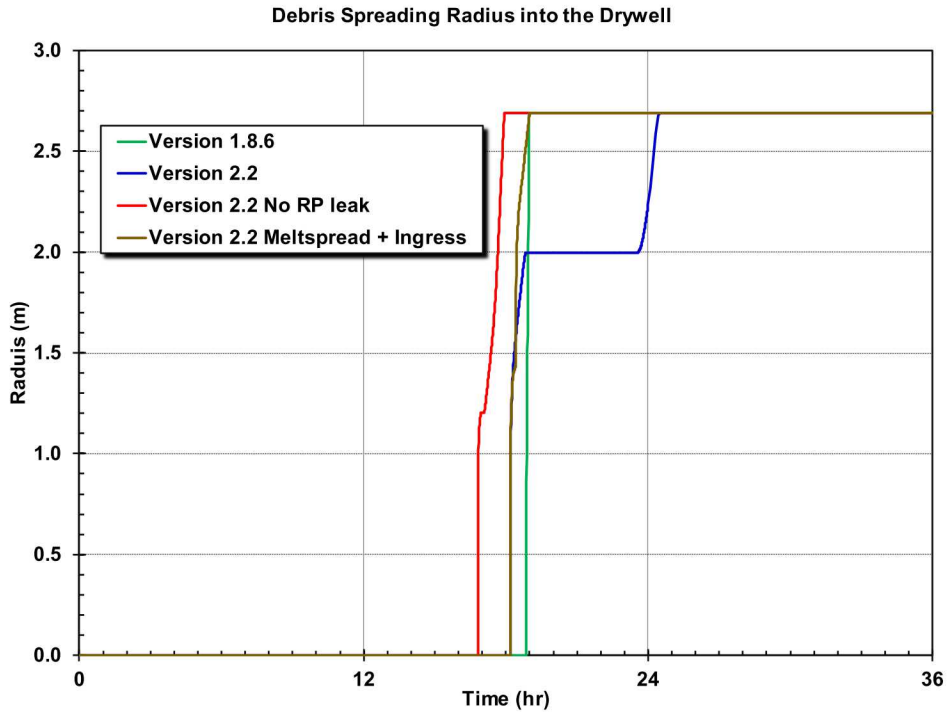

Figure 4-23. Comparison of the debris spreading radius into the drywell with NUREG/CR-7155 and MELCOR 2.2 for Realization 86 with a thermally-failed SRV and thermally-failed MSL

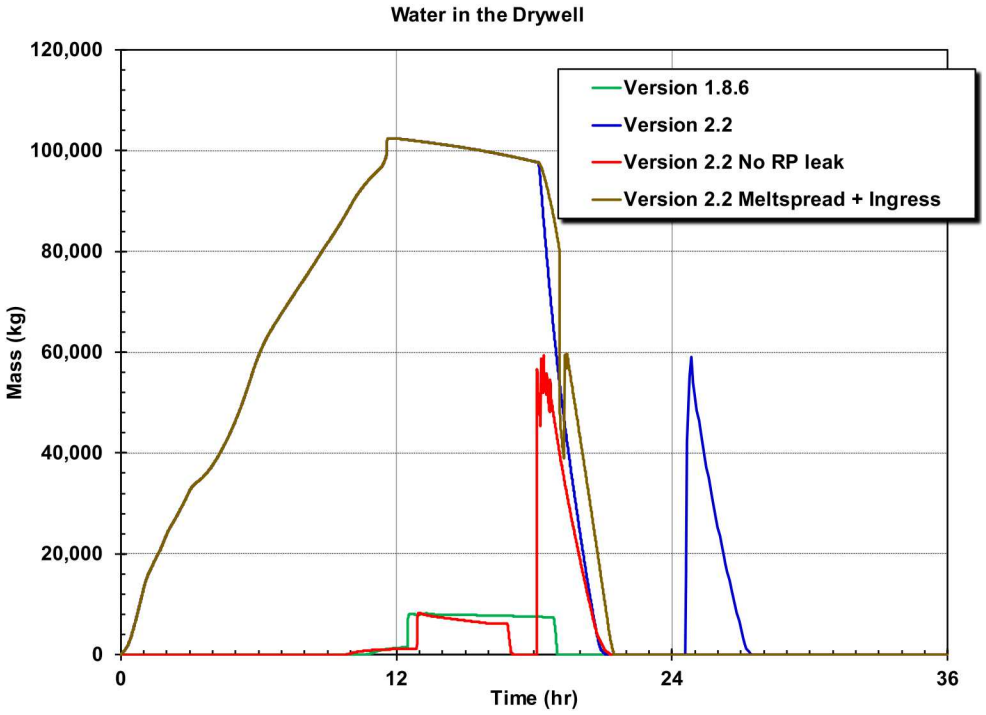

Figure 4-24. Comparison of the water mass in the drywell with NUREG/CR-7155 and MELCOR 2.2 for Realization 86 with a thermally-failed SRV and thermally-failed MSL

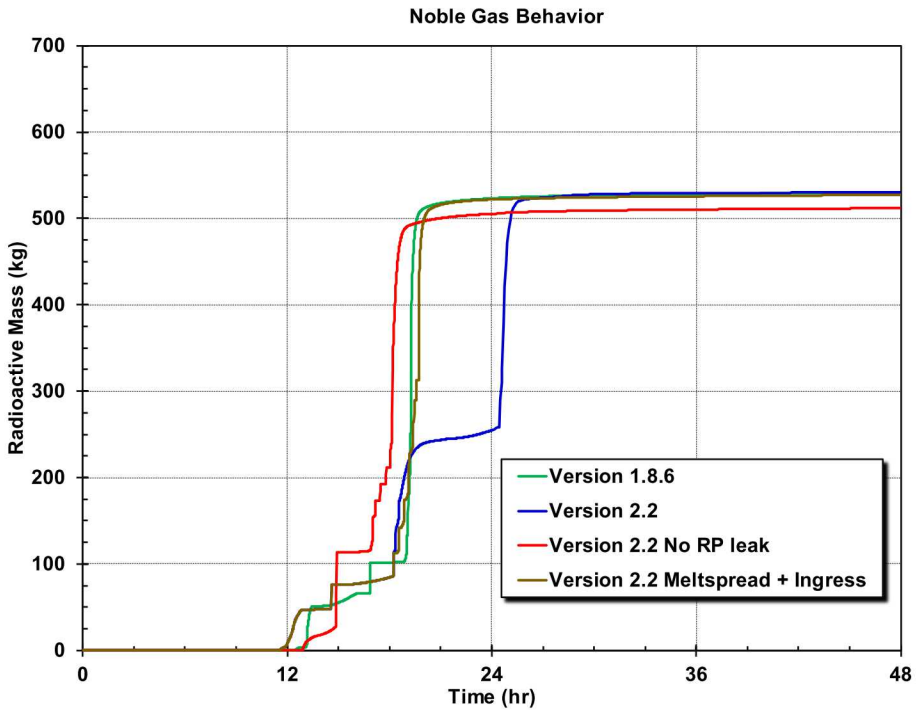

Figure 4-25. Comparison of the xenon release to the environment with NUREG/CR-7155 and MELCOR 2.2 for Realization 86 with a thermally-failed SRV and thermally-failed MSL

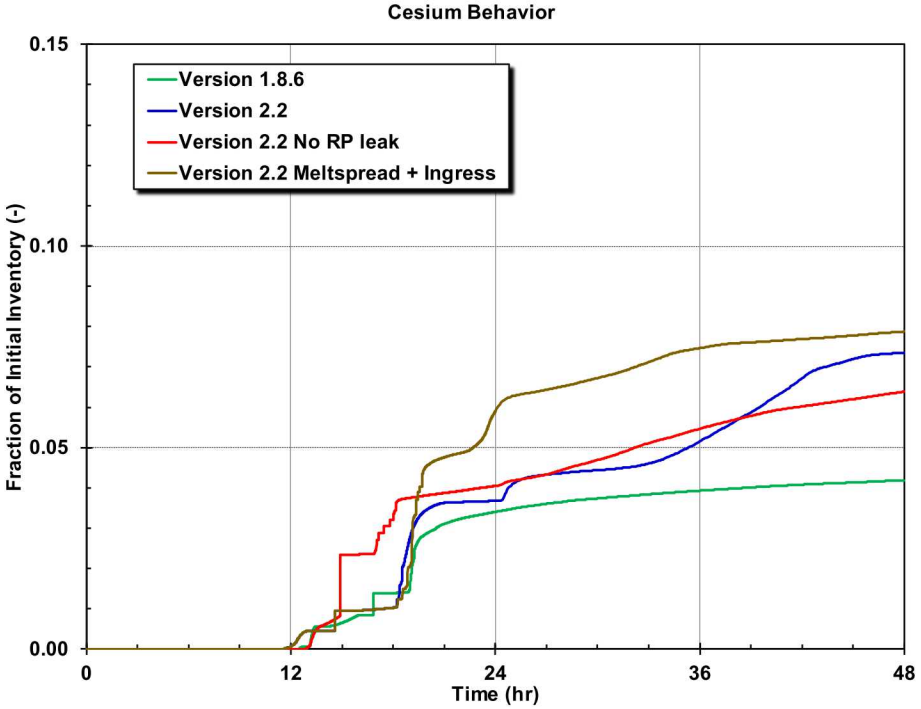

Figure 4-26. Comparison of the cesium release to the environment with NUREG/CR-7155 and MELCOR 2.2 for Realization 86 with a thermally-failed SRV and thermally-failed MSL

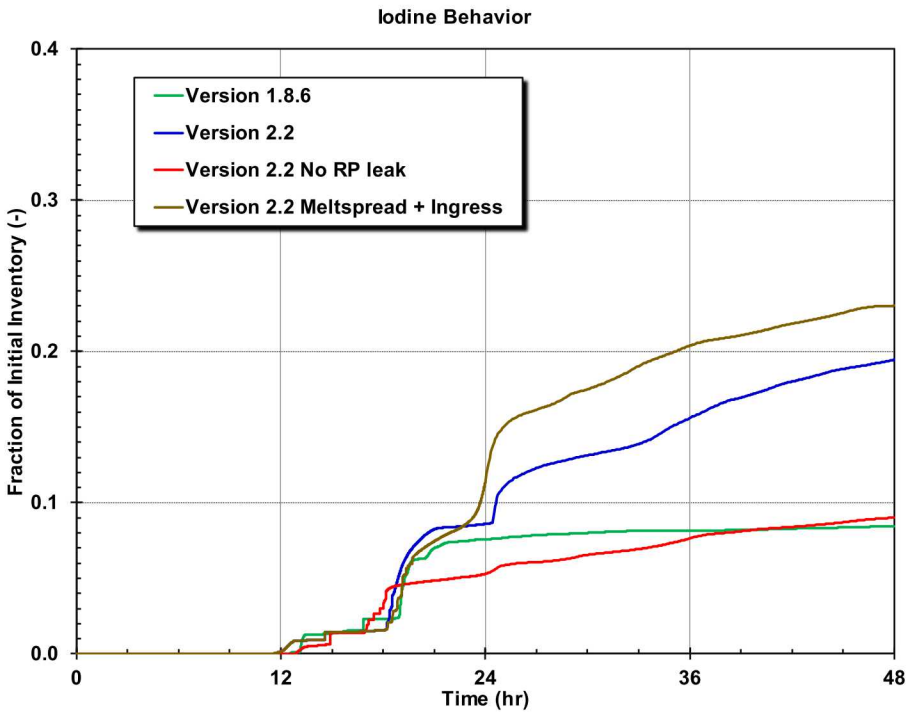

Figure 4-27. Comparison of the iodine release to the environment with NUREG/CR-7155 and MELCOR 2.2 for Realization 86 with a thermally-failed SRV and thermally-failed MSL

This page left blank

5. SUMMARY

A first-of-a-kind UA of the accident progression, radiological releases, and offsite consequences was performed for an unmitigated LTSBO severe accident scenario at the Peach Bottom Atomic Power Station. The study was completed in 2015 and documented in NUREG/CR-7155. Since 2015, two other SOARCA UAs were completed for two PWR plants. The PWR UAs incrementally updated the approach and methodology, including using the latest release of the MELCOR 2.2 computer code. There were also advances made in the state-of-the-art modeling related to NRC efforts using the Peach Bottom model in NUREG-2206, which provided the technical basis for the containment protection and release reduction rulemaking for boiling water reactors with Mark I and Mark II containments. The scope of the effort included documenting Peach Bottom input model changes since the NUREG/CR-7155 study and the reference calculations to assess the changes of the new computer code and the model input updates. The following insights were derived from the project.

- New MELCOR 2.2 benchmarks using the updated Peach Bottom model were compared to three reference cases from the NUREG/CR-7155. The new results qualitatively show the same responses and source term results, thereby confirming the conclusions from the NUREG/CR-7155 study.
- The Peach Bottom input model has been updated to support future research and uncertainty studies.
    - The MELCOR 2.2 code includes substantial model improvements and corrections since the MELCOR 1.8.6 calculations.
    - The updated Peach Bottom model also includes corrections and enhancements developed since the NUREG/CR-7155. These updates include:
        - RP seal leakage,
        - MSIV leakage,
        - FTC SRV modeling for five valves,
        - A two-control volume wetwell nodalization for localized heating,
        - Updated in-vessel falling debris heat transfer coefficient, and
        - Improvements to the ex-vessel debris spreading and water ingression heat transfer.
- New and updated uncertainty parameters and distributions were developed for the Peach Bottom model since the NUREG/CR-7155 study, which include:
    - An updated SRV stochastic FTC area,
    - Variable eutectic fuel melting temperatures,
    - An aerosol aerodynamic shape factor distribution based on the PWR UA work,
    - A new in-vessel falling debris heat transfer uncertainty distribution, and
    - An updated and continuous cesium speciation distribution.
- The new MELCOR 2.2 results also illustrate new behaviors:
    - The importance of RP leakage on the ex-vessel debris spreading behavior and radionuclide transport to the drywell,
    - The potential for delayed liner melt-through with improved ex-vessel debris modeling, and
    - The counter balancing effects of a delayed drywell liner melt-through radionuclide release versus sustained drywell head leakage without liner melt-through.

This page left blank

REFERENCES

[1] NUREG-1935. "State-of-the-Art Reactor Consequence Analyses (SOARCA) Report." U.S. Nuclear Regulatory Commission, Washington, DC. November 2012.

[2] NUREG/CR-7155. "State-of-the-Art Reactor Consequence Analyses Project, Uncertainty Analysis of the Unmitigated Long Term Station Blackout of the Peach Bottom Atomic Power Station." U.S. Nuclear Regulatory Commission, Washington, DC. May 2016.

[3] NUREG/CR-7245. "State-of-the-Art Reactor Consequence Analyses Project: Sequoyah Integrated Deterministic and Uncertainty Analysis." U.S. Nuclear Regulatory Commission, Washington, DC. October 2019.

[4] NUREG/CR-7262 (DRAFT). "State-of-the-Art Reactor Consequence Analyses Project: Uncertainty Analysis of the Unmitigated Short Term Station Blackout of the Surry Power Station." U.S. Nuclear Regulatory Commission, Washington, DC. August 2019.

[5] NUREG-2206. "Technical Basis for the Containment Protection and Release Reduction Rulemaking for Boiling Water Reactors with Mark I and Mark II Containments." U.S. Nuclear Regulatory Commission, Washington, DC. March 2018.

[6] ORNL. "Ex-Vessel Core Melt Modeling Comparison between MELTSPREAD-CORQUENCH and MELCOR 2.1." ORNL/TM-2014/1, Oak Ridge National Laboratory. March 2014.

[7] U.S. NRC. "Peach Bottom Atomic Power Station, Units 2 and 3 – Safety Evaluation Regarding Implementation of Mitigating Strategies and Reliable Spent Fuel Pool Instrumentation Related to Orders EA-12-049 and EA-12-051 (CAC Nos. MF0845, MF0846, MF0849, and MF0850; EPID NOS. L-2013-JLD-0017 AND L-2013-JLD-0018)." NRC ML18113A334, U.S. Nuclear Regulatory Commission, Washington, DC. May 9, 2018.

[8] Shaukat, S. K., J. E. Jackson, and D. F. Thatcher. "Regulatory Analysis for Generic Issue 23: Reactor Coolant Pump Seal Failure." NUREG-1401, U.S. Nuclear Regulatory Commission, Washington, DC. April 1991.

[9] Gauntt, R. O., et al. "Analysis of Main Steam Isolation Valve Leakage in Design Basis Accidents Using MELCOR 1.8.6 and RADTRAD." SAND2008-6601, Sandia National Laboratories. October 2008.

[10] "Wetwell Modeling Nodalization Study and SN/AP Post Processing," 6th Meeting of the European MELCOR User Group, UJD, VUJE, Bratislava, Slovakia. April 15-16, 2014. Accessed at: https://www.psi.ch/en/emug/2014-bratislava.

[11] Cook, D. H. "Pressure Suppression Pool Thermal Mixing." NUREG/CR-3471, ORNL/TM-8906, U.S. Nuclear Regulatory Commission and Oak Ridge National Laboratory. 1984.

[12] NUREG/CR-7008. "MELCOR Best Practices as Applied in the State-of-the-Art Reactor Consequence Analyses (SOARCA) Project." U.S. Nuclear Regulatory Commission, Washington, DC. August 2014.

[13] Dhir, V. K. and Purohit, G. P. "Subcooled Film-Boiling Heat Transfer from Spheres." *Nuclear Engineering and Design 47*, (1978): pp. 49-66.

[14] Farmer, M. T. "Melt Spreading Code Assessment, Modifications, and Applications to the EPR Core Catcher Design." ANL-09/10, Argonne National Laboratory. March 2009.

[15] Humphries, L. L. "MELCOR 2019 Workshop CAV Package Overview." SAND2019-6156PE, Sandia National Laboratories. June 2019.

[16] Ghosh, S.T., et al. "Estimating Safety Valve Stochastic Failure to Close Probabilities for the Purpose of Nuclear Reactor Severe Accident Analysis." NRC2017-3538, Proceedings of the Thirteenth NRC/ASME Symposium on Valves, Pumps, and In Service Testing for Operating and New Reactors. July 2017.

[17] Pontillon, Y., et al. "Lessons learnt from VERCORS tests. Study of the active role played by UO2–ZrO2–FP interactions on irradiated fuel collapse temperature." *Journal of Nuclear Materials 344*, (2005): pp. 265–273.

[18] NUREG/CR-7110 Volume 1, Rev. 1. "State of the Art Reactor Consequence Analysis Project Volume 1: Peach Bottom Integrated Analysis." U.S. Nuclear Regulatory Commission, Washington, DC. May 2013.

[19] NUREG/CR-7110 Volume 2, Rev. 1. "State-of-the-Art Reactor Consequence Analysis Project Volume 2: Surry Integrated Analysis." U.S. Nuclear Regulatory Commission, Washington, DC. January 2012.

[20] Gauntt, R. O. "Synthesis of VERCOS and Phebus Data in Severe Accident Codes and Applications." SAND2010-1633, Sandia National Laboratories. April 2010.

[21] Gauntt, R. O. "MELCOR 1.8.5 Modeling Aspects of Fission Product Release, Transport, and Deposition – An Assessment with Recommendations." SAND2010-1635, Sandia National Laboratories. April 2010.

[22] Haste, T., et al. "Main Outcomes of Fission Product Behavior in the Phebus FPT3 Test." 4th European Review Meeting on Severe Accident Research (ERMSAR-2010), Bologna, Italy. May 11-12, 2010.

[23] Helton, J. C., R. L. Iman, J. D. Johnson, and C. D. Leigh. "Uncertainty and Sensitivity Analysis of a Model for Multicomponent Aerosol Dynamics." *Nuclear Technology 73,* (1986): pp. 320-342.

[24] Helton, J. C., R. L. Iman, J. D. Johnson, and C. D. Leigh. "Uncertainty and Sensitivity Analysis of a Dry Containment Test Problem for the MAEROS Aerosol Model." U. S. Nuclear Regulatory Commission. *Nuclear Science and Engineering 102,* (1989): pp. 22-42.

[25] Kasper, G., T. Niida and M. Yang. "Measurements of viscous drag on cylinders and chains of sphere with aspect ratios between 2 and 50." Great Britain. *J. Aerosol Science, 16 (6)*, (1985): pp. 535-556. 1985.

[26] Hinds, W. C. *Aerosol Technology*. Wiley. 1982.

[27] Brockmann, J. E., et al. Appendix F, "Uncertainty in Radionuclide Release Under Specific LWR Accident Conditions," in "Range of Possible Dynamic and Collision Shape Factors." SAND84-0410 Volume 2, Sandia National Laboratories, Albuquerque, New Mexico. 1985.

[28] Kissane, M.P. "On the nature of aerosols produced during a severe accident of a water cooled nuclear reactor." *Nuclear Engineering and Design 238,* (2008): pp. 2792-2800.

[29] Humphries, L. L. "MELCOR Code Development Status MCAP 2016." SAND2016-12141PE, Sandia National Laboratories. September 2016.

[30] Humphries, L. L. "Quicklook Overview of Model Changes in MELCOR 2.2: Rev 6342 to Rev 9496." SAND2017-5599, Sandia National Laboratories. November 2017.

[31] Humphries, L. L. "Quicklook Overview of Model Changes in MELCOR 2.2: Rev 9496 to Rev 11932." SAND2018-13524, Sandia National Laboratories. November 2018.

[32] Humphries, L. L. "MELCOR Code Development Status MCAP 2016." SAND2019-6157PE, Sandia National Laboratories. June 2019.

DISTRIBUTION

Email—External

Name	Company Email Address	Company Name
Tina Ghosh	Tina.Ghosh@nrc.gov	U.S. NRC
Salman Haq	Salman.Haq@nrc.gov	U.S. NRC
Alfred Hathaway	Alfred.Hathaway@nrc.gov	U.S. NRC
Hossein Esmaili	Hossein.Esmaili@nrc.gov	U.S. NRC

Email—Internal

Name	Org.	Sandia Email Address
KC Wagner	8852	kcwagne@sandia.gov
Technical Library	9536	libref@Sandia.gov

This page left blank

Sandia National Laboratories

Sandia National Laboratories is a multimission laboratory managed and operated by National Technology & Engineering Solutions of Sandia LLC, a wholly owned subsidiary of Honeywell International Inc. for the U.S. Department of Energy's National Nuclear Security Administration under contract DE-N/A0003525.